Fall 1987

The development of glass-ceramic matrix composites and the crystallization of two glass-ceramic matrices

William M. Carty

Department:

THE DEVELOPMENT OF GLASS-CERAMIC MATRIX COMPOSITES AND THE CRYSTALLIZATION OF TWO GLASS-CERAMIC MATRICES

BY

WILLIAM MICHAEL CARTY, 1962-

A THESIS

Presented to the Faculty of the Graduate School of the

UNIVERSITY OF MISSOURI-ROLLA

In Partial Fulfillment of the Requirements for the Degree

MASTER OF SCIENCE IN CERAMIC ENGINEERING

1987

Approved by

Robert C. Moore (Advisor) Delbert E. Day

ABSTRACT

In order to develop ceramic matrix composites for high temperature applications, two glass-ceramic matrices, one an yttrium aluminosilicate (YAS), the other a magnesium aluminosilicate (cordierite), were chosen as possible matrix compositions. Two seperate sets of experiments were performed. Specimens were hot pressed and heat treated then analyzed for the crystallization produots and C.T.E. Specimens were also prepared containing commercially available ceramic fibers and coated ceramic fibers to investigate fiber/matrix interactions and the effect of fiber additions on the crystallization of the glass matrices. DTA was employed to approximate the crystallization temperature of the glasses and to determine the effect of dopant and fiber additions on the glass crystallization. Glass specimens hot pressed above 1000°C for 15 minutes would crystallize while specimens hot pressed for shorter times, i.e. 2 minutes, would remain amorphous. The cordierite matrix crystallized to α-cordierite. The YAS glass would crystallize to mullite and α-$Y_2Si_2O_7$ when hot pressed at, or below 1250°C and to mullite and β-$Y_2Si_2O_7$ when hot pressed at 1300°C. Thermal expansion measurements on YAS glass specimens showed the α- to β-$Y_2Si_2O_7$ phase transfomation to be displacive and occur at 1280°C. Fiber additions enhanced crystallization, but without protective coatings, they chemically bonded to the matrix eliminating fiber pullout and causing brittle failure of the composite during testing. Fiber coatings would effectively reduce this interaction and allow fiber pullout to occur.

ACKNOWLEDGEMENTS

The author wishes to express his sincere appreciation to his advisor, Dr. Robert E. Moore, for his guidance and helpful suggestions. Appreciation is also extended to his committee members: Dr. Delbert Day, Curator's Professor of Ceramic Engineering and Director of the Graduate Center for Materials Research and to Dr. Lokesh Dharani, Assistant Professor of Engineering Mechanics.

The financial support for this project provided in part by the McDonnell Aircraft Company of the McDonnell-Douglas Corporation, St. Louis, Missouri is gratefully acknowledged. Special thanks are extended to Mr. Tim Hackett, an employee of McDonnell Aircraft, who served as technical coordinator for this work.

Thanks are extended to the undergraduate research aides Mike Long, Greg Wesling and Chris Heller for their help in performing experimental work and for their friendship. Also, special thanks are extended to Lorie Peeler, Senior Secretary of the Ceramic Engineering Department for her help in preparing this manuscript.

Finally, grateful appreciation and affection are extended to the author's family and friends, particularly, Robert and Helen Carty, Sylvia Bryant, Andrew Skoog and Marvin Pennell, for their support and encouragement which made this project so much more meaningful.

TABLE OF CONTENTS

Page

Page

Page

LIST OF ILLUSTRATIONS

LIST OF TABLES

I. INTRODUCTION

The need for high temperature structural materials has necessitated research and development of fiber and particulate toughened ceramic composites. Wood, teeth and bones are some examples of naturally occuring composites which are composed of a matrix phase and a reinforcing phase.[1-3] The matrix phase is usually a continuous, homogeneous medium which bonds to the reinforcing fibers or particulates to form a material which exhibits synergistic behavior. Ceramic materials are of particular interest as matrix materials because of their high strength and high usage temperature.

Unlike most metals or plastics, ceramics are brittle and generally fail in tension.[4] Therefore, if ceramics are to be used for high temperature structural applications they must be toughened to reduce the possiblility of catastrophic failure. The incorporation of ceramic fibers or particulates into a ceramic matrix gives rise to mechanisms which impede crack growth and dissipate crack energy imparting toughness to the matrix.

The potential application of ceramic composites for high temperature applications requires that the composite be thermally and dimensionally stable in an oxidizing atmosphere. Refractory glasses, glass-ceramics and ceramic oxides exhibit excellent oxidation resistance and low coefficients of thermal expansion (C.T.E.), making them solid candidates for these applications providing they can be mechanically toughened. Glass-ceramic matrix composites are of particular interest because of their ease of densification and their potentially high usage temperatures after ceraming. This thesis will examine the behavior of various commercially available ceramic fibers

in an yttrium aluminosilicate and a magnesium alumino-silicate glass-ceramic matrix, the crystallization procedure for these matrices, and the effect of fiber additions on their crystallization behavior.

Particulate and whisker reinforced composite systems are beyond the scope of this thesis and were not studied.

II. LITERATURE SURVEY

A. STRENGTHENING AND TOUGHENING

The terms strengthening and toughening are often confused; just because a material is strong does not mean that that a material will be tough.[3-6] The strength of a composite is determined by the force required to produce ultimate failure. A material which can support a large stress is considered a strong material. The toughness of a material is determined by the way the material fractures. A tough material fails in a non-catastrophic manner, whereas a brittle material fails catastrophically (see Figure 1). Ceramics, like metals, possess high strength; unlike metals, however, which exhibit ductile flow and other mechanisms to slow crack growth, ceramics have very poor toughness and generally undergo brittle failure. If a ceramic contains a flaw of critical size as defined by Griffith,[7] it will fail at a predicted stress which is much lower than the strength of the flaw-free material. The size of the critical flaw can be expressed using the Inglis equation:

$$F = 2R(c/\rho)^{1/2} \qquad (1)$$

where ρ is the radius of the crack tip, c is one half the flaw length, R is the applied stress, and F is the maximum stress realized at the crack tip. By substituting the ultimate tensile strength of the material for F, the maximum tensile stress the material can withstand, R, can be calculated. The critical flaw size for a structural ceramic material is accepted to be less than 10um.[8] If the material contains a particle or a fiber which can impede crack growth or can somehow promote absorption of the crack energy, produced by the increase in

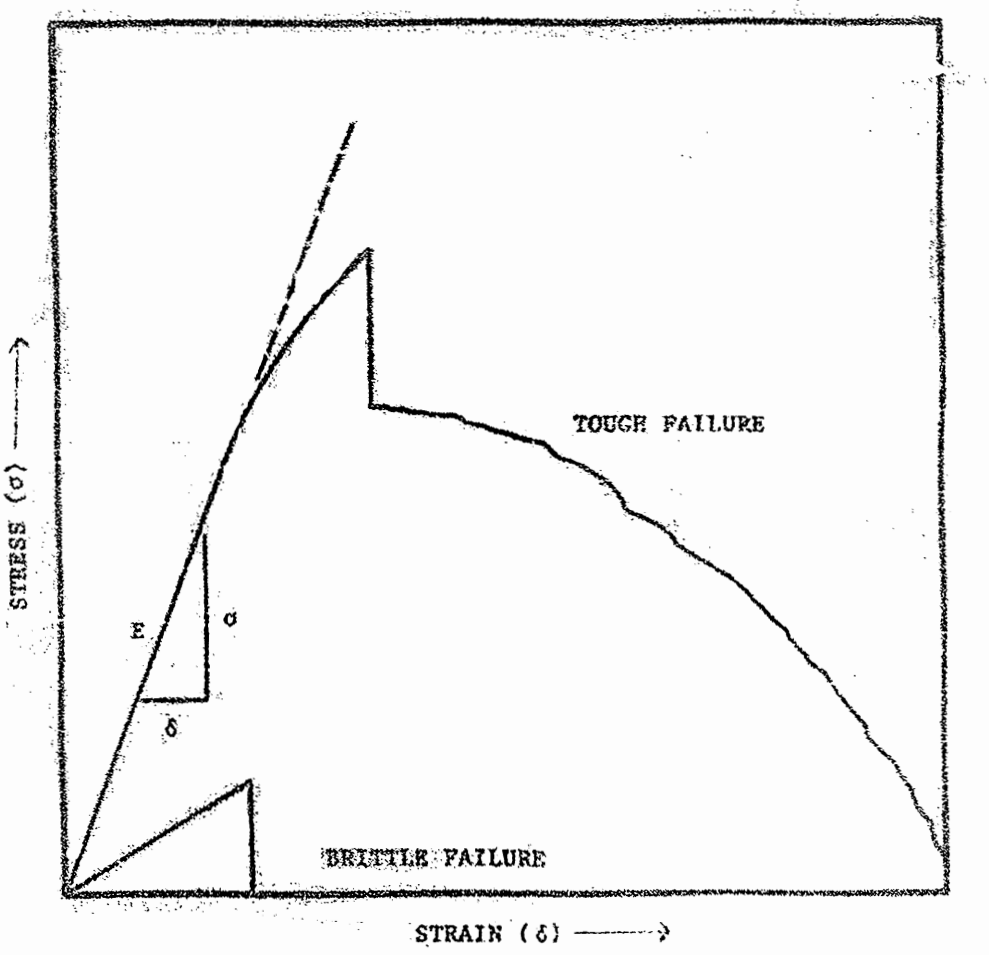

Fig. 1. Stress versus strain curves resulting from brittle and tough failure (Ref. 4).

surface area associated with crack propagation, the material may exhibit toughness.

1. Criteria for Strengthening in a Ceramic Composite. Three criteria must be fulfilled in a fiber reinforced ceramic to strengthen the ceramic with fiber additions.

a. Elastic Modulus Mismatch. The elastic modulus, E, of the reinforcing fiber must be considerably greater than that of the matrix. E is defined as the slope of the stress versus strain curve (Figure 1). When the strain becomes too great, the specimen fails. For optimum strengthening of a composite, the E of the fiber must be much greater than the E of the matrix. In general, the fibers will elongate much less under a given load than will the matrix, allowing the composite to withstand greater loads without failure.

The elastic modulus (E_c) of a composite can be determined using the Rule of Mixtures (ROM):[9,10]

$$E_c = E_m V_m + E_f V_f \qquad (2)$$

where E_m and E_f are the elastic modulus of the matrix and fiber, respectively, and V_m and V_f are the volume fractions of the matrix and fiber, respectively. Figure 2 illustrates the resulting E_c for a ceramic matrix composite. Such a matrix will only be strengthened if it contains a critical fiber volume fraction (V_f^*).[2,9-11] Equation 3 can be used to calculate V_f^*.[10]

$$V_{f^*} = [\sigma_{mu} - (\sigma_m)_{\varepsilon_{f^*}}] / [\sigma_{fu} - (\sigma_m)_{\varepsilon_{f^*}}] \qquad (3)$$

Where σ_{fu} and σ_{mu} are the ultimate tensile strength of the fiber and matrix, respectively; $(\sigma_m)_{\varepsilon_{f^*}}$ is the strength of the matrix at the stress required to produce the matrix failure strain in the fiber. Figure 3 illustrates the strength of a composite as a function of V_f

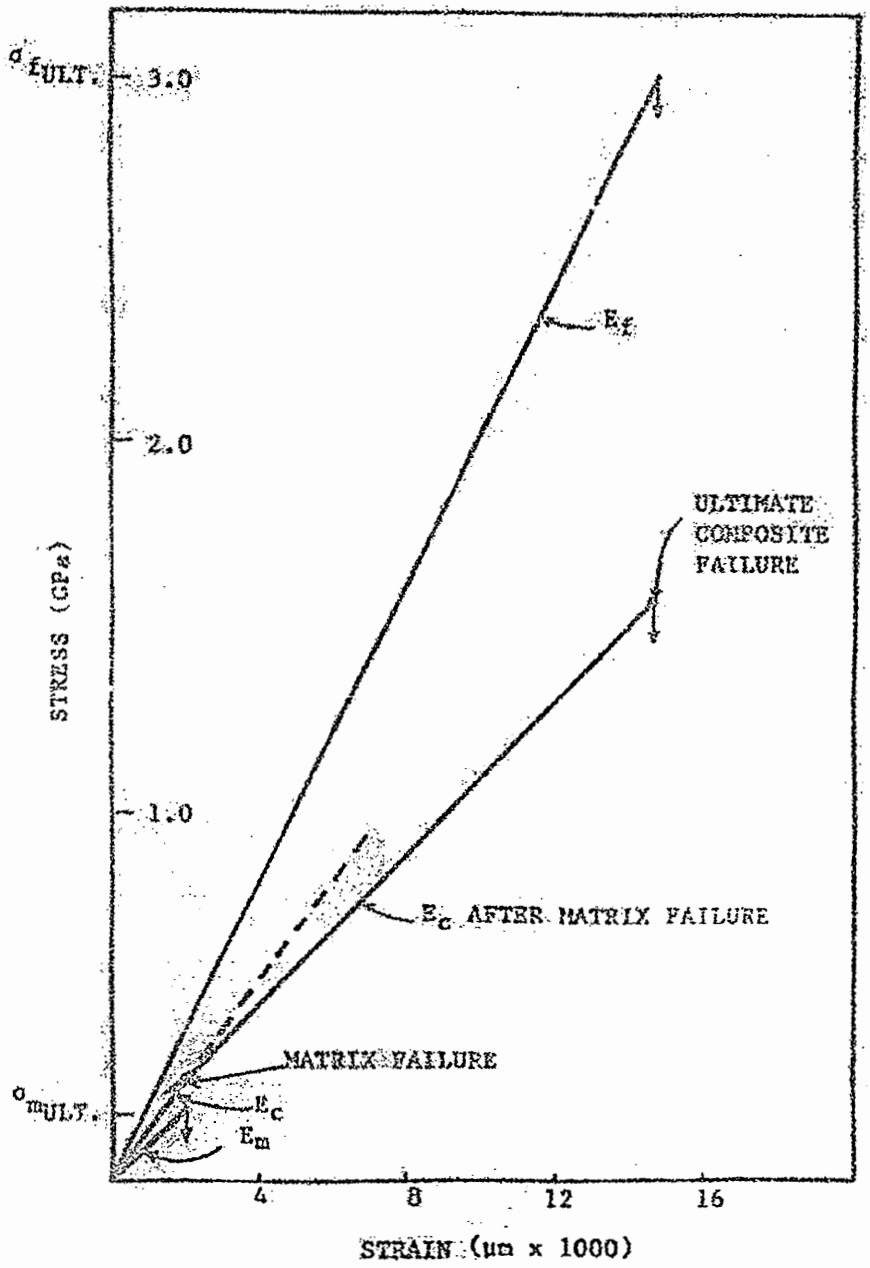

Fig. 2. Elastic modulus for a 0.50 volume fraction Nicalon fiber reinforced LAS glass-ceramic matrix composite (Ref. 9).

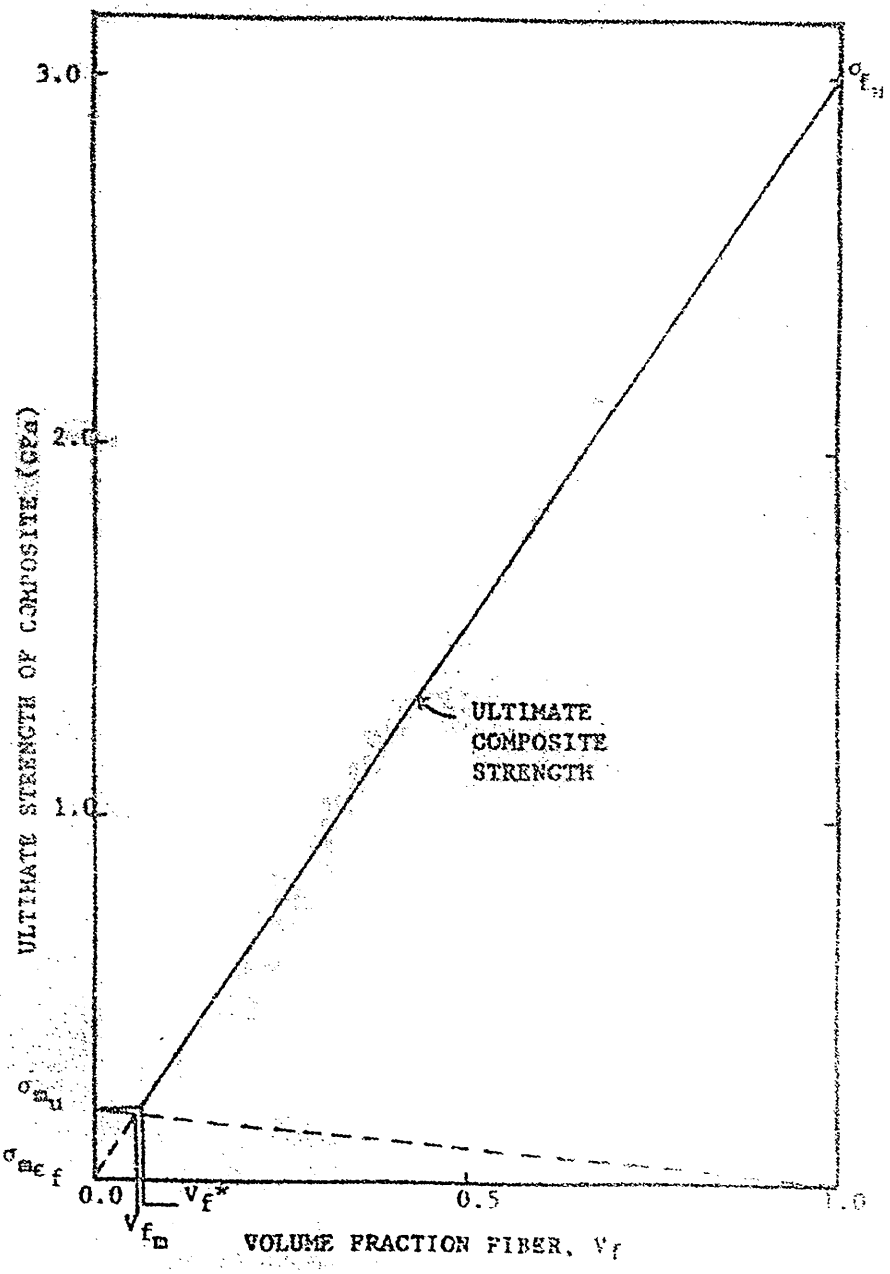

Fig. 3. Ultimate composite strength versus fiber volume fraction for a Nicalon fiber reinforced LAS glass-ceramic matrix composite (Ref. 9,10).

for a composite possessing the component properties of Nicalon fiber in a lithium aluminosilicate (LAS) matrix.

b. C.T.E. Mismatch. The coefficient of thermal expansion (C.T.E.) of the reinforcing fiber and the C.T.E. of the matrix must be similar. The coefficient of thermal expansion is the amount a material expands or contracts during heating or cooling and is dependent on the chemical and physical make-up of that material.[12] The C.T.E. difference, i.e. mismatch, between the matrix and the fibers can have a profound effect on the strength of the composite, particularly if the composite is processed at a high temperature as in the case of ceramic composites.[1,4,5,8,9,13-17] There are three cases which can occur:

i. $C.T.E._f < C.T.E._m$

ii. $C.T.E._f = C.T.E._m$

iii. $C.T.E._f > C.T.E._m$

i. $C.T.E._f < C.T.E._m$. When the $C.T.E._f$ is less than the $C.T.E._m$, the matrix surrounding the fiber is placed in tangential tension and radial compression upon cooling as the matrix tries to shrink around the fiber. If the mismatch is large enough, these stresses may cause radial cracking of the matrix around the fiber and a considerable decrease in composite strength as illustrated in Figure 4.

ii. $C.T.E._f = C.T.E._m$. The ideal situation is when the $C.T.E._f$ and the $C.T.E._m$ are matched since this yields a composite free of residual stress.

iii. $C.T.E._f > C.T.E._m$. It is more desirable to have the $C.T.E._f$ greater than the $C.T.E._m$ if a mismatch occurs. This mismatch places the relatively weak matrix in tangential compression and radial tension, equal to one-half of the compressive stress (Figure 5). This

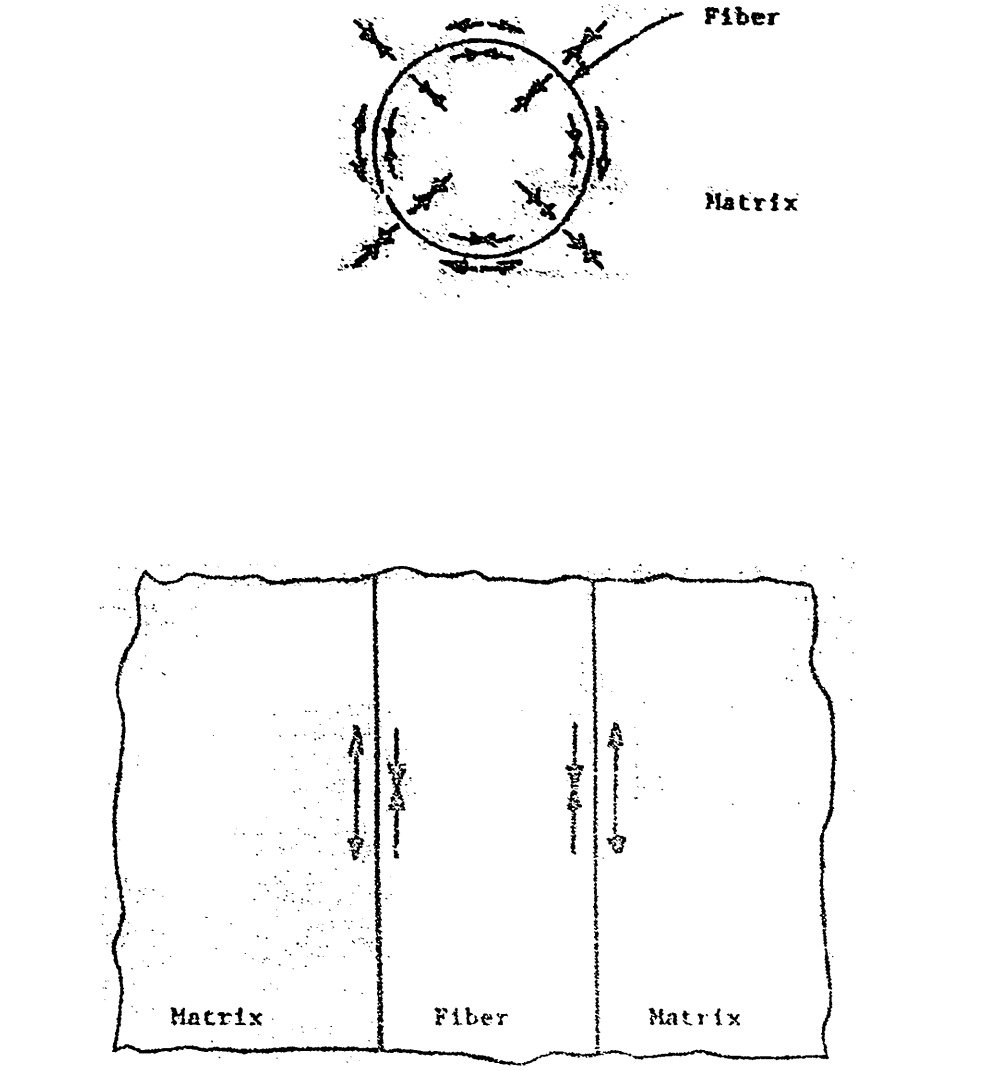

Fig. 4. Schematic representation of stresses developed during cooling for a single fiber with low C.T.E. surrounded by an infinite matrix of high C.T.E.

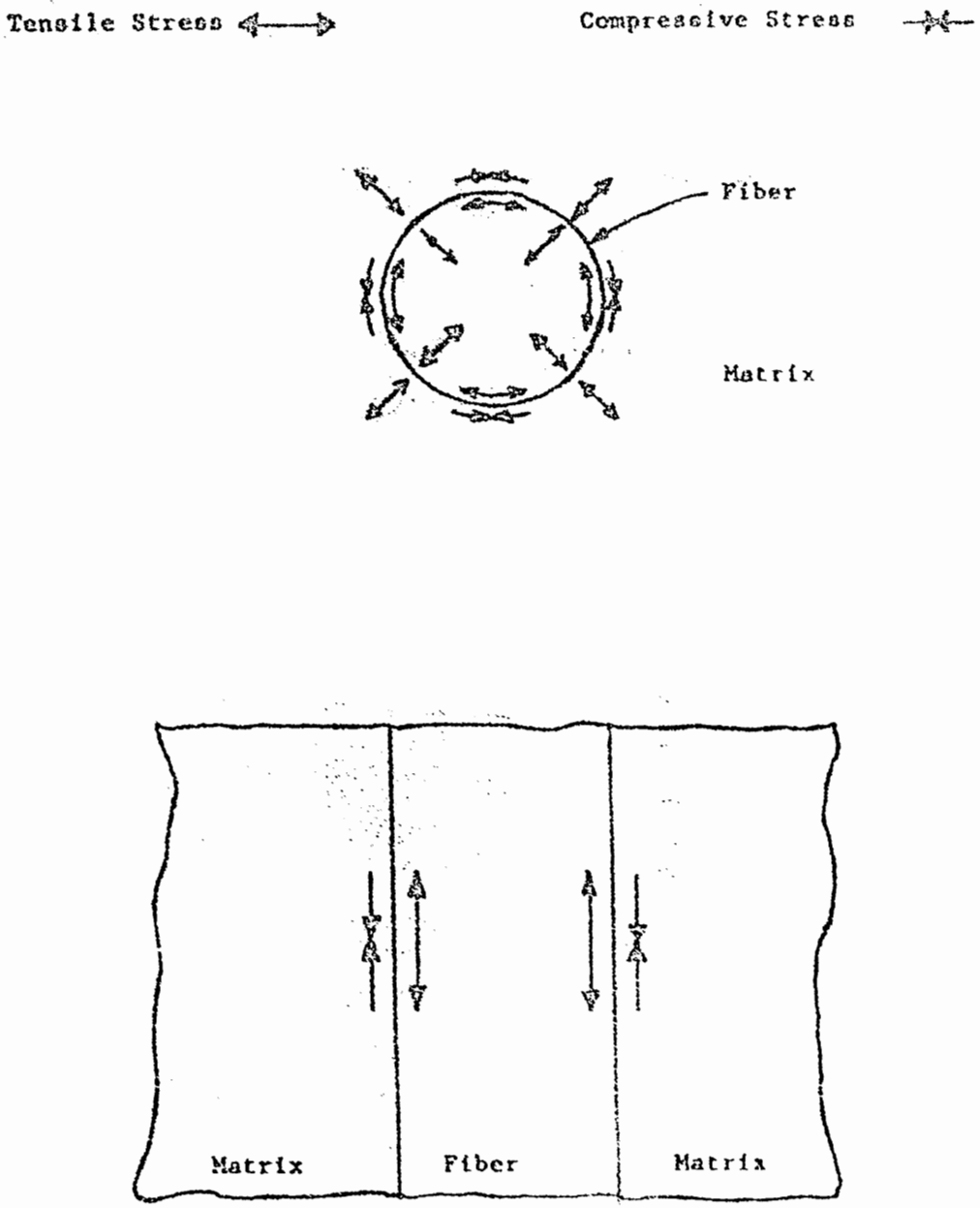

Fig. 5. Schematic representation of stresses developed during cooling for a single fiber with high C.T.E. surrounded by an infinite matrix of low C.T.E.

is desirable for ceramics, as ceramics are stronger in compression. If the C.T.E. mismatch is large enough in this situation, the fibers are placed in radial tension which can result in debonding of the fiber from the matrix or in fiber breakage, either of which is detrimental to the strength of the composite.

c. Fiber to Matrix Bond. The reinforcing fiber and the matrix must be intimately bonded together, either chemically or mechanically to provide efficient load transfer from the matrix to the fiber. If this bond is not strong, the composite will not be able to act in a synergistic fashion, and a reduction in the strength of the composite will result.[3-5,9,10]

2. Criteria for Toughening in a Ceramic Composite. There are basically two types of toughening in fiber reinforced ceramic composites: crack deflection due to C.T.E. mismatch,[4,5] and crack energy absorption due to fiber debonding and pull out.[4-6,9,15,18]

a. C.T.E. Mismatch Toughening. When the $C.T.E._f$ is greater than the $C.T.E._m$, the matrix is placed in compression around the fibers. In this case, a crack propagating through the matrix will be deflected before reaching the fiber at the compressive zone surrounding the fiber.[4,5] This type of toughening is not very effective and necessitates a strong interfacial bond to produce the compressive force in the matrix. The strong interface negates the toughening achieved through fiber pull out and is, therefore, an inefficient method for toughening.

b. Fiber Debonding and Pullout. In order for the fiber to debond and pull out of the matrix, the fiber/matrix interface must be weak. There can be no chemical reaction between the fiber and the matrix or

any corrosion of the fiber by the matrix at the interface. If there is a strong chemical bond between the fiber and the matrix, a crack propagating through the matrix will propagate through the fiber, resulting in brittle failure of the composite as illustrated in Figure 6.[5,6] If the interface is weak, however, the fiber will debond from the matrix, allowing the fiber to remain intact and carry the load. Once the matrix has cracked through, the entire load is transferred to the fibers which will fail at their weakest point and pull out,[6,9,18] as shown in Figure 7, producing a tough composite. The stress required for ultimate failure must then be large enough to overcome the frictional forces associated with the pull-out of the fibers.[4,6,9]

B. GLASS AND GLASS-CERAMIC MATRICES

1. Glass Formation. The American Society for Testing and Materials (ASTM) defines a glass as "an inorganic product of fusion which has been cooled to a rigid condition without crystallization."[19] If a melt cannot be cooled quickly enough to freeze the amorphous structure of the liquid, the material will crystallize. The minimum speed at which the melt needs to be cooled is known as the critical cooling rate. Thus, by the ASTM definition, any inorganic material which can be cooled quickly enough will form a glass. Often, however, the rate of cooling required to form a glass is so high it makes glass formation impractical. Using this criterion it is possible to compositionally determine a glass formation range. Figure 8 shows the glass formation region for the Y_2O_3-Al_2O_3-SiO_2 system [20,21] and the MgO-Al_2O_3-SiO_2 system[22] based on the criterion described by ASTM.

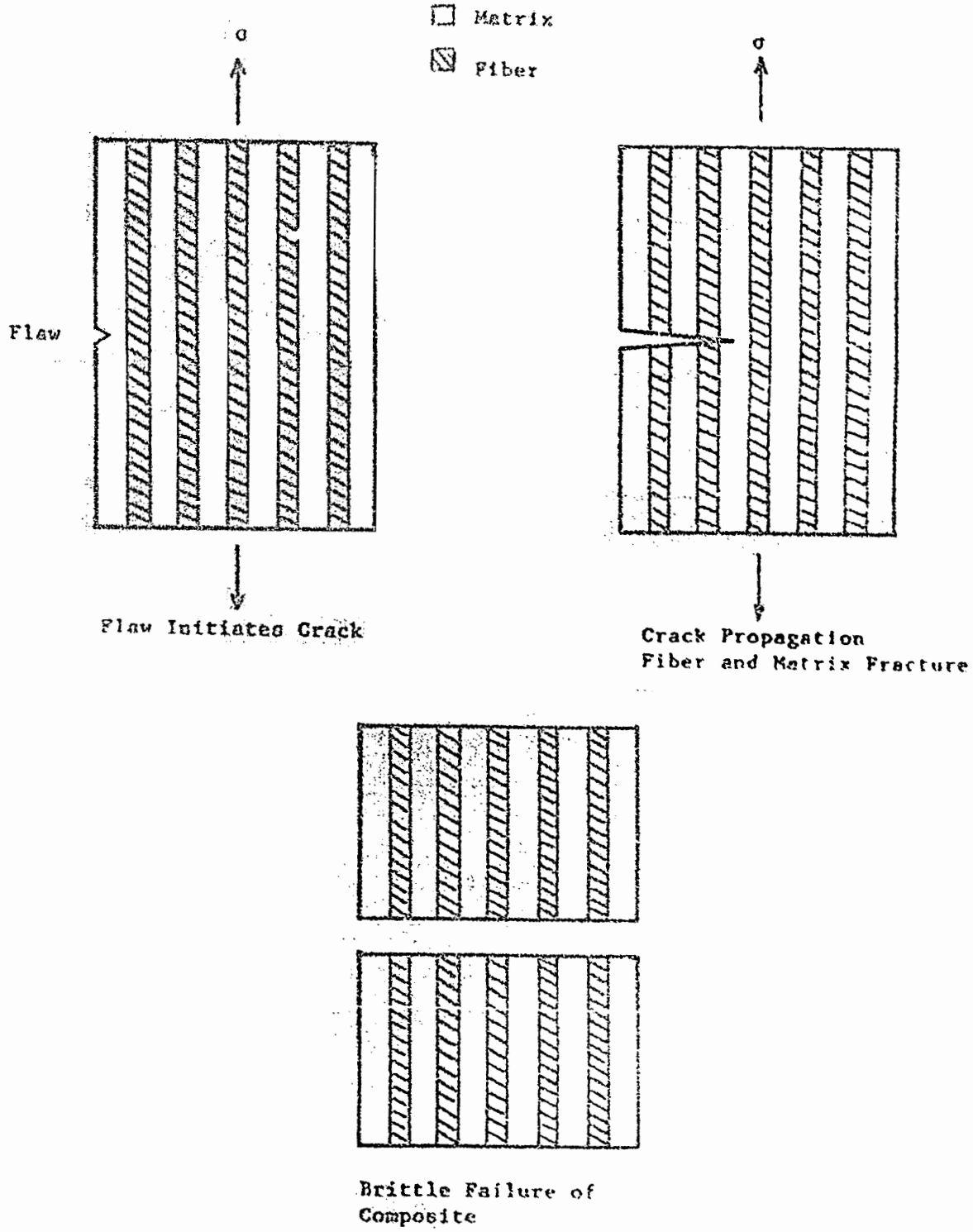

Fig. 6. Schematic representation of strong fiber/matrix interface resulting in brittle fracture.

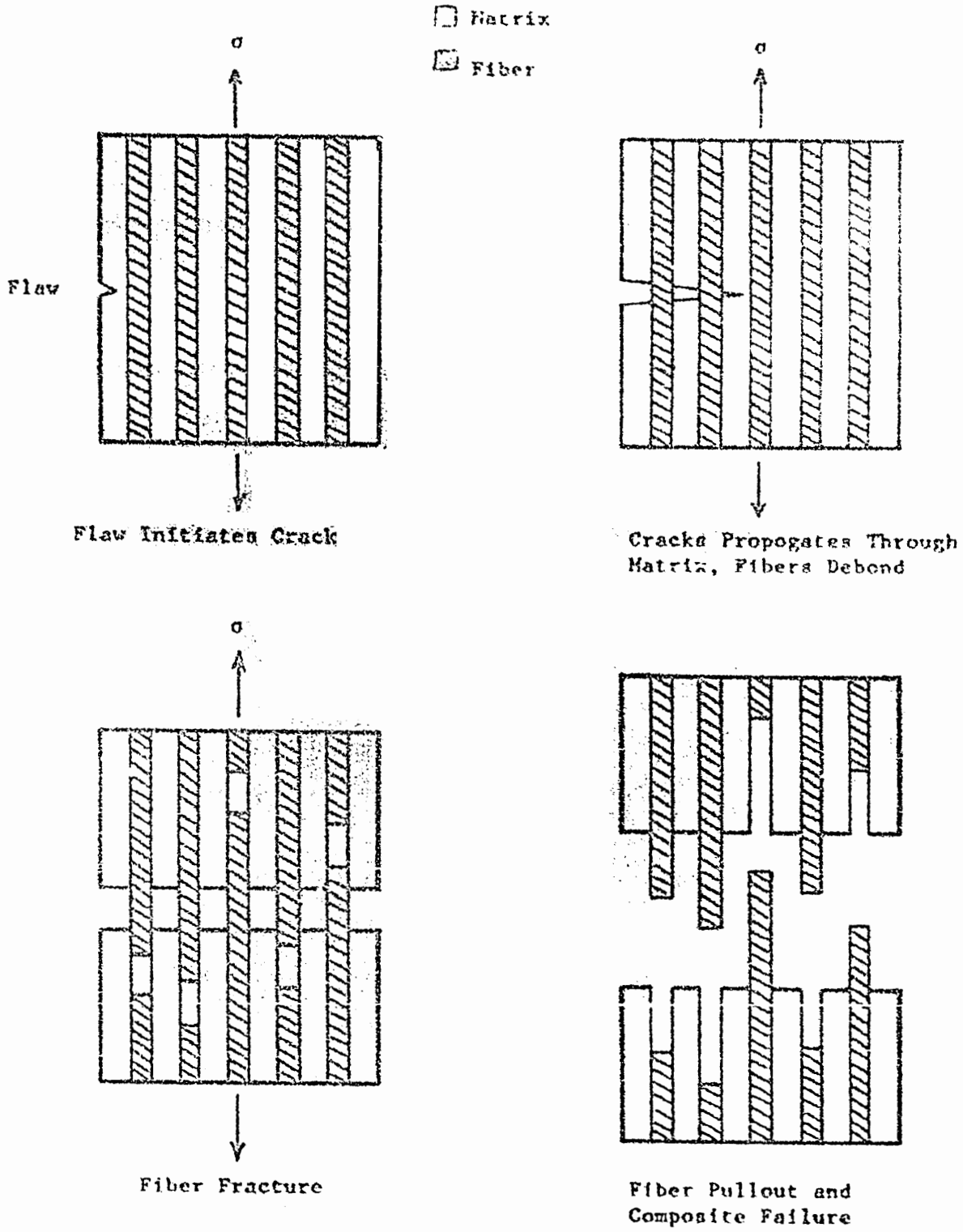

Fig. 7. Schematic representation of weak fiber/matrix interface resulting in fiber debonding and pullout.

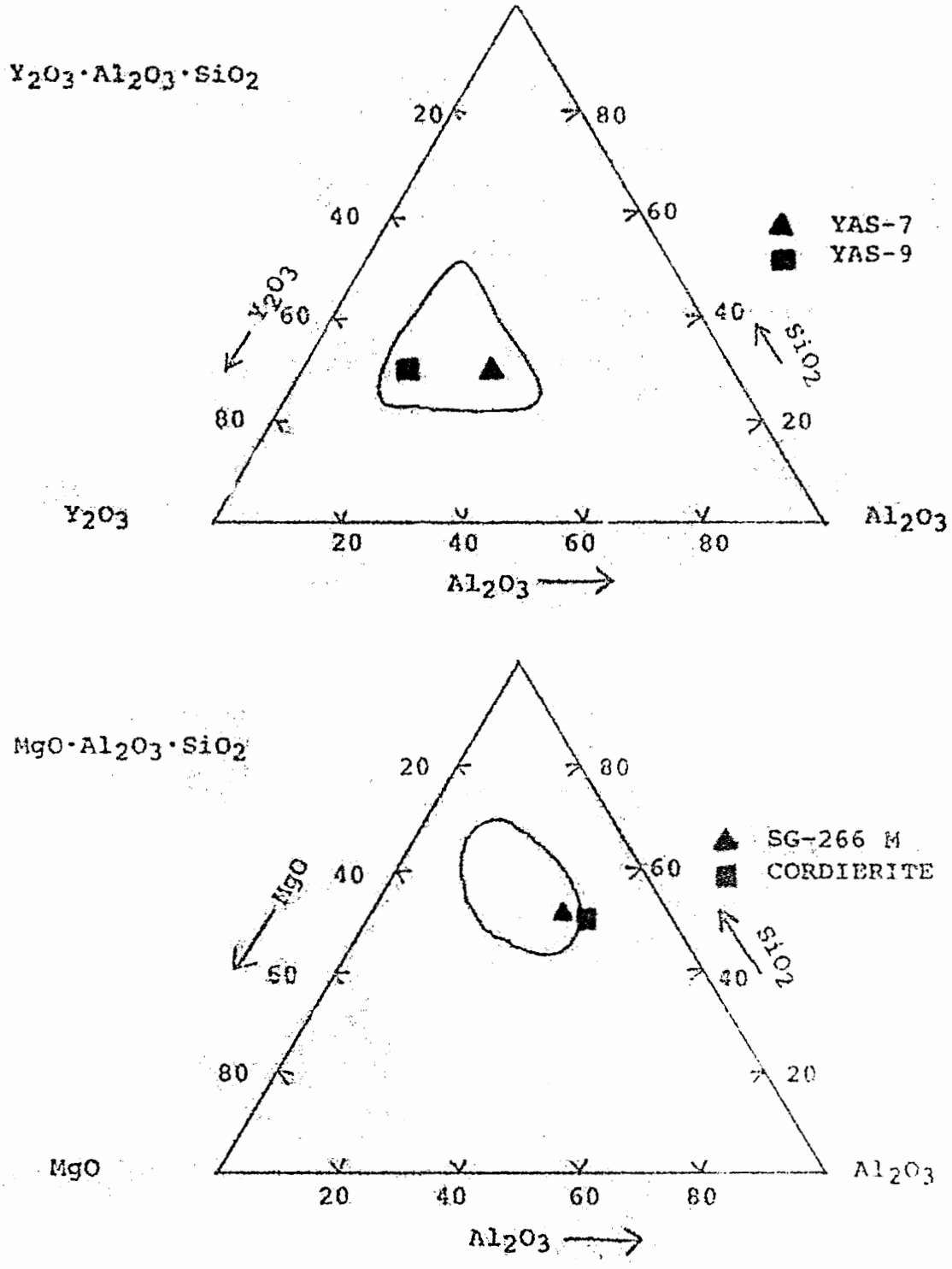

Fig. 8. Glass formation regions in the YAS (Ref. 21) and the MAS (Ref. 22) systems.

2. Glass-Ceramic Formation. Glass-ceramics are defined as "polycrystalline solids prepared by the controlled crystallization of glasses."[22] This crystallization is usually accomplished through heat-treatment resulting in the nucleation and growth of a fine grained network of crystals. Nucleation and crystal growth are the two steps essential to the crystallization of the glasses.[22,23]

a. Homogeneous and Heterogeneous Nucleation. There are two types of nucleation: homogeneous and heterogeneous. In homogeneous nucleation, the nucleation sites are of the same composition as the crystals which grow upon them. In heterogeneous nucleation the crystals are not the same composition as the nucleation sites. Heterogeneous nucleation is by far the more common of the two types.

b. Differential Thermal Analysis. Melting, or the transformation from a solid to a liquid, requires energy and will appear as an endothermic peak using Differential Thermal Analysis (DTA). The reduction in free energy associated with the crystallization of a glass results in the evolution of heat which can be detected as an exothermic peak using DTA. DTA can be used to determine the annealing point of a glass, the optimum nucleation and crystallization temperatures, the effect of nucleation agents on the crystallization behavior, the crystallization activation energy, and the sensitivity of glass to surface crystallization effects experienced with powdered glass samples.[22,24]

For crystalline materials, DTA is useful in determining the temperature at which a polymorphic phase transformation occurs. If the polymorphic transformation requires heat, an endothermic reaction occurs; if heat is produced, an exothermic reaction occurs. If the polymorphs have different specific heats and little heat is absorbed

or evolved during the polymorphic transformation, a discontinuity occurs in the DTA curve.[24]

The problem of thermal lag between the specimen and the furnace can be minimized and the sensitivity maximized through the use of small specimens. Small specimens allow faster response time and, therefore, yield better defined DTA peaks than do larger specimens which require greater reaction time. The standard practice for describing the temperature at which a reaction occurs is to determine the onset of the peak, not the temperature at which the peak reaches its maximum value.[24]

c. Effect of Fiber Additions. The introduction of fibers into a glass during the fabrication of composites has an effect on the crystallization of the glass matrix.[14,25,26] The fibers apparently provide a substrate upon which crystallization can begin. TEM analysis at the interface of a Nicalon fiber imbedded in an LAS matrix showed nucleation of β-spodumene.[26]

d. Effect of Hot-Pressing Temperature. The crystallization of the glass-ceramic matrix can be affected by the hot-pressing temperature. Hot-pressing at 1300°C results in well defined surface X-ray diffraction (XRD) patterns for cordierite.[27] Ba-cordierite matrix composites densify as low as 950°C and remain amorphous up to 1200°C.

3. Effects of Crystallization.

a. Mechanical Behavior. The crystallization of a glass to a glass-ceramic increases its strength and toughness. As a glass, the material is usually single phase and homogeneous. After the glass has crystallized, however, it has a polycrystalline structure which

possesses some fracture toughness through crack deflection along grain boundaries.[4]

b. Density. The density change associated with crystallization depends upon the composition of the crystal species.[22] In the case of cordierite, the density increases with the beginning of crystal growth, then decreases as crystallization continues and is completed.[28]

c. Thermal Expansion. If a glass-ceramic is completely crystalline it should possess a thermal expansion curve identical to a crystalline solid. If there is much residual glass phase, the material may show a curve similar to that of the glass. As a sample crystallizes, the C.T.E., like density, is dependent upon the crystalline phases evolved.[22] C.T.E. follows the ROM which allows the extent of crystallization to be calculated, provided C.T.E. is coupled with another analytical technique, such as XRD, which can identify and quantify the crystalline phases present.

d. High Temperature Behavior. In most cases the glass-ceramic will be dimensionally stable at temperatures higher than the original glass.[22] As noted earlier, glasses soften over a temperature range and, therefore, begin to deform long before the glass reaches a viscosity of $10^{7.6}$ poise (defined as the softening point). In certain cases, however, glass-ceramics begin to deform or creep at a lower temperature than their glass counterparts. This can occur when the ceraming process does not completely crystallize the glass and the remaining glass has a lower softening point and therefore a different composition than the original glass. Creep in the glass-ceramic can then occur: the glass phase will segregate to the grain boundaries of

the glass-ceramic system providing a lubricant for grain boundary sliding.[5]

4. Crystallization in Cordierite and YAS Glasses

a. Crystallization of Cordierite. The crystallization behavior, polymorphism and effectiveness of nucleating agents, in the cordierite system have been extensively studied using DTA.[28-33] The crystallization of cordierite occurs through heterogeneous nucleation.[28-31] Using powder XRD techniques, a decrease in the 'd' spacings was observed, suggesting that solid solution of the silicon and aluminum ions in the cordierite structure occurs when heat treated at temperatures above 1200°C. In this system, surface crystallization occurs readily so the DTA results are very sensitive to particle size.[31,32] Increasing the particle size decreases the crystallization temperature. Two exotherms have been observed. The first, at 954°C, corresponds to the crystallization of μ-cordierite; the second, at 999°C, to the crystallization of α-cordierite. The addition of TiO_2 promotes phase separation and enhances crystallization.[28] When ZrO_2 is added, the nucleation and crystallization peaks shift to higher temperature, whereas, CeO_2 inhibits crystallization.[29] Sol-gel derived cordierite, doped with 2.0% ZrO_2, shows exothermic peaks at 1000°C and 1200°C. If the powder was heated at 900°C, μ-cordierite was formed.[33] The optimum temperature for nucleation is 830°C.

b. Crystallization of Yttrium Aluminosilicates. Little work has been done on the formation and the crystallization of glasses in the $Y_2O_3 \cdot Al_2O_3 \cdot SiO_2$ (YAS) system.[34-36] Figure 9 shows the phase diagram for the yttrium aluminosilicate system.[37] Crystallization of YAS compositions with CaO additions (up to 55 mole %)[38] and ZnO additions (up to 45 mole %)[39] have been studied.

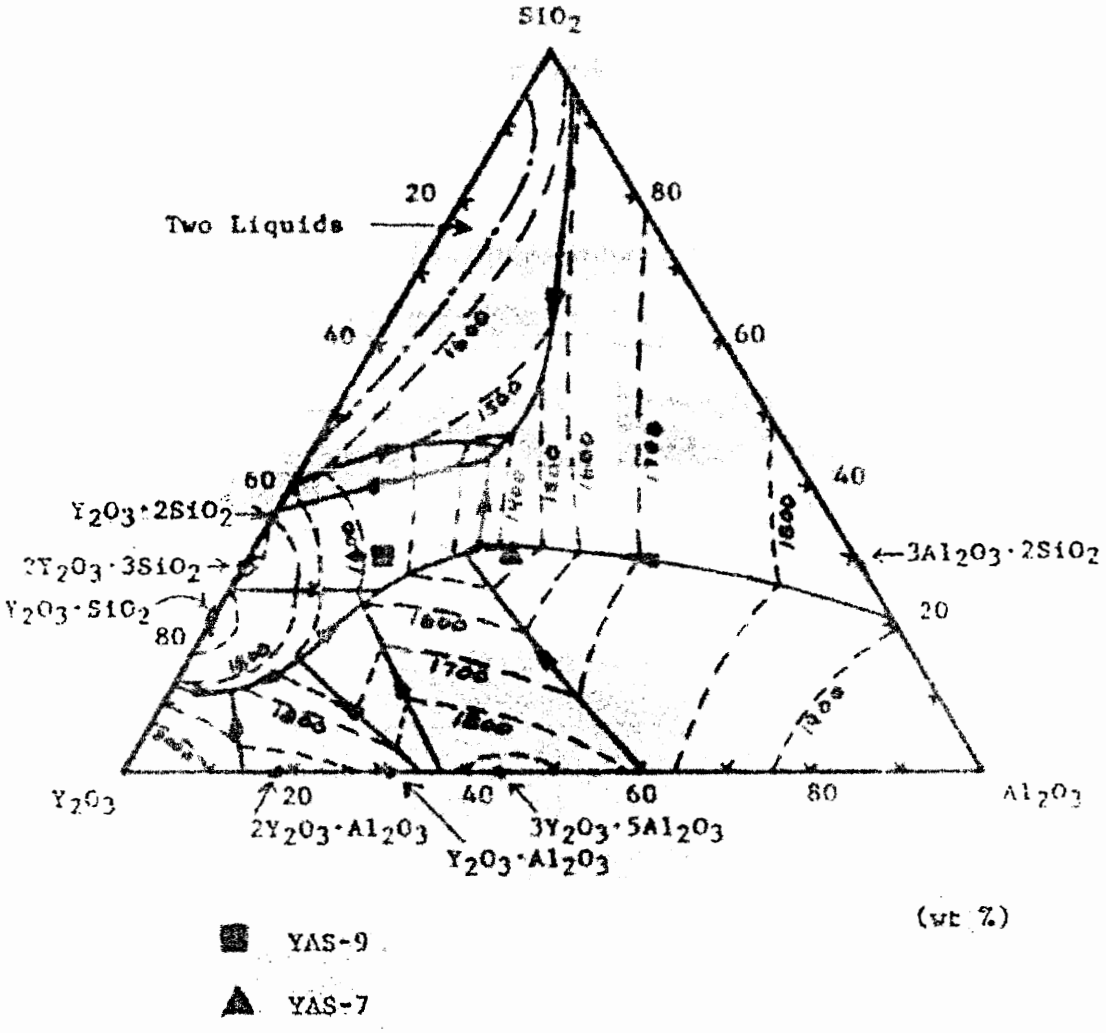

Fig. 9. Yttrium aluminosilicate phase diagram (Ref. 37).

Of particular interest in the YAS system are compositions which would produce polymorphic yttrium diorthosilicate ($Y_2Si_2O_7$). $Y_2Si_2O_7$ naturally occurs as yttrialite,[40] a metamict mineral which devitrifies at 1000°C to form y-$Y_2Si_2O_7$.[41,42] Several studies using synthesized yttrialite[41-45] have been conducted to determine the transformation temperatures and the crystallographic structures (Table I).

C. COMMERCIALLY AVAILABLE CERAMIC FIBERS

Table II lists the commercially available fibers together with their properties.

1. Nicalon Fiber. Nicalon fiber is produced by the pyrolysis of a poly-carbosilane and is, for all practical purposes, infinitely long. Characterization of this fiber has shown its composition to vary both throughout its cross section and from fiber to fiber.[27,46,47] In addition to these variants, elemental species such as Mg and Al can diffuse into the fiber from certain matrices and accelerate a chemical interaction between the fiber and matrix, in turn creating a very strong interface which usually results in a brittle composite.

Because of chemical interaction, the promotion of a weak interface has been of particular interest in the development of Nicalon composites. The easiest method of producing a weak interface is through heat treatment of the fiber at 1300°C or above. This heat treatment results in the formation of a carbon layer due to diffusion of free carbon from the interior of the fiber to the fiber surface. Unfortunately, however, this migration of carbon also results in a degradation of the fiber and its mechanical properties. The strength

TABLE I

POLYMORPHS OF YTTRIUM DIORTHOSILICATE (REF. 41)

Polymorph Designation	Structure (Space Group)	Unit Cell (A)	Angle	Transformation Temperature (°C)
α	Triclinic (PT)	a = 6.592 b = 6.642 c = 12.255 V = 133.6 (A³)	α = 94.03° β = 89.23° γ = 93.13°	
				1225°C
β	Monoclinic (C2/M)	a = 6.875 b = 8.970 c = 4.721 V = 142.5 (A³)	β = 101.74°	
				1445°C
γ	Monoclinic ($P2_1/n$)	a = 5.579 b = 10.857 c = 4.696 V = 142.2 (A³)	β = 95.99°	
				1535°C
δ	Orthorhombic ($Pna2_1$)	a = 13.661 b = 5.020 c = 8.152 V = 139.8 (A³)		

TABLE II

COMMERCIALLY AVAILABLE CERAMIC FIBERS

Name	AS-4	HM-S	Nicalon	SCS-6
Composition (weight %)	94% C	C	30.0 C 11.8 O 54.3 Si	* C SiC
Diameter (μm)	8	8	10-20	141
Cross Section	round	round	round	round*
Filaments / Tow	12,000	NL	500	1
Density (g/cm^3)	1.80	1.91	2.56	3.3
C.T.E. (10^{-6}/°C) Range (°C)	-2.2 NL	0 150-600	3.1 NL	4.4 NL
Elastic Modulus (GPa)	235	345-414	180-200	430
Ultimate Tensile Strength (GPa)	3.6	1.7-2.4	2.5-3.2	4.1
Ultimate Strain to Failure (%)	1.53	NL	1.5	NL
Manufacturer	Hercules	Hercules	Dow Corning	AVCO
Reference	M	48	M	3

*see Figure 10.

NL = Not Listed
M = Manufacturer's Information

TABLE II (CONT.)

COMMERCIALLY AVAILABLE CERAMIC FIBERS

Name	Nextel 440	Nextel 480	Fiber FP	Tyranno
Composition (weight %)	2 B_2O_3 70 Al_2O_3 28 SiO_2	2 B_2O_3 70 Al_2O_3 28 SiO_2	>99 Al_2O_3	25-33 C .1-.2 N 15-20 O 45-53 Ti 0.5-5 Si
Diameter (um)	10-12	10-12	20	8-10
Cross Section	oval	oval	round	round
Filaments / Tow	1,000	1,000	200	800
Density (g/cm3)	3.10	3.05	3.95	2.3-2.5
C.T.E. (10^{-6}/°C) Range (°C)	4.38 25-1000	4.99 25-1000	5.7 NL	3.1 0-500
Elastic Modulus (GPa)	200-240	220	380	190
Ultimate Tensile Strength (GPa)	1.4-2.1	1.9	1.4	2.8
Ultimate Strain to Failure (%)	NL	NL	NL	1.4-1.7
Manufacturer	3M	3M	DuPont	Sumitomo
Reference	50	50	M	49

NL = Not Listed
M = Manufacturer's Information

of Nicalon fiber is considerably decreased after exposure to temperatures >1000°C in an oxidizing atmosphere.

2. Nextel 440 and 480 Fiber. Nextel fiber has a mullitic composition and is also formed by a polymer precursor method. Nextel fiber is oval in cross section and, because it is an oxide, is relatively stable in an oxidizing atmosphere. The addition of an oxide fiber into an oxide matrix will always result in chemical interaction. Nextel 440 and 480 fibers have a temperature limit of approximately 1000°C. They begin to recrystallize above this temperature and lose strength.[50] Little work has been done with Nextel in glass and glass-ceramic matrices due to the chemical reaction problem. Some work has been done by the manufacturer with fiber coatings to reduce fiber/matrix interactions.

3. SCS-6 (Silicon Carbide Filament). SCS-6 fiber is produced by the chemical vapor deposition (CVD) of stoichiometric SiC on a carbon fiber substrate; the result is a large diameter (140μm) fiber composed mainly of β-SiC crystallites. A SEM photomicrograph of a typical SCS-6 fiber cross section is shown in Figure 10. Previously, this fiber has been used principally in metal matrix composites. Smaller diameter fibers, such as Nicalon, when incorporated into various glass matrices, have produced composites with better mechanical properties than those obtained using SCS-6 filaments.[51] For an equal volume of SCS-6 fiber and Nicalon fiber, the higher surface area of the Nicalon fibers would provide a greater fiber/matrix interfacial area, stronger bonding and hence greater composite strength. SCS-6 is generally more stable in air due to the purity of the SiC layers and their oxidation resistance.[3] At temperatures greater than 1000°C, the crystallites of SiC begin to grow resulting in a considerable decrease in strength.

Fig. 10. SEM photomicrograph of the fractured cross section of a silicon carbide CVD fiber, SCS-6, showing carbon filament substrate and silicon carbide layers.

D. FABRICATION AND PROCESSING OF CERAMIC COMPOSITES

1. Discontinuous Fiber. The major objective realized in the production of discontinuous fiber composites is the effective mixing of the matrix and fibers to achieve a uniform distribution of fibers in the matrix. The aspect ratio of a fiber, defined as the length divided by the diameter, can have a considerable effect on the mixability of the matrix and fibers. The smaller the aspect ratio, the better the matrix and fibers mix. Larger aspect ratios result in clumps of fibers oriented directionally, producing property anisotropy; an aspect ratio greater than 20 may result in large voids and breakage upon orientation of the fiber during mixing and hot pressing.[52] However, 8 μm diameter carbon fibers 3 millimeters long (aspect ratio = 375) were easily mixed with matrix powders while fibers 10 millimeters long (aspect ratio = 1250) would clump together into discrete bundles.[53] If the fibers and matrix are not intimately and uniformly mixed the mechanical properties may be severely affected. The best composite properties are obtained with unidirectional, continuous fibers employing a high fiber volume fraction. Optimal strength properties are observed when testing composites parallel to the fiber direction.

2. Continuous Fiber. The most widely accepted method for producing ceramic matrix composites involves using slurries of the matrix powder and continuous fiber tows. The use of a continuous filament winder and a glass slurry has the advantages of speed, uniformity and ease of fabrication compared to the production of composite pre-pregs using hand lay-up techniques.[14] The winder produces unidirectional laminas which can be oriented to give

composite specimens with any degree of fiber orientation. In the manufacturing process, a sizing is applied to the fiber tow to reduce fiber damage during handling. Prior to prepreg fabrication, however, this sizing must be removed so that the individual fibers in the fiber tow can separate and intimately mix with the matrix. In particular, the sizing on Nicalon fiber is a vinyl acetate which is not soluble and therefore must be burned off.[26]

3. Densification Using Hot Pressing. With the exception of sol-gel derived ceramic matrices, all glass and glass-ceramic matrix composites are densified through the simultaneous application of heat and pressure in a process known as hot pressing. In hot pressing, the material is densified in a graphite die which has been protected with a lining of graphite foil,[25,33] molybdenum foil,[48] or a boron nitride wash.[54,55] The literature[14,25,33,48,53-61] describes many variations in the hot press atmosphere. The specimens are pressed either in a vacuum or in a non-reactive atmosphere such as argon or nitrogen. Table III contains the hot pressing parameters used for the densification of various glass and glass-ceramic matrix composites.

The temperature at which the specimen densifies differs with the matrix material and, in some cases, with the fiber volume fraction.[14,53] The optimum temperature for the hot pressing of glass matrix composites occurs when the glass viscosity reaches $\approx 10^6$ poise.[61] This is just above the softening point of the glass which is defined as $10^{7.6}$ poise. Excessively high hot pressing temperatures, i.e. above 1300°C in the case of Nicalon, result in substantial fiber degradation and are generally avoided.[25,33]

The hot pressing pressures used do not appear to follow any trend ranging from 3.5 MPa (500 psi) for Pyrex[53] to 35 MPa (5000 psi) for

TABLE III

HOT PRESSING PARAMETERS FROM PREVIOUS WORK

Fiber	Matrix	Temperature	Pressure	Atmosphere	Time	Reference
HM Carbon	Pyrex (7740)	700-1000°C	6.9MPa	V/Ar	NL	53
HM Carbon	LAS	1230°C	10.4	V/Ar	NL	53
HM-S	L·A·8S	1375°C	6.9	N2	5 min	48
Nicalon	Pyrex (7740)	1200°C	14	V	60 min	51,56
Nicalon	Vycor (7930)	1600°C	>6.9	V	NL	56
Nicalon	SiO2	1520°C	35	V	30 min	54
Nicalon + Coating	SiO2	1350°C	35	V	20 min	54
Nicalon	LAS (9608) + ZrO_2	>1300°C	>6.9	V	NL	57
Nicalon	LAS + ZrO_2 + Nb_2O_5	1450°C	7.0	V	15 min	54
Nicalon	LAS I, II, III	1000-1350°C	6.9	NL	15-30 min	58
Nicalon	LAS	1250-1300°C	7	V	15 min	59
Nicalon	MAS I	1260-1270°C	13.8	V	15 min	25
Nicalon	MAS II	1255-1260°C	13.8	V	15 min	25
Nicalon	Cordierite	1370°C	35	V	1 min	54
Nicalon	Cordierite	~1325°C	12.1	V	NL	59
SCS-6	Pyrex (7740)	1150°C	6.9	Ar	20 min	51
Fiber FP	SiO_2 + 2% B_2O_3	1400°C	34.5	NO	30 min	55
Fiber FP	Pyrex (7740)	*	2-13.8	NL	2 min	61
Fiber FP	Vycor (7900)	*	2-13.8	NL	2 min	61

*Hot Pressing Temperature is the temperature where the glass has a viscosity of 10^6 poise.

cordierite.[14] In general, the densification pressure is 6.9 MPa (1000 psi) and is applied at the temperature corresponding to the softening point of the matrix as described above. The time required for densification is approximately two minutes[61] but densification times up to 60 minutes have been reported.[25]

E. GLASS AND GLASS-CERAMIC MATRIX COMPOSITES

1. Carbon Fiber Reinforced Glasses and Glass-Ceramics. Carbon fiber has been used extensively for the reinforcement of polymer and epoxy matrix composites because of its high strength and modulus. The first use of carbon fiber to reinforce glasses resulted in significant increases in both strength and toughness.[48,62] Due to the negative axial expansion of the carbon fibers, it is possible to produce a composite with an extremely small C.T.E. If, as discussed earlier, the matrix C.T.E. is sufficiently high and produces a large C.T.E. mismatch between the fiber and the matrix, the composite will be weakened. Carbon is also not chemically reactive in most glass and glass-ceramic matrices so the fiber/matrix interface will be weak resulting in toughening by fiber pullout mechanisms. Unfortunately, however, carbon fiber has an upper usage temperature of 450°C due to rapid chemical and physical degradation of the fiber from oxidation,[5,63] therefore, this low usage temperature essentially eliminates carbon fiber from consideration as a reinforcement for high temperature composites.

a. Discontinuous Carbon Fiber Composites. Ideally, discontinuous carbon fiber additions should increase the strength and toughness of a matrix isotropically. This is not usually the case, however, due to

preferred orientation resulting from the hot pressing of the composite.[15,52,64] The strength and toughness may not be improved because only a small percentage of fibers are actually parallel to the tensile axis.

The ultimate strength of the composite can be calculated following the ROM if the length of the discontinuous fiber is greater than the critical length and if the discontinuous fibers are aligned parallel to the tensile axis. If the length of the fiber is less than a critical length, the average fiber strength must be substituted for the ultimate fiber strength. Discontinuous fibers which are misaligned will produce stress concentration effects similar to Griffith flaws, thereby reducing the strength of the composite;[5] as expected, aligned fibers produce better results. In addition, poor mixing of the discontinuous fibers can produce fiber agglomerations which can result in defects and lower strengths.[15] For example, the strength reduction, from 100 MPa to 40 MPa, observed in a Pyrex matrix composite containing 30 volume percent discontinuous fiber, was due to poor mixing.[53]

b. Continuous Carbon Fiber Composites. Continuous unidirectionally aligned carbon fiber composites exhibit excellent strength and toughness compared to the unreinforced matrix. The C.T.E. mismatch problem is more pronounced in unidirectional laminas and can result in microcracking perpendicular to the fiber direction. The calculated stress due to the C.T.E. mismatch for Pyrex and LAS reinforced with 50 volume percent carbon fiber was less than the strength of the matrix; therefore, no microcracking was observed.[65] In one study the LAS matrix composite was already a glass-ceramic when the carbon fiber which was added[48] seems to nullify the advantages of

using glass-ceramic matrices. The composite pre-preg was hot pressed at 1375°C, a temperature which was high enough for liquid formation and subsequent densification of the LAS matrix. In addition, the crystalline phases in the glass-ceramic were different after hot-pressing suggesting that the fibers affected the crystallization.[46]

2. Ceramic Fiber Reinforced Glasses and Glass-Ceramics. Ceramic fibers have properties similar to carbon fibers in terms of elastic modulus and ultimate tensile strength. The density and the C.T.E. of ceramic fibers are usually greater than carbon fibers (see Table II). Problems which are often encountered using carbon fibers such as C.T.E. mismatch between the fiber and the matrix and poor oxidation stability are reduced with the use of ceramic fibers. The increased chemical compatibility between ceramic fibers and a ceramic matrix results in a strong fiber/matrix interface and brittle composite failure. This problem of fiber/matrix chemical interaction has been greatly reduced, however, through the use of fiber coatings and careful processing to yield fiber pullout and significantly toughened glass and glass-ceramic composites.

a. Continuous Ceramic Fiber Composites. The incorporation of ceramic fibers into various glass and glass ceramic matrices has resulted in some useful composite systems. These matrices include Pyrex,[51,53,56,61,65] Vycor,[54-56,61] a barium sialon,[56] and various compositions in the magnesium aluminosilicate (MAS) system[25,54,59] and the lithium aluminosilicate (LAS) system.[48,53,54,57,58,65] Table IV contains a summary of the reported data for ceramic fiber reinforced glass and glass-ceramic matrix composites. Only Nicalon fiber reinforced Pyrex and LAS have been studied in detail.

TABLE IV

EXISTING GLASS AND GLASS-CERAMIC MATRIX COMPOSITE SYSTEMS

Matrix	Fiber	Volume Fraction	Fracture Behavior	Reference
Discontinuous, Random Orientation				
Pyrex	HM Carbon	0.1-0.4	Tough	53
LAS	HM Carbon	0.2	Tough	53
Discontinuous, Aligned Orientation				
Pyrex	HM Carbon	0.1-0.3	Tough	53
Pyrex	Celion Graphite	0.3-0.35	Tough	64
Continuous, Unidirectional Orientation				
Pyrex	HM Carbon	0.4	Tough	65
Pyrex	Nicalon	0.35-0.50	Tough	51,56
Pyrex	SCS-6	0.35,0.65	Tough	51
Pyrex	Nicalon	0.35	Tough	56
				56
LAS	HM Carbon	0.36	Tough	65
LAS	Nicalon	0.50	Tough	54,57
L-A-BS	HM-S	0.36	Tough	48
Compglas	(Nicalon)	NL	Tough	8,54
Cordierite	Nicalon	0.30	Brittle	54
Ba-Cord.	Nicalon	0.40	Tough	27
Ba-MAS	Nicalon	0.40	Tough	27
Ba-SiAlON	Nicalon	0.50	Tough	66

The limited temperature stability of the Nicalon fiber can be exploited to produce a toughened composite. Nicalon does not exhibit a uniform chemical composition throughout the fiber.[47] If the fiber is treated in air, a SiO_2 layer will form on the fiber; when heated under non-oxidizing conditions, a carbon rich layer is formed. Composite specimens are usually densified in a hot press using a non oxidizing atmosphere. If the hot pressing temperature is high enough, the carbon rich layer will form and act as a barrier to reduce fiber/matrix interaction.[51,56,57] This situation would be ideal except that the development of the carbon layer occurs through degradation of the fiber, which reduces its strength.[47]

Unfortunately, the research literature is incomplete regarding many of the investigated composite systems. Important information omitted includes fiber fractions,[67] hot pressing parameters,[55,57,66] mechanical testing parameters,[25,33] and even mechanical testing results.[10] The omission of this information makes it exceedingly difficult to compare the various composite systems.

b. Coated Ceramic Fiber Composites. Coated ceramic fibers are used to reduce the fiber/matrix interaction and to provide an oxidation barrier for elevated temperature use. Two coatings which will fulfill this requirement are carbon and boron nitride.[67,68] Unfortunately, carbon and boron nitride coatings are not thermodynamically stable at elevated temperatures in an oxidizing atmosphere so they would not provide acceptable fiber coatings for use in high temperature composites.[5,63,69] If the coating does not react with the matrix or fiber, a weak fiber/matrix interface will result, allowing toughening of the ceramic through fiber pullout.

Increases in both strength and toughness have been obtained through the use of coated fibers.[70] Unfortunately, the coating material was not disclosed due to the possibility of patentability making the results inaccessible for comparisons. Coatings are also sometimes formed in situ as in niobium pentoxide (Nb_2O_5) doped LAS glass ceramics containing Nicalon fibers. The niobium will form a NbC layer at the fiber/matrix interface efficiently reducing interaction after reacting with carbon from the Nicalon fiber. The NbC will precipitate at the interface in the form of small crystallites which are detectable using transmission electron microscopy (TEM).[58,59] The NbC layer provides a slippage system, allowing toughening of the composite through fiber pullout.[54] This is significant because this type of reaction and barrier formation has not been observed in other ceramic fiber reinforced matrix composite systems.

F. MECHANICAL TESTING OF CERAMIC COMPOSITES

As the development of ceramic fiber reinforced ceramic matrix composites continues, it is becoming increasingly important to develop standard testing techniques to determine the mechanical properties of strength and toughness. Although one testing procedure for monolithic ceramics, i.e. flexure testing, is commonly used to measure strength of ceramic composites; ideally, this procedure should not be used without modifications to test ceramic composites because composites do not behave isotropically and do not exhibit linear elastic behavior.[2,4,8,71,72] Similarly, testing procedures for polymer matrix composites are not applicable because ceramic matrices are not

ductile, and some degree of matrix ductility is assumed in the testing of polymer matrix composites.[73]

1. Sample Preparation. Because ceramic materials exhibit a dependence of strength on surface flaws, it is important to eliminate surface flaws whenever possible. Testing in the as-formed condition without any subsequent machining or polishing is acceptable in some cases. If a specimen is polished, the scratches produced by polishing must be less than the critical flaw size, otherwise, the testing results may not reflect the actual strength of the material. The critical flaw size varies depending on the ceramic material under investigation.[8] Diamond abrasives are usually used for polishing because they are more effective and result in less damage to the specimen such as fiber plucking from the polished surface.

2. Testing Techniques.

a. Flexure Testing. Flexure testing methods, commonly known as 3 or 4-point bending tests, are used to determine the modulus of rupture (MOR) and may be applicable to short, discontinuous, randomly oriented fiber composites provided they exhibit isotropic behavior.[52] MOR tests are designed so that the outer fiber tensile stress developed on the tensile side of the testing specimen can be calculated. This type of testing is applicable for monolithic ceramics because monolithic ceramics generally fail in tension rather than compression. As a ceramic composite specimen is loaded, however, matrix microcracking begins on the tensile side of the specimen, effectively reducing the elastic modulus, causing an increase in the compressive stress on the compression side. This microcracking, and the accompanying elastic modulus change, cause further deviation from the linear elastic behavior predicted by linear elastic theories used to develop the

equations for the calculation of the outer fiber tensile stress (MOR) of the specimen at failure.

The MOR test is applicable to unidirectional fiber reinforced ceramic composites with some modifications. Studies show that the ultimate shear strength of unidirectional fiber reinforced ceramic composites is 10 to 100 times lower than the ultimate tensile strength, resulting in shear/compression failure in bending rather than tensile failure.[8,71] This type of failure is observed experimentally.[25,74,75] In order to eliminate shear/compression failure, the minimum span to depth (S/d) ratio can be calculated for a given composite system. For example, the minimum S/d ratio for a Nicalon fiber reinforced LAS II matrix composite was 15-17 and 30-34 for 3-point and 4-point flexure, respectively.[8] In much of the research literature regarding testing performed on ceramic composites, the minimum S/d ratio for the system being investigated is not calculated. Table V contains S/d ratios and the resulting mechanical data for various systems.

The advantage of flexure testing is that it is easily adapted to high temperature testing of ceramic composites.[74] Loading jigs can be fabricated from refractory materials such as SiC or Al_2O_3. This technique is also conducive to continuous load/deflection measurements using optical methods.[76]

b. Tensile Testing. Tensile testing of any ceramic material presents problems with perfectly aligning and gripping the specimen. The low shear strength exhibited by ceramics can produce shear failure originating at the specimen grips. Imperfect alignment can result in torsion and shear stress development in the specimen yielding unreliable results.

TABLE V

MECHANICAL PROPERTY DATA FOR GLASS AND GLASS-CERAMIC MATRIX COMPOSITE SYSTEMS

Matrix	Fiber	V_f	Test*	S/d ratio	Strength MPa	Ref.
Discontinuous, Random Orientation						
Pyrex	HM Carbon	0.10	F-3	NL	60	53
Pyrex	HM Carbon	0.30	F-3	NL	40	53
LAS	HM Carbon	0.20	F-3	NL	60	53
Discontinuous, Aligned Orientation						
Pyrex	HM Carbon	0.10	F-3	NL	90	53
Pyrex	HM Carbon	0.30	F-3	NL	140	53
Pyrex	Celion Gra.	0.35	F-3	5.5	35	64
Pyrex	Celion Gra.	0.35	F-4	32	320	64
Pyrex	Celion Gra.	0.35	T	NA	150	64
Continuous, Unidirectional Orientation						
Pyrex	HM Carbon	0.40	F-3	30	680	65
Pyrex	Nicalon	0.35	F-3	20	470	56
Pyrex	Nicalon	0.40	F-3	NL	290	51
Pyrex	Nicalon	0.50	F-3	20	800	56
Pyrex	SCS-6	0.35	F-3	NL	650	51
Pyrex	SCS-6	0.65	F-3	NL	830	51
Vycor	Nicalon	0.35	F-3	20	440	56
LAS	HM Carbon	0.36	F-3	30	680	65
LAS	Nicalon	0.50	F-3	25	620	57
L-A-BS	HM-S	0.36	F-3	30	880	48
Compglas†	(Nicalon)	NL	F-3	10	860	54
Compglas	(Nicalon)	NL	F-3	15	144	8
Compglas	(Nicalon)	NL	T	NA	84	8
Cordierite	Nicalon	0.30	F-3	10	110	54
Ba-Cord.	Nicalon	0.40	F-4	16	375	27
Ba-MAS	Nicalon	0.40	F-4	16	550	27
Ba-SiAlON	Nicalon	0.50	F	NL	250	66

*F = Flexure Testing; 3 and 4 = 3- and 4-point bending respectively, where designated; and T = Tensile Testing.
†Compglas is a registered trademark of UTRC.
"NL" and "NA" = not listed and not applicable respectively.

The best specimen design for tensile testing of ceramic composites is the three-pin configuration illustrated in Figure 11. The three-pin configuration minimizes the gripping problem effectively but is expensive and still requires perfect alignment. Additional problems which arise from machining the 'dog-bone' shape, such as fiber damage, surface flaws, and microcracking of the matrix, can result in strength degradation.[8,71]

The gripless tensile specimen (Figure 12) may provide an answer to some tensile testing problems; however, the machining of the specimens is a problem. The actual testing is performed using four-point flexure apparatus and results in a uniform tensile stress in the lower part of the beam.[8] This makes the gripless tensile testing specimen ideal for high temperature testing if the oxygen embrittlement problem resulting from specimen machining could be overcome.[74,77]

Elevated temperature tensile testing is difficult because of gripping problems. In the case of polymer matrix composites, the specimen is bonded with an epoxy which would not be usable as a bonding material for high temperature testing specimens because of its limited temperature stability.[73,77]

c. Toughness Testing. Test specimens for toughness are generally single-edge notched beams (SENB), circumferentially notched beams, or chevron notched beams where the notches are produced with a thin (0.05") diamond saw or with a wire saw and a cutting slurry. Flaws are also introduced with shaped diamond indentors such as Vickers or Knoop indentors. This notching, or indenting, of test specimens introduces a flaw of critical size which can be propagated through the material in a controlled manner as illustrated in Figure 1. The area

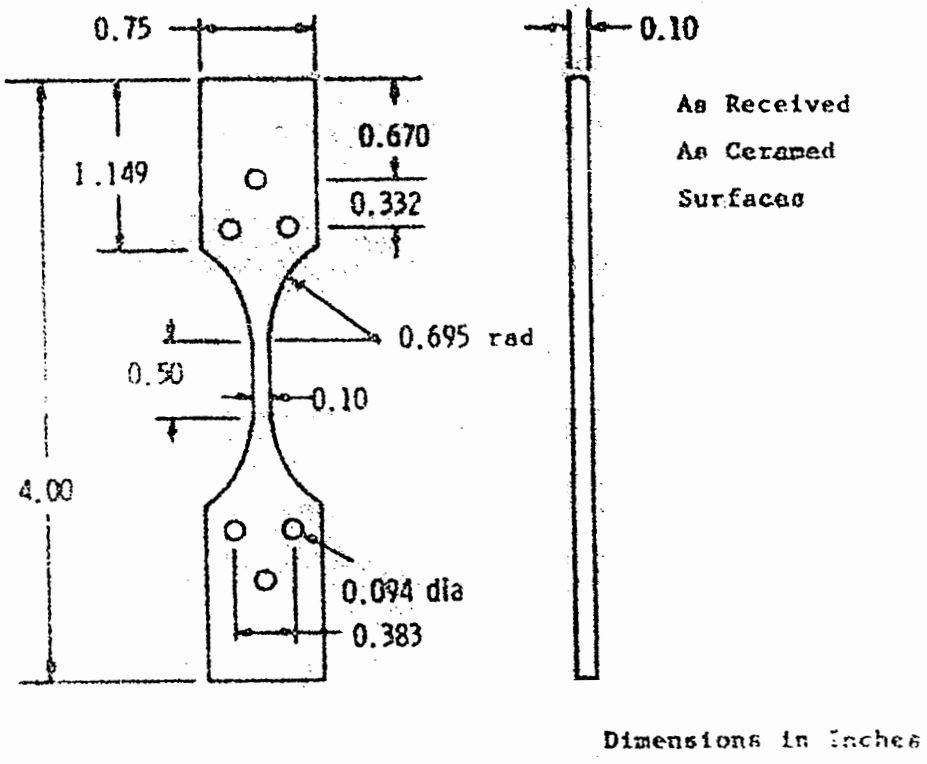

Fig. 11. Schematic representation of a 3-pin tensile testing configuration for tensile testing continuous fiber reinforced ceramic matrix composite specimens (Ref. 8).

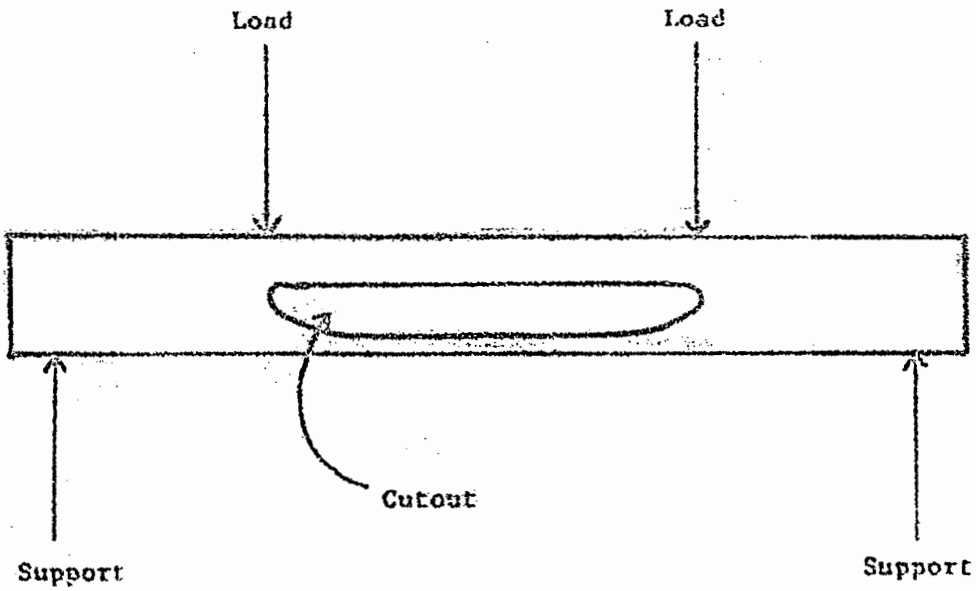

Fig. 12. Schematic representation of a gripless tensile testing configuration for testing continuous fiber reinforced ceramic matrix composite specimens in 4-point flexure (Ref. 8).

under the load/deflection curve can be used to determine the work required to produce new surface and hence to measure the toughness of the material.

Flexure testing of notched beams is the most common method of toughness testing. Researchers disagree on the effect of notch depth on the toughness of the composite.[4,60,71] The rate of loading does not appear to have any effect on measured values.[60]

d. Fiber/Matrix Interfacial Bonding. The degree of interfacial bonding between the matrix and a reinforcing fiber is the determining factor for toughening in ceramic composites. The measurement of the bond strength can be obtained by pushing out individual fibers with a diamond indentor. From the applied load, the diameter of the fiber, and the distance the fiber moves, it is possible to approximate the bond strength. The elastic modulus and Poisson's ratio of the fiber must also be known.[71,78] The major problem associated with this testing method is that the fiber must be perfectly perpendicular with the polished surface. If the fiber is not perpendicular, shear stresses develop at the fiber/matrix interface which cannot be accounted for when determining the interfacial bond strength.

It is also possible to calculate the interfacial shear strength by measuring the distance between matrix microcracks perpendicular to the fiber direction.[71] These cracks are usually uniformly spaced and can be measured using a light microscope. Equation 2 is used to calculate the frictional stress, τ, between the matrix and the fiber using the matrix microcrack spacing, 2d.[71]

$$2d = \sigma_c R / [2\tau V_f (1 + E_f V_f / E_m V_m)] \quad (4)$$

Where σ_c equals the stress where the composite starts to exhibit nonlinear elastic behavior and R is the fiber diameter. The C.T.E.

for the matrix and the fiber should be included in this equation because residual stresses resulting from C.T.E. mismatch could contribute to the matrix microcracking.

III. EXPERIMENTAL PROCEDURE

A. MATRIX PREPARATION

The cordierite matrix composition, listed in Table VI, differs slightly from theoretical cordierite ($2MgO \cdot 2Al_2O_3 \cdot 5SiO_2$). This material, SG-266M, received from Ferro Corporation as a frit with particle size of 5-20μm, was used for all preliminary processing experiments because it was relatively inexpensive and considerably more plentiful than the YAS matrix material. The terms SG-266M and cordierite will be used interchangeably in this thesis.

Two YAS compositions were initially selected from ten compositions investigated for liver cancer research.[29] YAS-7 and YAS-9 (Table VI) were picked because of their refractoriness, their relatively low SiO_2 content, and low C.T.E. These glasses were batched from reagent grade Y_2O_3, Al_2O_3 and SiO_2 and melted in platinum crucibles using a molybdenum disilicide hairpin heating element furnace. The glass was quenched in water, crushed, and ball milled to pass 230 mesh. YAS-9 was too refractory to be efficiently melted and was eventually eliminated. YAS-7 was cast and annealed at approximately 850°C to provide stock for mechanical testing specimens.

B. COMPOSITE FABRICATION

1. Woven Cloth. The first attempt at the fabrication of composite samples utilized #1 weave Nextel 440 cloth. Slurries of SG-266M and methanol were prepared and 1" squares of cloth were dipped into the slurry. They were then interleaved with excess glass, and hot

TABLE VI

GLASS-CERAMIC MATRIX COMPOSITIONS AND PROPERTIES

	Cordierite		Yttrium Aluminosilicate		
	Theoretical	SG-266M	YAS-7	YAS-9	Eutectic
Composition (wt. %)					
MgO	13.8	13.3			
Y_2O_3			40	55	32
Al_2O_3	34.9	32.0	30	15	22
SiO_2	51.3	52.7	30	30	46
BaO		2.0			
Melting Temperature	1550°C	1450°C	~1450°C	~1500°C	1345°C
Density		2.63	3.39	3.80	
C.T.E. ($\times 10^{-6}$/°C)		2.69	5.0	5.7	
Reference	79	20	20	20	34

pressed. SEM analysis showed the matrix was unable to penetrate the tight weave of the cloth.

In an effort to impregnate the cloth, a solution with the composition of theoretical cordierite was prepared using reagent grade magnesium and aluminum nitrate salts and tetraethylorthosilicate (TEOS) with enough excess methanol to completely dissolve the nitrates. The solution was heated between 55 and 60°C until the volume decreased by approximately 50%. Nextel cloth squares were placed in the solution and impregnated with the aid of a vacuum. The specimens were dried, then impregnated again. These impregnated squares were then hot pressed with excess SC-266M powder. Visual observation of the hot pressed disk fracture surface showed the matrix still had not penetrated the cloth sufficiently, and efforts to impregnate woven cloth were abandoned.

2. Chopped Fiber Composites.

a. Slurry Method. The production of chopped fiber composites was accomplished by wetting 1/4" chopped fiber with a minimum amount of water. Initially, dry glass powder was added to the chopped fibers and mixed until no agglomerates were evident. As the volume percent fiber increased, the mixing of the fiber with the matrix powder became a problem: in some cases, clumps of fiber were evident in hot pressed specimens. It was then discovered that wetting the matrix powder before mixing resulted in easier mixing and better fiber dispersion. All prepregs were hand mixed to minimize fiber damage.

b. Tape Casting. Tape casting techniques were applied to produce prepreg sheets of discontinuous fibers mixed with matrix.[80] Equal amounts of Tam tape casting binder #Z3216 and SC-266M were ball milled for three hours in a polyethylene jar containing 200 grams of Al_2O_3

media. The resulting slurry produced uniform tapes with good green strength. Ten volume percent 1/4" chopped Nextel 440 fiber was added and ball milled for 30 minutes resulting in the grinding of the fibers to lengths less than 1/16". Another slurry was produced and the fibers were mixed manually to produce a bulky slurry. Tape casting of this slurry was impossible due to the segregation of the fiber fraction from the matrix at the doctor blades; as a result, tape casting was abandoned.

c. Roller Casting. Tape casting mixtures consisting of binder, glass powders and chopped fibers were placed in a plastic bag as a wet ball and rolled using a metallurgical rolling mill. The bag was passed through the rolling mill until a sheet approximately 1/16" thick was formed; the bag was then cut and the prepreg was allowed to dry. If large amounts of binder were used the prepreg would have a uniform distribution of holes which was undesirable. The prepreg possessed enough green strength to be easily handled.

Discs were cut from the sheet, heat treated to remove the binder phase, and then hot pressed. Binder burnout temperatures ranged from 500°C to 1000°C. Lower burnout temperatures were more desirable due to the susceptibility of the matrix phase to crystallize while in powder form.

Roller casting experiments were curtailed when excellent results were obtained simply by mixing the fibers and matrix using the slurry method. Roller casting is a promising technique for the production of large sheets and merits further investigation.

3. Continuous Fiber Composites.

a. Filament Winder Methods. The most practical method for producing unidirectional laminas is through the use of a continuous fiber impregnator and a filament winder. The fiber tow is passed over a series of rollers and through a slurry of the desired matrix; the tow is then wound on to a drum.

Preliminary work with this method was carried out using SC-266M, water, and an ammonium alginate called Superloid from the Kelco Chemical Company. The water to glass ratio was 1:1; 0.5% Superloid was added to suspend the glass and 1.0% PVA was added to provide green strength. Fiber tows of Nicalon were dipped into the slurry then draped over a beaker and allowed to dry. The dried, impregnated fiber tow was then examined using a Jena microscope to qualitatively determine the extent of matrix powder infiltration into the fiber bundle.

One kilogram of this suspension was prepared and unidirectional prepregs were produced using a commercial filament winder at McDonnell Douglas Astronautics Company, St. Louis, Missouri. Prepregs composed of carbon fiber and carbon coated Nextel 480 fiber were dried, cut, and hot pressed to provide specimens for microstructural evaluation.

b. Hand Lay-ups. The fabrication of unidirectional lay-ups is tedious and results in non-uniform and inconsistent laminas. The use of AVCO SCS-6 fiber necessitates hand lay-up due to the stiff nature and large diameter of the fiber. Other unidirectional fiber lay-ups, however, should be prepared using a filament winder to produce optimum results.

C. DENSIFICATION OF SPECIMENS

1. Hot Pressing in an Argon Atmosphere. The densification of all monolithic and composite samples was accomplished using a Centorr uniaxial hot press (Figure 13). The prepreg or powder specimen was placed in a boron nitride coated 1.6" diameter graphite die. The loaded die was inserted into the hot press and evacuated to ~50 millitorr; the hot press chamber was then purged with gettered argon. The argon flowed at a continuous rate of approximately two liters per minute throughout the hot press run. Figure 14 depicts the time/temperature profile for a densification pressure of 3.5 MPa (500 psi) applied at 900°C. Comparison of the hot pressed density to the reported glass density for the two matrices indicated that higher pressure during hot pressing was unnecessary. Density of the hot pressed billets was measured in distilled water using the Archimedes technique.

Densification of the cordierite and YAS-7 matrices occurred at 915°C and 980°C respectively, suggesting that processing temperatures greater than 1300°C, as reported for LAS, are unnecessary.[14,48,57-60] For these matrices, the specimens were held at maximum temperature for one minute and allowed to cool naturally. In some cases higher densification temperatures up to 1300°C were used to determine the effect of hot pressing temperature on the crystallization of the matrix and to study the behavior of various fibers in the matrix. Table VII lists the hot pressing parameters and the average specimen density of the specimens prepared for this thesis.

2. Vacuum Hot Pressing. One sample of YAS-7 was hot pressed at 1100°C at 10^{-4} to 10^{-5} torr vacuum. After the sample densified, the chamber was purged with argon to minimize oxidation of the heating

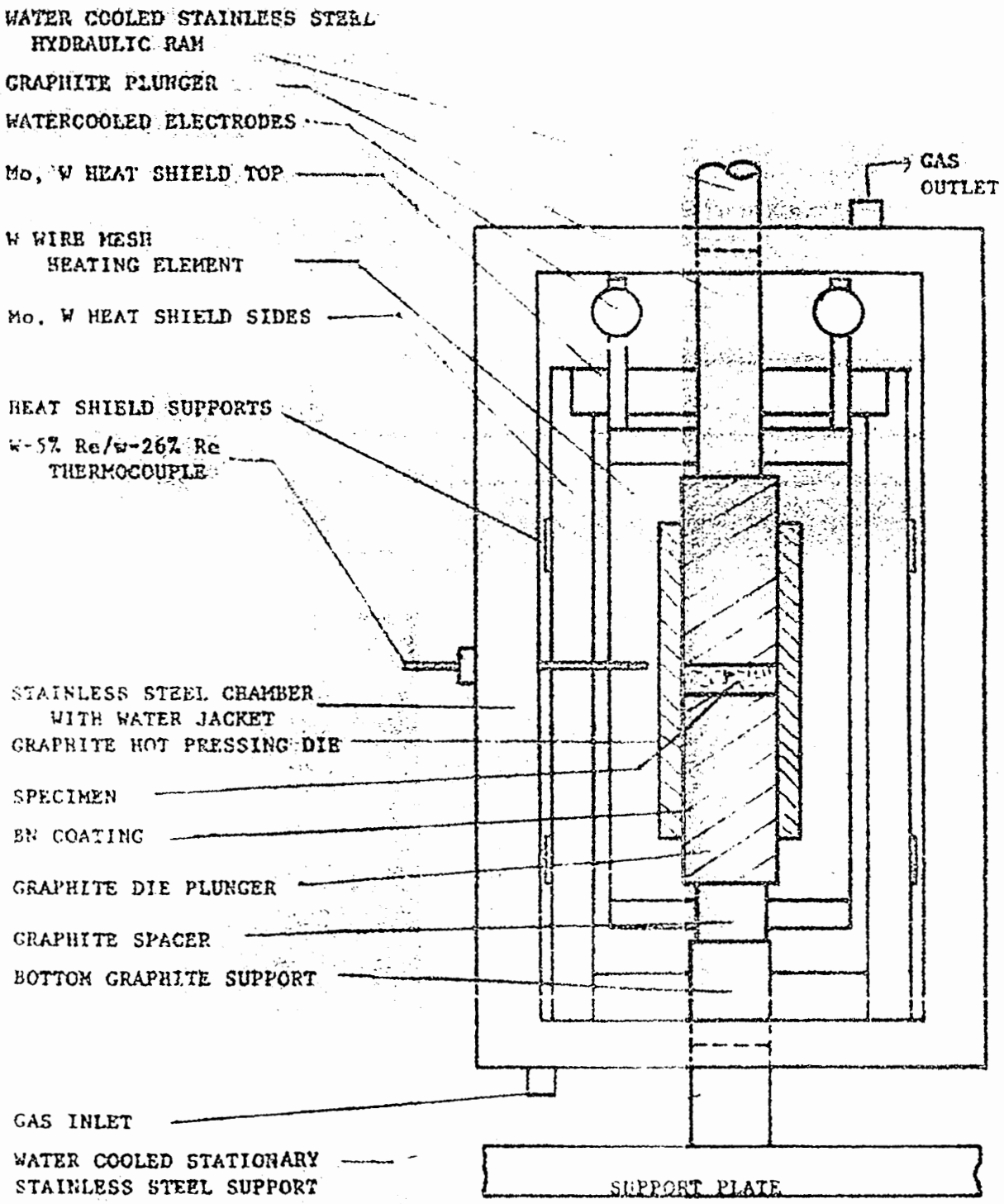

Fig. 13. Schematic representation of the Centorr hot press chamber.

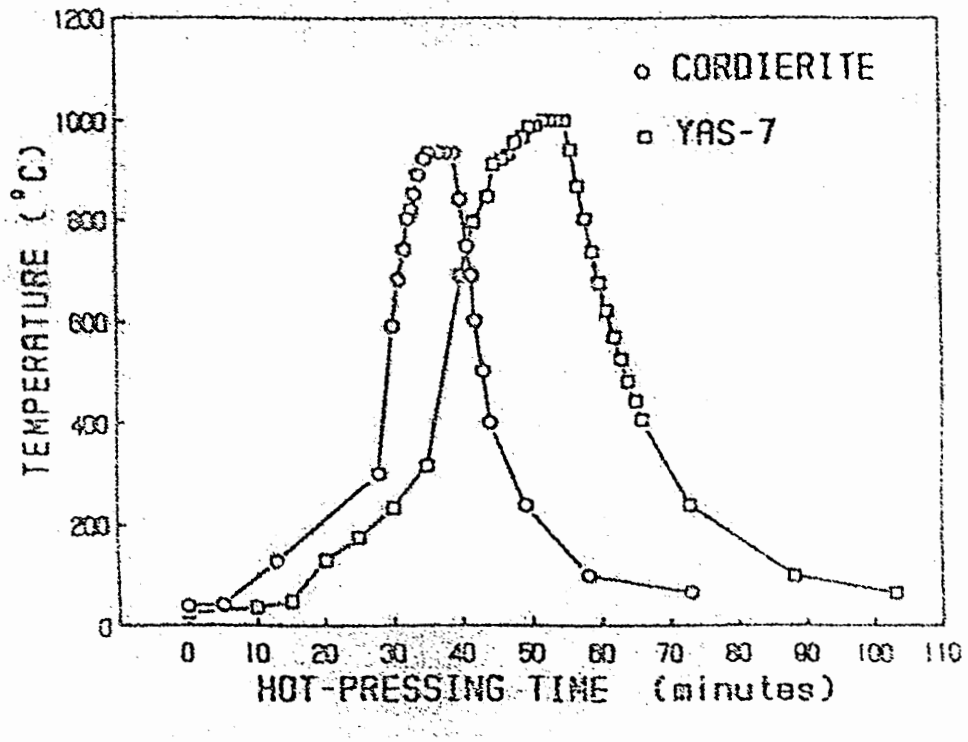

Fig. 14. Typical temperature versus time profile for the densification of glass-ceramic matrix specimens hot pressed in an argon atmosphere.

TABLE VII

HOT PRESSING PARAMETERS FOR YAS-7 AND CORDIERITE SPECIMENS

Fiber	%	Temp. I	Temp. II	Time (minutes)	Density (g/cm^3)
YAS-7					
None	--	900	1000	4/15	3.47
None	--	900	1100	6/15	3.46
None	--	900	1150	5/15	3.48
None	--	900	1200	9/15	3.48
None	--	900	1250	12/15	3.49
None	--	900	1300	8/15	3.39
None*	--	900	1100	150/10	3.51
N440†	10	900	1010	8/1	
N440	20	900	980	12/1	3.34
N440	30	900	1000	11/1	3.36
CCN480*††	20	900	1100	40/1	3.45
Tyranno	10	900	1150	12/1	3.29
Tyranno	10	900	1000	8/1	3.31
SCS-6	NA	900	1200	11/1	
Fiber FP	10	900	1150	12/1	3.54
Cordierite					
None	--	900	950	2/15	2.57
None	--	900	1050	3/15	2.53
None	--	900	1150	5/15	2.53
None	--	900	1250	13/15	2.53
Carbon	UN	900	1000	4/3	
N440	10	900	1000	2/15	2.59
N440	10	900	1150	5/15	
N440	10	920	1160	6/1	
NI-N440	NA	855	930	6/1	
CCN 480*	20	900	915	35/1	2.70
Nicalon	NA	850	950	5/2	
Nicalon cloth		900	1100	5/2	
Fiber FP	10	900	1000	2/15	2.62
Fiber FP	10	900	1150	14/15	2.68
Tyranno	10	900	1000	1/15	2.54
Tyranno	10	900	1150	7/15	2.53

*Vaccum hot pressed, all other specimens hot pressed in argon.
†N440 = Nextel 440 fiber
††CCN480 = Carbon Coated Nextel 480 fiber.
"Temp. I" is the temperature at which the densification pressure (3.5 MPa) was applied during hot pressing.
"Temp. II" is the maximum temperature achieved.
"Time" equals the time after the densification pressure was applied to the maximum temperature was reached/the time at maximum temperature.

elements and heat shields. Some specimens were hot pressed in a three inch diameter boron nitride coated graphite die using a larger hot press located at the McDonnell-Douglas Research Labs in St. Louis, Missouri. These specimens were hot pressed in a vacuum of 10^{-5} torr and were held at maximum temperature for 1 minute. The densification pressure used at MDRL was between 3.5 and 5.2 MPa (500 and 750 psi).

As a specimen is heated in a vacuum, volatile species on the surface outgas and cause an increase in pressure (decrease in vacuum). If the temperature continues to increase at this point, a vacuum protection circuit is tripped, shutting off the power to the heating elements resulting in a rapid loss of temperature. Therefore, the time/temperature profile for vacuum hot pressed specimens is not identical to the time/temperature profile illustrated in Figure 14, due to the interruption of heating during hot pressing to allow recovery of the vacuum.

3. Temperature Measurement. The temperature of the hot press chamber is measured with a W-5% Re/W-26% Re thermocouple placed 1/8" from the graphite die. Investigation of the die temperature with a micro-optical pyrometer showed that the thermocouple will at times lag the graphite die temperature up to 140°C. The thermocouple reading is believed to be accurate however, because when pressure is applied at 900°C, a YAS-7 specimen will start to densify at 950°C corresponding to the reported glass softening temperature of 940°C.[20]

D. MECHANICAL TESTING

1. Sample Preparation. Mechanical testing specimens were cut from hot pressed billets and cast glass bars using a diamond saw. These specimens were polished progressively using 320 and 600 grit SiC

paper, followed by 6 μm and 1 μm diamond paste to eliminate any surface flaws which could affect mechanical behavior. Specimens for toughness measurements, specifically K_{1c}, were notched through approximately 20% of the specimen thickness using a wire saw and a 400 grit silicon carbide slurry.

2. Testing Procedures. Whenever possible five specimens were tested. All specimens were tested in three point bending with a span of 1" employing an Instron mechanical test unit; the crosshead speed was 0.05"/minute. The test specimens averaged 0.3" thick, resulting in a span to thickness (S/d) ratio of approximately three. The S/d ratio needs to be approximately 15-17 for a unidirectional composite specimens to fail in tension;[8] a value less than this causes the specimen to fail in compression and/or shear. Load values were recorded on chart paper and converted to pounds.

E. GLASS-CERAMIC CRYSTALLIZATION STUDIES

1. Dopant Additions and DTA Studies. To determine the effect of dopants on the crystallization of SG-266M and YAS-7, 0.5% and 2.0% of TiO_2 and ZrO_2 were separately added to the glass powders in the form of alkoxides. Two percent CaO was also evaluated in YAS-7. The doped glass powders were remelted and quenched in water to assure homogeneous distribution of the dopants. Powder XRD was used to determine whether significant crystalline phases were present.

Doped and undoped glass powders were ground and sized between 270 and 400 mesh (53-38μ) for use in DTA experiments, eliminating particle size effects on the position and size of the crystallization exotherm, and allowing comparison between specimens. The weights of the specimens were also held constant at 200.0 milligrams. DTA was

conducted in air, over a temperature range of 25-1200°C, at a heating rate of 10°C/minute, using a Mettler DTA-TGA Model AT-1 located in the Graduate Center for Materials Research (UMR).

2. Heat Treatment of Matrices.

a. Heat Treatment of Cast YAS-7. Several studies were conducted on the YAS-7 glass matrix in order to determine the optimum heat treatment schedule required for crystallization. Specimens of cast glass were heat treated for 25 hours at four separate nucleation temperatures; then the specimens were heat treated for 20 hours at a higher temperature to promote crystallization. The heat treatment temperatures (°C) are listed in Table VIII. These glass samples, in the form of slivers approximately 1/16" x 3/16" x 1", were cut from cast bars during the preparation of mechanical testing specimens. The specimens were heated in air on alumina plates in two small "Rapid-temp" furnaces; in each case, the specimens remained transparent and showed signs of softening. The higher temperature heat treatments were performed first and resulted in considerable softening. A second group of specimens was then heat treated just below 940°C, the reported softening point of YAS-7.

b. Heat Treatment of Hot Pressed YAS-7. A specimen of YAS-7 was hot pressed and a small specimen approximately 3/16" x 1/4" x 3/4" was cut from the edge of the disc. This specimen was then heat treated in air at 1000°C for 25 hours; during this time it changed in color from dark gray to light gray. There was no evidence of the softening or deformation that was seen in the cast glass specimens. When the specimen was broken, the fracture cross section was uniformly gray in color. Similar specimens of YAS-7 containing 10%, 20% and 30%

TABLE VIII

HEAT TREATMENT TEMPERATURES FOR CAST YAS-7 SPECIMENS

Nucleation Temperature (°C)	Crystallization Temperature (°C)
840	910
840	935
860	910
860	935
900	1020
900	1035
925	1020
925	1035

uncoated chopped Nextel 440 fiber were hot pressed at UMR and heat treated using the same parameters as for the monolithic specimens.

Twelve small specimens were cut from an 1100°C hot pressed specimen, and heat treated in the following manner: The specimens were placed in a furnace and heated to 950°C. After two hours two specimens were removed and the temperature was increased 50°C to 1000°C. This process was repeated until the last two specimens were removed after two hours at 1200°C.

3. Analysis of Crystallizaton Studies.

a. XRD Analysis. A General Electric XRD5 or XRD7 was used with a scanning speed of 2°/minute and with an intensity factor of 1k or 2.5k. Powder XRD provided qualitative information and estimates regarding the extent of the crystallization of the glass ceramic matrices. It also provided immediate information as to the effectiveness of various crystallization trials.

Samples of the hot pressed matrices were ground and passed through a 270 mesh, packed into a plexiglass specimen holder, and X-rayed using $Cu_{K\alpha}$ radiation with a wavelength of 1.5418A. Powder XRD patterns of mullite, cordierite, and yttrium diorthosilicate (Appendix A) were generated according to the expected crystal phases, as deduced from phase diagrams. These patterns were then used to aid in identifying the phases appearing in powder XRD patterns obtained from the crystallization of the glass-ceramic matrices.

b. Dilatometer Measurements. Specimens for thermal expansion measurements were cut from hot pressed billets, or cast glass rods, to approximately 1/4" square cross section and to a length of 1" ±0.005". The measurements were performed using an Orton automatic dilatometer equipped with an alumina specimen holder and push rod. The heating

rate was 5°C per minute; temperature was measured with a Pt/Pt-10%Rh thermocouple.

c. Microstructure Analysis. Microstructural analyses of the matrix and of the fiber reinforced matrices were performed using two different scanning electron microscopes (SEM). The SEM at the Graduate Center for Materials Research (UMR) is a Jeol JSM-35 CF thermionic emission microscope with a W target; the SEM at McDonnell Douglas is an International Scientific Instrument (ISI) thermionic emission SEM with a W filament. Fracture surfaces were examined in each instance to obtain the best graphic evidence of fiber/matrix interaction and fiber pullout. The specimens were mounted on either aluminum or steel mounts using silver or carbon paints and coated with a thin (<100Å) layer of either carbon or a gold-palladium mixture to make the specimen surface conductive.

IV. EXPERIMENTAL RESULTS AND DISCUSSION

A. THE DETERMINATION OF HOT PRESSING PARAMETERS

Developing hot pressing methods and techniques was, by necessity, an early goal, so that hot pressed specimens could be reproducibly fabricated and evaluated. Glass presents a unique hot pressing problem because the viscosity of glass decreases with increasing temperature. This behavior will cause the glass to extrude around the die punches and make specimen removal difficult and sometimes cause the die to fracture upon removal of the specimen. Determining the minimum temperature at which the specimen will densify will minimize the extrusion tendency and still allow complete densification. The cordierite and YAS-7 matrices behave differently in terms of densification. The cordierite matrix powder will readily consolidate and densify to essentially zero percent porosity. YAS-7 however, appears dense and its hot pressed density compares closely with the cast glass density, giving the appearance of a fully dense specimen. Only SEM analysis of fraccure surfaces reveals that approximately 10% closed porosity remains.

Specimens of YAS-7 matrix, hot pressed in an argon atmosphere showed a large amount of porosity in an apparently crystalline matrix (Figure 15). Vacuum hot pressing of YAS-7 specimens failed to eliminate the matrix porosity (Figure 16) and therefore has no advantage over hot pressing YAS-7 specimens in argon. The density of the specimen hot pressed in a vacuum was 3.51 g/cm^3 compared to 3.48 g/cm^3 for the specimen hot pressed in argon under identical conditions which suggests that a small reduction in the porosity may have resulted from the vacuum hot pressing.

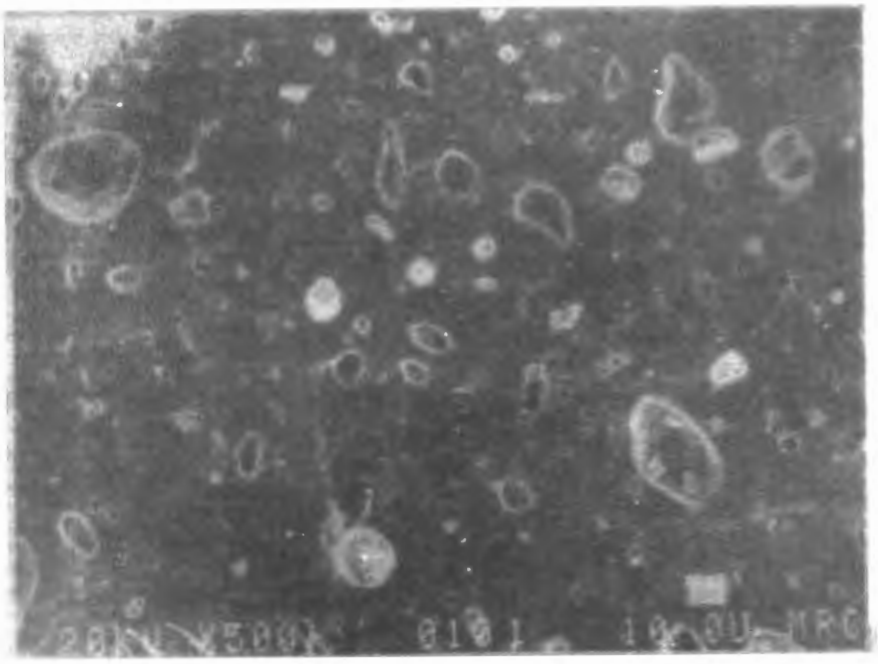

Fig. 15. SEM fractograph of a monolithic YAS-7 specimen, hot pressed in argon at 1100C for 15 minutes, illustrating a high degree of matrix porosity.

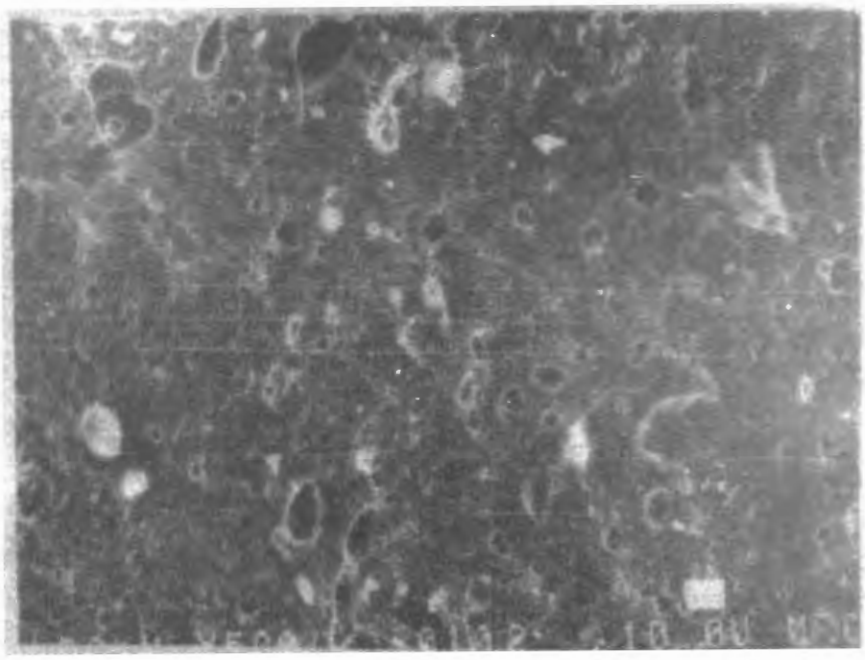

Fig. 16. SEM fractograph of a monolithic YAS-7 specimen, vacuum hot pressed at 1100C for 10 minutes, illustrating similar matrix porosity to specimens hot pressed in argon.

The porosity observed in the YAS-7 matrix could be a result of trapped gases, the evolution of dissolved gases present in the glass powder, a result of chemical reactions associated with the crystallization of the glass, or a result of chemical reaction between the hot pressing environment and the glass powder during hot pressing. If the porosity is a result of trapped gases, a simillar problem should be observed in the cordierite matrix during hot pressing and the problem should be eliminated when the specimens are hot pressed in a vacuum. If dissolved gases are causing the porosity, then the glass should foam upon subsequent heating, as during the fabrication of glass spheres for cancer research,[20] which is not observed either. This evolution of porosity therefore, may be due to chemical interaction between the YAS-7 glass and the boron nitride die coatings and/or the graphite dies, or from the process of crystallization in the glass.

A densification pressure of 3.5 MPa was sufficient to fully densify the specimens. Pressures up to 14 MPa were tried but only resulted in increased glass extrusion around the die punches. The hot pressing parameters for specimens used in this study are listed in Table VII.

B. COMPOSITE FABRICATION

The fabrication of fiber composites requires that the fiber and the matrix be intimately mixed. Most commercially available fibers are manufactured with a sizing which improves handling and reduces fiber damage. Nextel fiber has a starch sizing[50] which is water

soluble while Nicalon and carbon fiber usually have an acetate sizing which must be burned off prior to fabrication.[26]

1. Woven Cloth. Attempts to impregnate woven Nextel 440 cloth and woven Nicalon cloth with a cordierite frit slurry was unsuccessful because the powder had a particle size much greater than the spacings in between the fibers in the fiber bundles. Stoichiometric cordierite was then produced through hydrothermal processing techniques,[81-84] from reagent grade $Mg(NO_3)_3 \cdot 6H_2O$, $Al(NO_3)_3 \cdot 9H_2O$, and $Si(C_2H_5O)_4$ (TEOS), and utilized in efforts to infiltrate the cloth bundle. The resulting solution was added to the cloth using vacuum impregnation and then heat treated to eliminate the volatiles. The process was repeated and the impregnated cloth was combined with excess cordierite glass powder and hot pressed. SEM analysis of a cut surface shows that the interior of the cloth was devoid of matrix glass (Figure 17). Polymer matrix composites are better suited for using woven cloth because the matrix is introduced as a liquid then cured to form a continuous matrix phase.[1] Moreover, hydrothermal methods produce low yields which make them impractical for large scale composite materials syntheais.

2. Tape and Roller Casting. Tape casting suspensions were produced by ball milling the matrix powder with a tape casting binder and then hand mixing the fiber into the ball milled mixture. Ball milling the fibers with the matrix powder and binder reduced the fiber to extremely short lengths. Tape casting is commonly used to produce electronic substrates or thin sheets of ceramic materials such as alumina and barium titanate.[80] Producing composite laminas using tape casting was unsuccessful because the fibers would segregate from the matrix at the tape casting doctor blade.

Fig. 17. SEM photomicrograph of a cut surface of a cordierite matrix specimen containing woven Nicalon cloth, hot pressed in argon at 1000C for 2 minutes, illustrating a lack on matrix in the cloth weave.

Roller casting was then investigated because rollers would not cause the chopped fiber to segregate from the matrix and might result in uniform thicknesses similar to tape casting. The tape casting mixture was added to plastic bags and repeatedly rolled using a metallurgical roller mill to achieve a sheet approximately 1/16" thick. The bag was then cut and the prepreg allowed to dry. Discs slightly smaller than the hot pressing die were cut from the prepreg, heat treated to remove the tape casting binder, and hot pressed. During heat treatment, the glass powder crystallized so the specimen did not densify during hot pressing. No other specimens were produced because of the success of the slurry method for composite fabrication.

3. Slurry Method. Wetting chopped fiber with water will help disperse the fibers and the water will help the matrix powder stick to the fibers. Better results are obtained when the matrix powder is added as a thick slurry to the wet fibers. Excess water will promote segregation of the matrix and fibers through sedimentation and should be avoided. The fibers tend to form a skeletal network which the matrix powder can settle through much like fine particles in a coarse particle network. The wet prepreg is placed in an alumina tube which has an inside diameter slightly smaller than the inside diameter of the hot pressing die. The prepreg is dried then placed in the BN coated hot pressing die with excess glass powder. (It is unclear whether the chemical interaction between the BN die coatings and the glass matrix powder constitute a problem; the excess powder was added only as a precautionary measure.)

SEM analysis of fracture surfaces of hot pressed specimens showed good fiber/matrix mixing and fiber bundles. The fibers had an aspect ratio of approximately 650 (1/4" long and 10μm diameter) and would be

expected to form discrete bundles during mixing.[52,53] Some orientation will always occur during hot pressing, but smaller aspect ratios should minimize the effects of the hot pressing and mixing and thereby reduce the anisotropy caused by fiber alignment.[52,53,64]

4. Unidirectional Fabrication Methods. The best strengthening and toughening of composites is obtained using aligned continuous fibers.[53,65] A filament winder was designed and constructed (Figure 18), but was not completed in time to produce unidirectional laminas. Preliminary experiments were conducted on a commercial filament winder (McDonnell-Douglas Astronautics Company) to test the feasibility of producing unidirectional laminas. The matrix powder was suspended in water containing 0.5% Superloid and 1.0% polyvinyl alcohol. Specimens of carbon fiber (Hercules AS-4) and the cordierite matrix were produced and hot pressed. Figure 19 illustrates the extensive fiber pullout the specimen experienced during fracture which would normally be associated with excellent toughness. However, SEM examination of the hot pressed surface showed regularly spaced matrix microcracks perpendicular to the fiber direction (Figure 20) which extend through the fiber layers into the specimen (Figure 21). It is likely that this type of matrix microcracking resulted from the large C.T.E. mismatch between the carbon fibers and the cordierite matrix effectively eliminating carbon fiber reinforced cordierite as a candidate for ceramic composites. This type of matrix cracking due to C.T.E. mismatch has been reported for other glass and glass-ceramic matrix composites.[48,53,65]

The axial stress, σ_a, developed upon cooling (ΔT) in the matrix due to the thermal expansion mismatch ($\alpha_m - \alpha_f$) between unidirectionally aligned fibers can be approximated using the following formula:

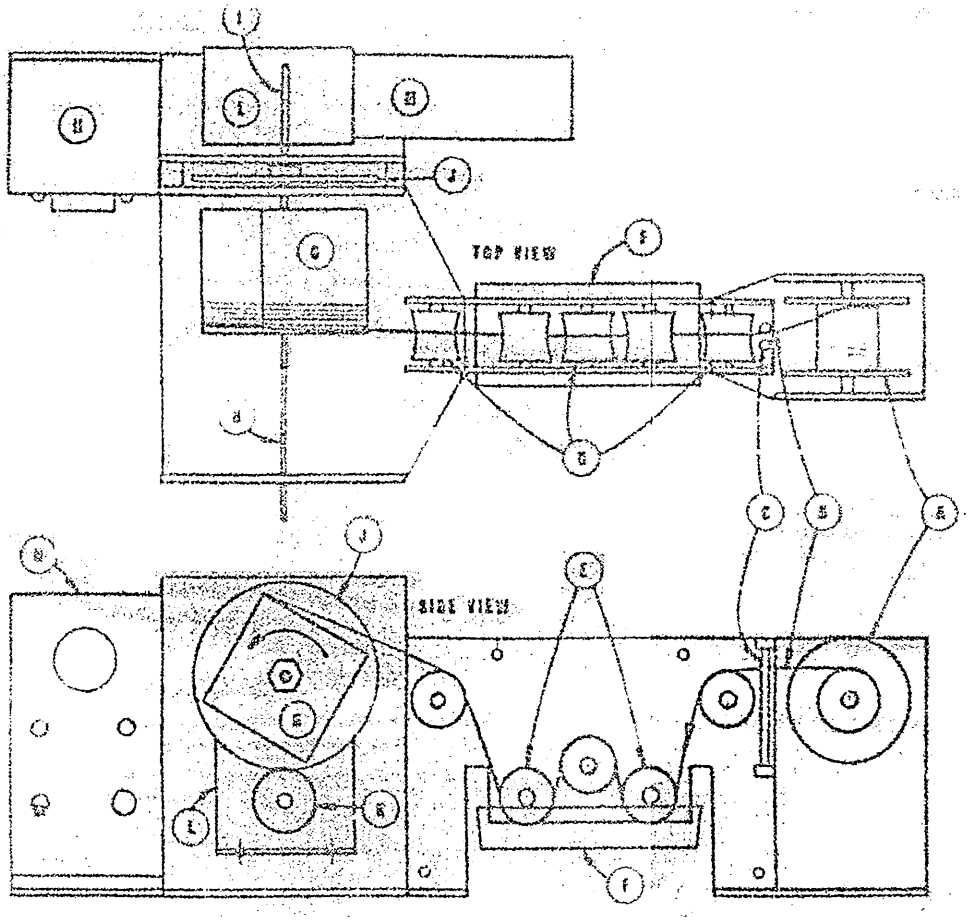

A. Source spool
B. Fiber tow
C. Guide rods
D. Guide rollers
E. Impregnation rollers
F. Slurry bath
G. Square Al take-up spool
H. Threaded rod for lateral movement
I. Hexagonal rod for rotational movement
J. Large drive sprocket
K. Small drive sprocket
L. Speed reducer
M. DC motor
N. Controller for DC motor

Fig. 18. Schematic representation of the experimental filament winder constructed at the University of Missouri-Rolla.

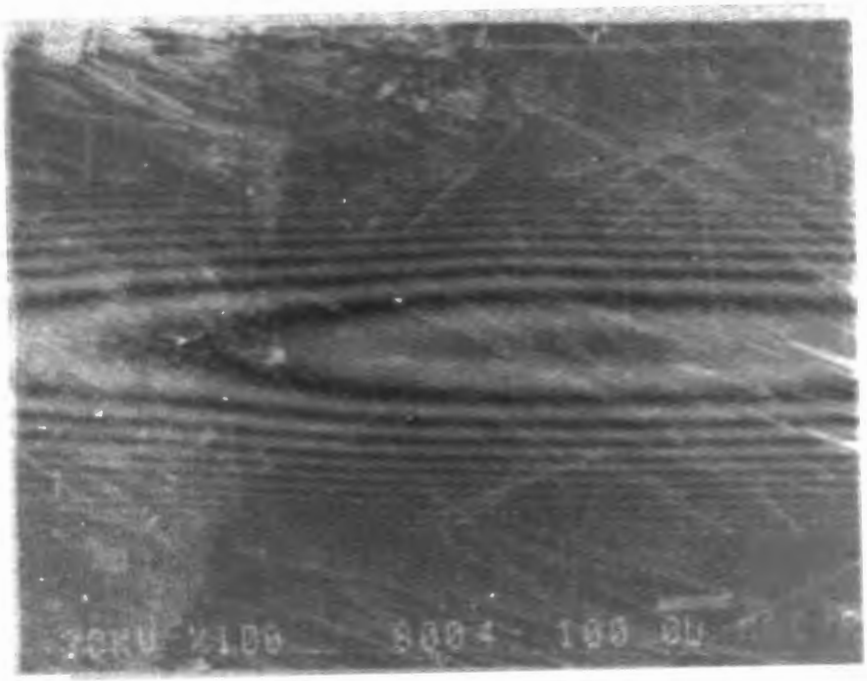

Fig. 19. SEM fractograph of a unidirectionally aligned carbon fiber reinforced cordierite matrix, hot pressed at 950C, showing extensive fiber pullout and high fiber volume.

Fig. 20. SEM photomicrograph of a hot pressed surface of a unidirectional carbon fiber reinforced cordierite matrix showing regularly spaced matrix microcracks perpendicular to the fiber direction.

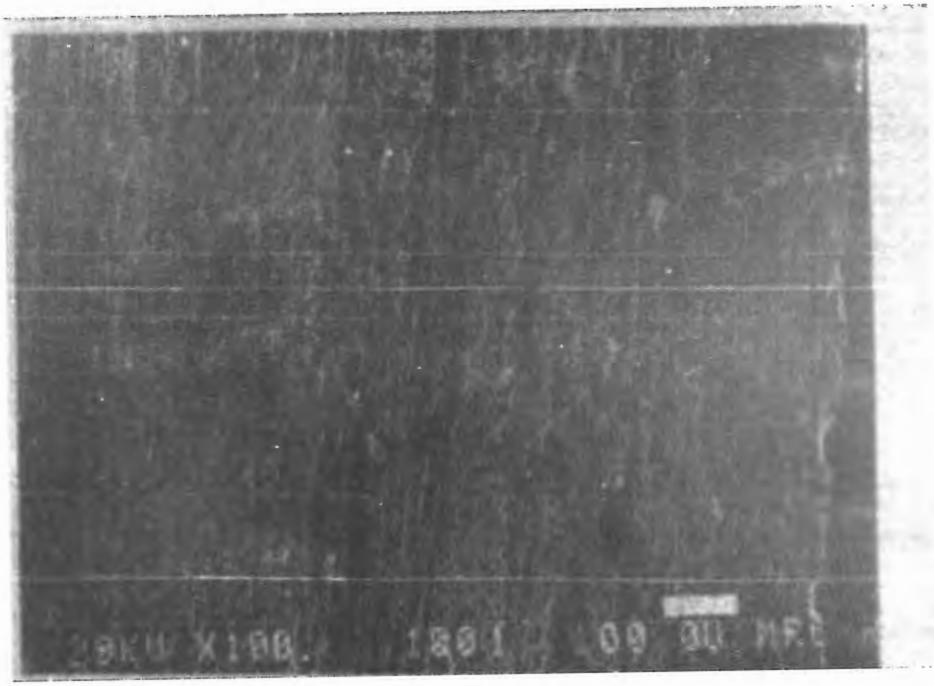

Fig. 21. SEM photomicrograph of a cut surface parallel to the fiber direction in a unidirectional carbon fiber reinforced cordierite matrix showing crack extension into the bulk of the specimen perpendicular to the fiber direction.

$$\sigma_a = (\alpha_m - \alpha_f)\,\Delta T\, E_f\, V_f \,/\, [V_f\,[(E_f / E_m - 1) + 1]] \quad (5)$$

where E_f and E_m are the elastic moduli of the fiber and the matrix, respectively. For a composite of 50 volume percent ($V_f = 0.50$) unidirectionally aligned AS-4 carbon fiber (Table II) reinforced cordierite matrix composite, the stress developed upon cooling from the glass softening point of 900°C is 300 Mpa, which is approximately 2.2 times the average bending strength of 135 MPa. Table IX lists the properties of various glass and glass-ceramic matrix composites and the estimated axial stresses developed upon cooling. The resulting axial stress is function of C.T.E. mismatch, elastic modulus and temperature range and if the stress exceeds the strength of the matrix, microcracking of the matrix will occur. Additional treatment of this subject appears in Appendix B.

C. CHOPPED FIBER COMPOSITES

1. Studies with YAS-7 Matrix Composites. The addition of uncoated Nextel 440 fiber and Tyranno fiber to YAS-7 greatly reduces the hot pressed porosity of the matrix; these additions also appear to retard the crystallization of YAS-7. As seen in Figures 22 and 23, the porosity of the YAS-7 matrix is greatly reduced when Tyranno fiber was added to YAS-7 and hot pressed at 1000°C (compare Figure 22 to Figure 15); brittle fracture has occurred and no fiber pullout is observed. Similar behavior is observed in Figure 24 with Nextel 440 fiber additions in the YAS-7 matrix. The Tyranno fibers appear as dark round and oval dots where the ovals are a result of transverse fiber fractures. The Nextel 440 fiber also appears as dark dots but in this case, the fibers are oval and in Figure 24, the fibers are

TABLE IX

APPROXIMATE AXIAL STRESSES RESULTING FROM FIBER/MATRIX C.T.E. MISMATCH FOR VARIOUS GLASS AND GLASS-CERAMIC MATRICES CONTAINING 0.50 VOLUME FRACTION UNIDIRECTIONALLY ALIGNED CARBON FIBER

Matrix	C.T.E. (10^{-6}/°C)	ΔT (°C)	E_m (GPa)	Axial Stress (σ_a, MPa)	Matrix Stress (σ_m, MPa)
Soda-Lime-Silica Glass*	9.0	480	60	220	100
Pyrex*	3.3	520	60	88	100
LAS*	1.5	1000	100	117	150
SG-266M** (cordierite)	2.7	900	97.4	300	135
YAS-7**	6.3	940	171	788	200

*Reference 65, Table III
**Experimental Data

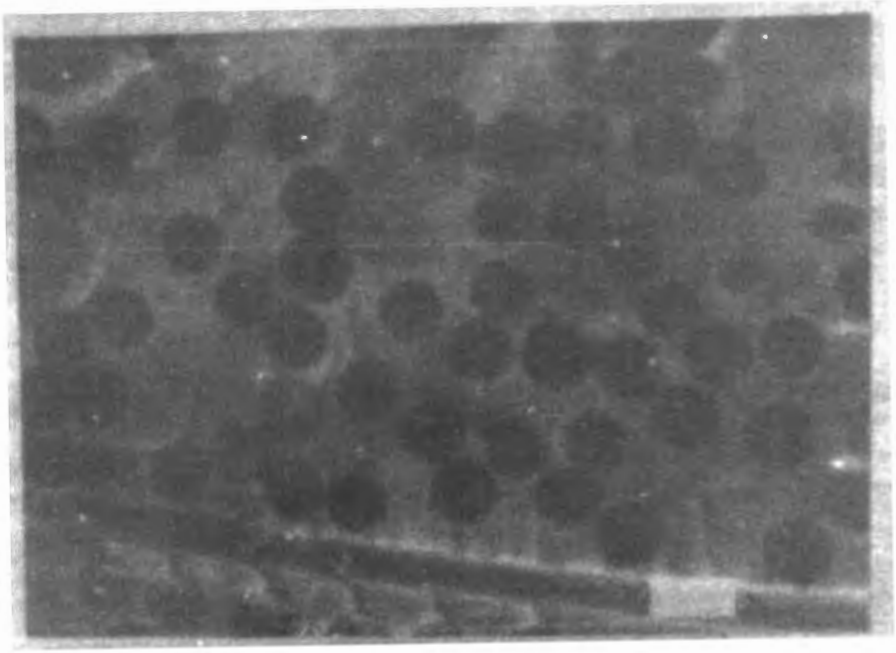

Fig. 22. SEM fractograph of Tyranno fiber reinforced YAS-7 specimen, hot pressed in argon at 1000C for 2 minutes, depicting reduced matrix porosity and brittle fracture.

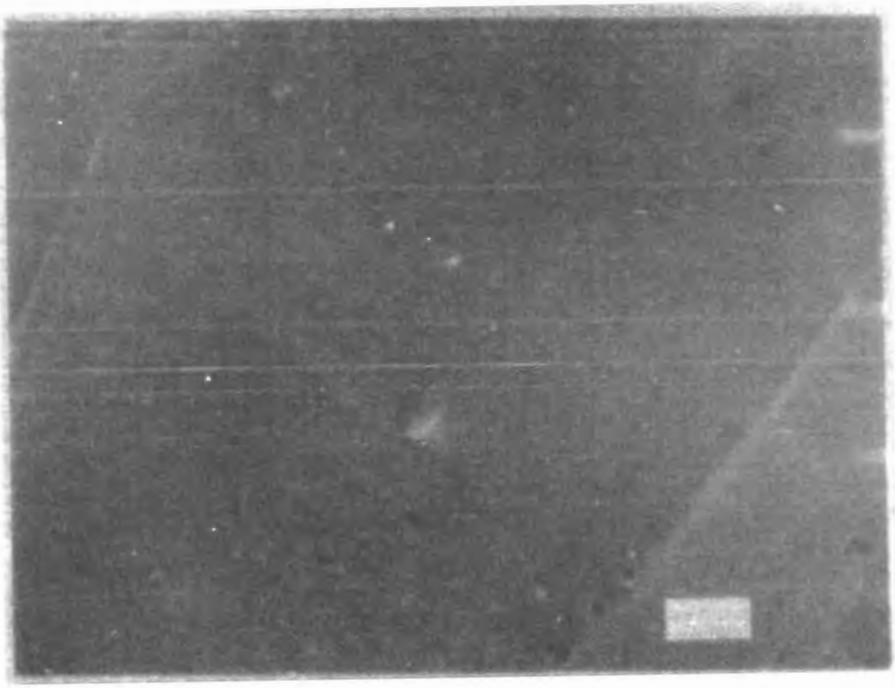

Fig. 23. SEM fractograph of a Tyranno fiber reinforced YAS-7 specimen, hot pressed in argon at 1000C for 2 minutes, depicting a region with 0% matrix porosity and smooth, glass-like fracture.

Bar = 10μm

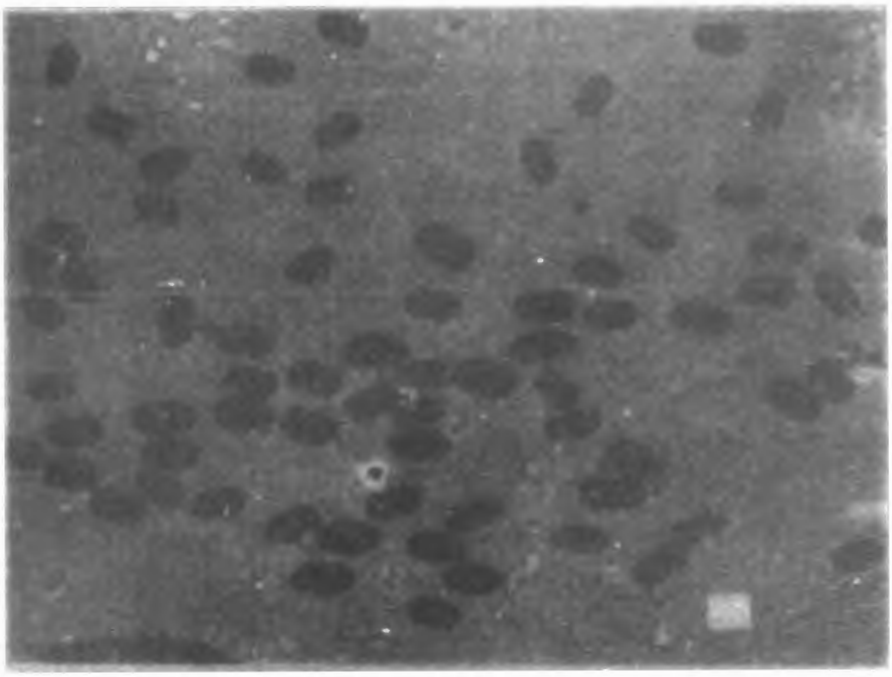

Fig. 24. SEM fractograph of a 10% Nextel 440 fiber reinforced YAS-7 specimen, hot pressed in argon at 1010C for 2 minutes, showing reduced matrix porosity and brittle fracture.

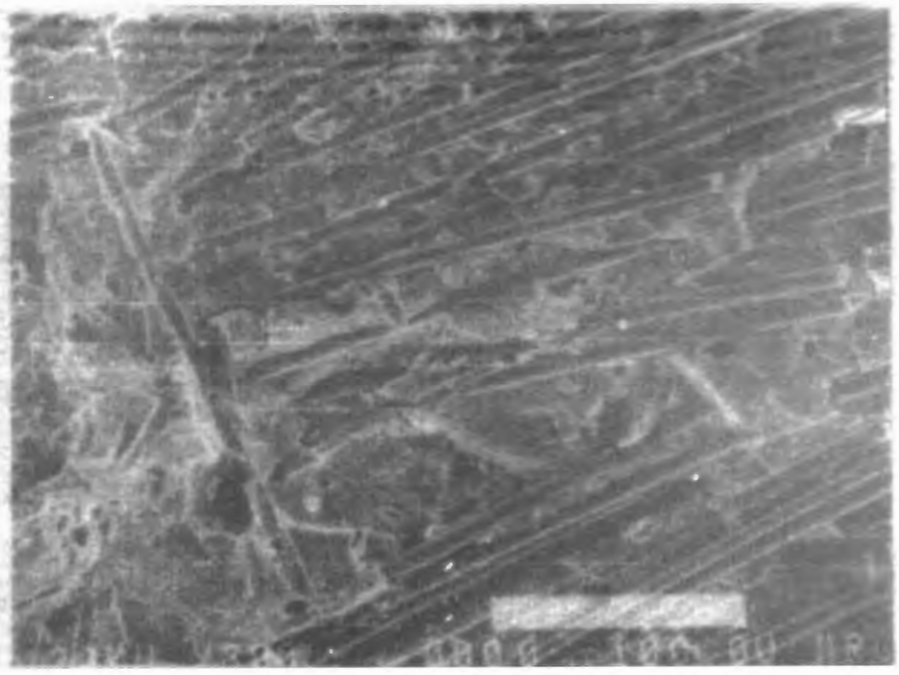

Fig. 25. SEM fractograph of a Tyranno fiber reinforced YAS-7 specimen, hot pressed in argon at 1150C for 2 minutes, depicting high matrix porosity and fiber pullout.

perpendicular to the fracture plane. The fiber surface area may provide a sink for porosity, allowing increased densification of the specimen. This implies that low porosity composites could be fabricated using YAS-7 improving the mechanical properties of the composite. When Tyrannno fiber is hot pressed at 1150°C the fibers exhibit pullout, the matrix fracture is no longer smooth and contains a large amount of porosity similar to the hot pressed monolithic matrix (Figure 25).

Strong fiber/matrix bonding resulted when Fiber FP was added to the YAS-7 matrix. No reduction in porosity was observed compared to monolithic YAS-7; the specimen with Fiber FP exhibited brittle fracture (Figure 26). The fibers are dark spots, the gray area is the YAS-7 matrix and the white and black areas are porosity. Examination of the fiber/matrix interface showed a poorly defined boundary at the interface suggesting a high degree of fiber/matrix chemical interaction (Figure 27). The fiber is the grainy structure in the lower left hand corner and the YAS-7 matrix is the relatively smooth area in the upper right. A fiber coating would be required to reduce this strong fiber/matrix interfacial bonding to produce a tougher composite.

SCS-6 fiber in YAS-7 resulted in severe matrix microcracking (Figures 28 and 29). An example of a single SCS-6 fiber is illustrated in Figure 10 and SCS-6 appears in the upper right hand corner surrounded by the YAS-7 matrix in Figure 28. These cracks are probably caused by C.T.E. mismatch.[4] This assumption is further supported by the characteristic crack networking which developed in regions between the fibers as shown in Figure 29. The magnification used to produce the SEM photmicrographs in Figures 22 and 28 is 1000x;

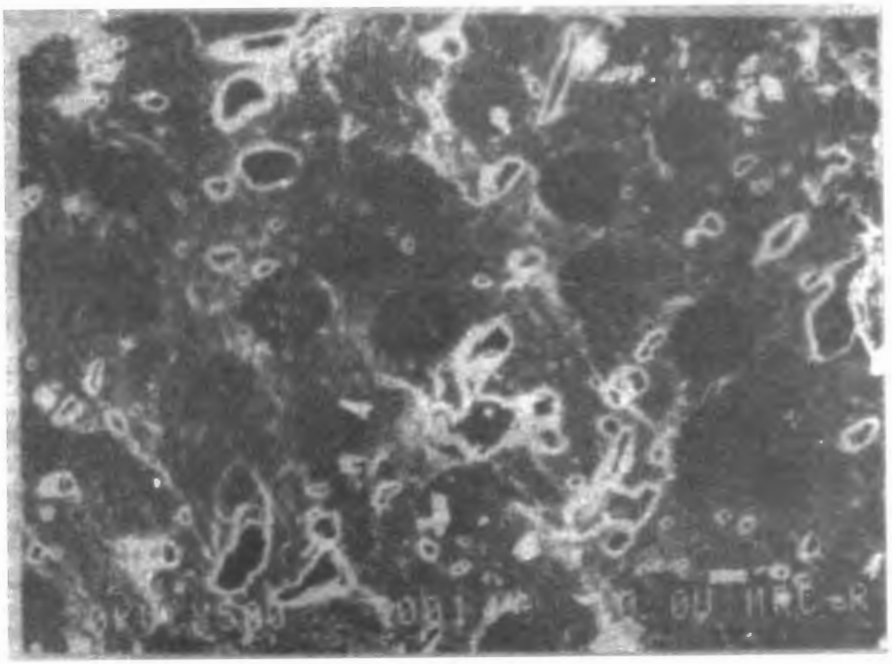

Fig. 26. SEM fractograph of a Fiber FP reinforced YAS-7 specimen, hot pressed in argon at 1150C for 2 minutes, showing high matrix porosity and brittle fracture.

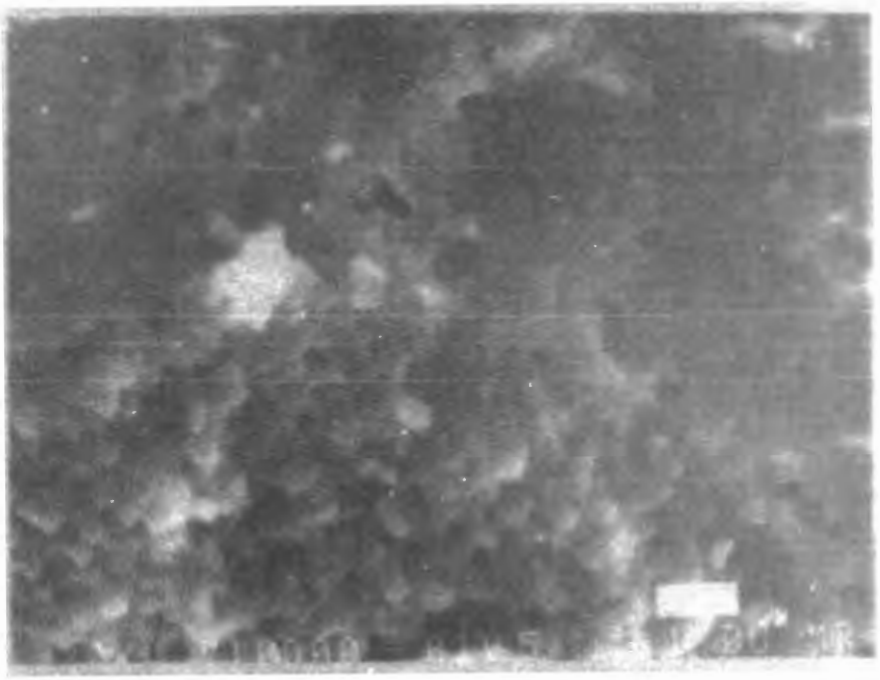

Fig. 27. SEM fractograph of the poorly defined Fiber FP/YAS-7 matrix interfacial region in a specimen hot pressed in argon at 1150C for 2 minutes.

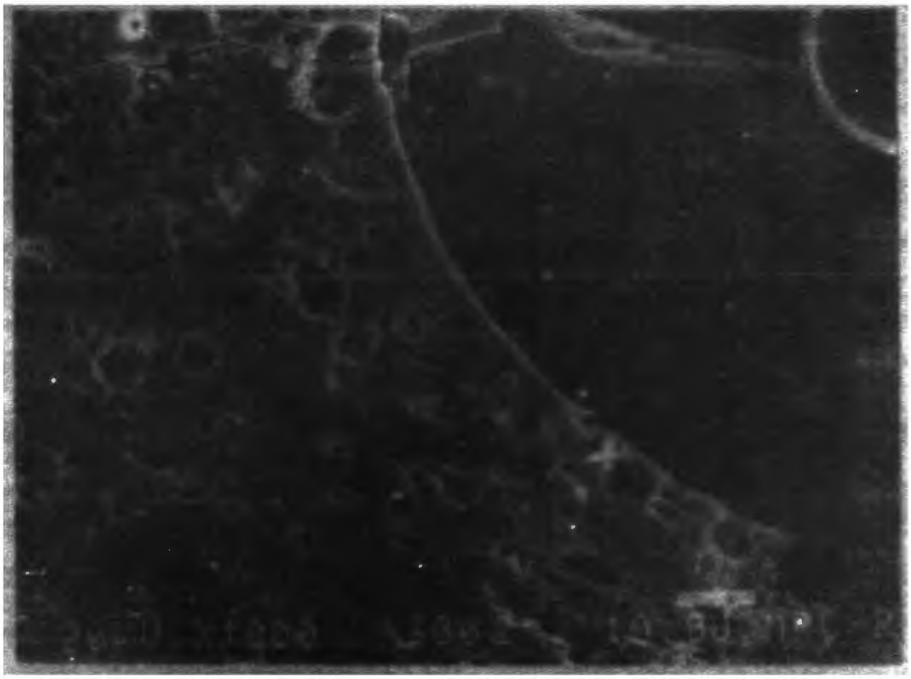

Fig. 28. SEM fractograph of YAS-7 containing SCS-6 fiber, hot pressed in argon at 1200C for 1 minutes, showing matrix microcracking originating at the fiber/matrix interface.

Fig. 29. SEM fractograph of YAS-7 containing SCS-6 fiber, showing the matrix microcracking network developed between the fibers.

this provides a comparison of the size of a typical SCS-6 fiber (141μm) to the typical fiber size of Tyranno (10μm).

Fiber debonding and pullout resulted when carbon coated Nextel 480 fiber was incorporated into the YAS-7 matrix. Matrix porosity appears to be reduced by the coated fiber additions (Figures 30 and 31). Figure 30 illustrates the high degree of mixing achieved between the fiber and the matrix. Also evident is the comparatively low YAS-7 matrix porosity. Noticeable in Figure 31 is the clumping associated with large aspect ratios. Limited fiber pullout was observed when SiC coated Nextel 440 fibers were used as well as a reduction in the matrix porosity (Figure 32). In some cases, boron nitride coated Nextel 440 fibers bonded to the matrix; in other cases, these fibers exhibited pullout from the matrix (Figure 33). SEM analysis of BN coated fibers showed the coating to be non-uniform which could account for the variable behavior of the fiber when incorporated into the matrix (Figure 34).

2. Studies with Cordierite Matrix Composites. As expected, when uncoated fibers such as Nextel 440, Nicalon, and Fiber FP are incorporated into the cordierite matrix, strong bonding results producing brittle fracture behavior. The use of fiber coatings is required to minimize fiber/matrix interaction. Nextel and Fiber FP are oxides and would be expected to chemically react and bond in an oxide matrix.[3] Nicalon fiber, although not a pure oxide fiber, develops a silica surface coating which will produce fiber/matrix bonding similar to that exhibited with oxide fibers.[25,27,47]

The Nicalon fibers, present in Nicalon fiber reinforced cordierite, could not be detected using SEM even though the fibers were visible under an optical microscope. The fibers were so tightly

Fig. 30. SEM fractograph of a carbon coated Nextel 480 fiber reinforced YAS-7 matrix composite, vacuum hot pressed at 1100C, depicting fiber pullout and intimate mixing.

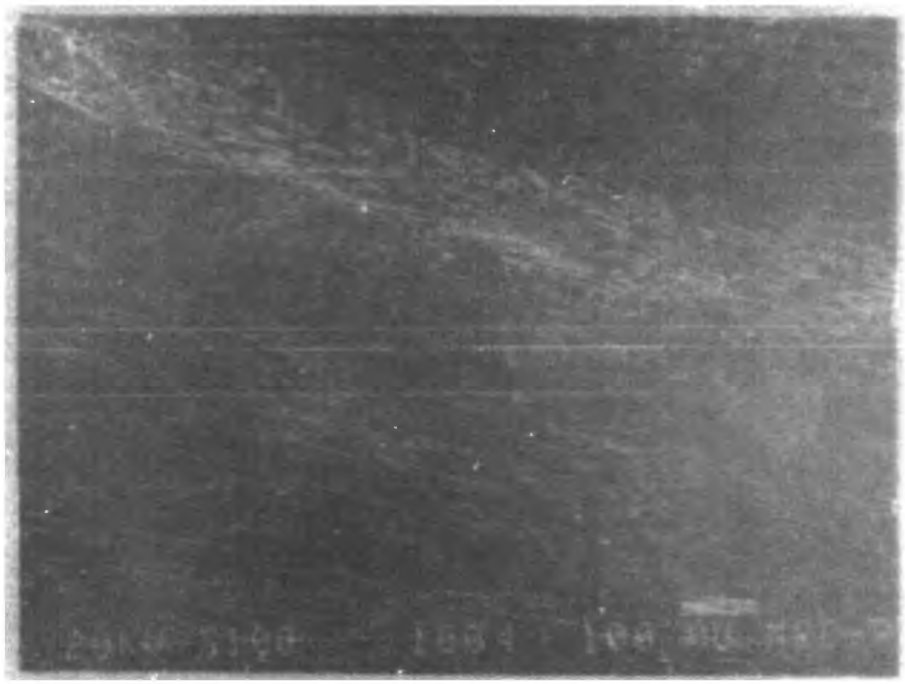

Fig. 31. SEM fractograph of a carbon coated Nextel 480 fiber reinforced YAS-7 matrix composite, vacuum hot pressed at 1100C, showing fiber clumping associated with large fiber aspect ratios.

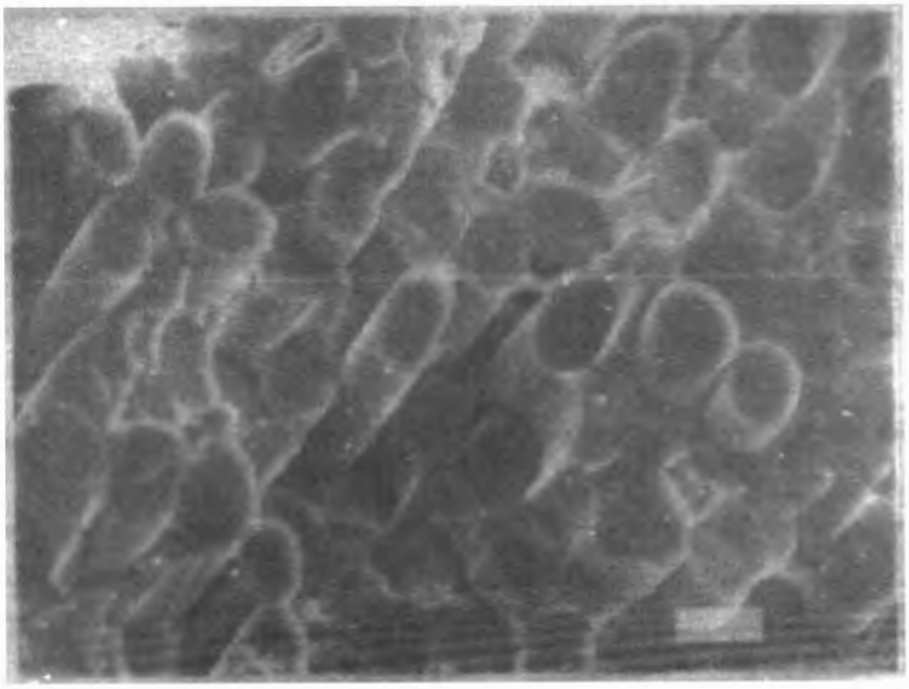

Fig. 32. SEM fractograph of YAS-7 containing silicon carbide coated Nextel 440 fiber, hot pressed in argon at 1100C, showing reduced matrix porosity and some fiber pullout.

Fig. 33. SEM fractograph of YAS-7 containing boron nitride coated Nextel 440 fiber, hot pressed in argon at 1100C, showing varying degrees of fiber/matrix bonding.

Bar = 10μm

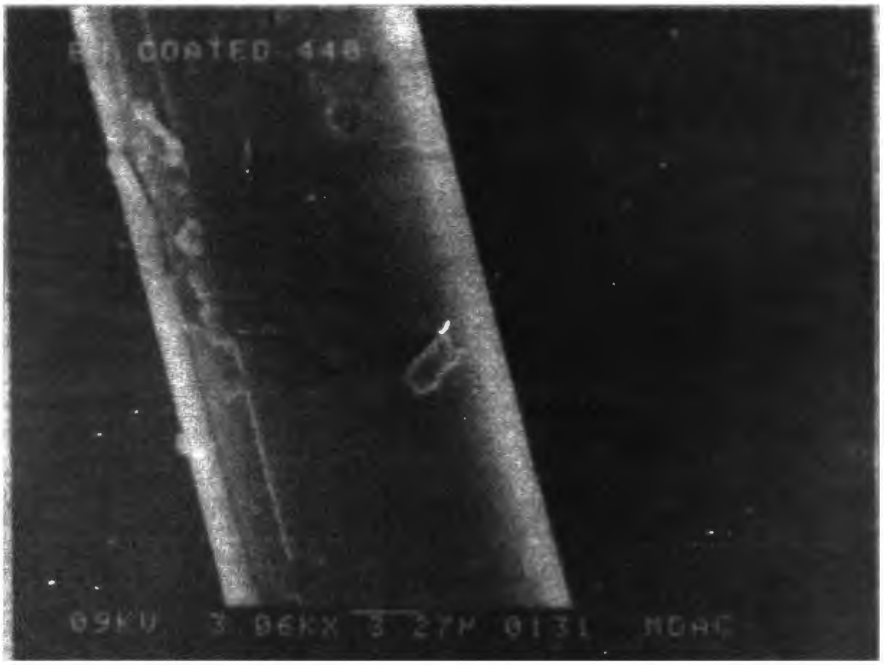

Fig. 34. SEM photomicrograph illustrating the non-uniform boron nitride coating on a Nextel 440 fiber.

bonded to the matrix that they fractured transversely, resulting in an oblong fiber fracture surface outline (white dots) as shown in Figure 35; the small black specks are small pores in the matrix.

Fiber FP has a higher C.T.E. than the matrix, thus placing the matrix in compression on cooling which could produce the hemispherical fractures shown in Figure 36 (also see Figure 5). Matrix microcracking ran between the fibers (rather than into the fibers), as anticipated from the C.T.E. mismatch theory (Figure 37).[4] Figure 38 shows that the fiber/matrix interface is clearly defined (the fiber is on the right), suggesting that the fiber/matrix interaction may be less than that observed in the YAS-7 matrix (Figure 27). Figures 36 and 38 are SEM photomicrographs depicting fracture surfaces of specimens which were hot pressed at 1150°C; Figure 37 is an SEM photomicrograph depicting the fracture surface of a specimen which was hot pressed at 1000°C. Hot pressing temperature apparently has no effect on the fiber/matrix bonding.

Fiber pullout occurred (Figures 39 and 40) when Nextel and Nicalon fibers coated with carbon (Figure 41) and nickel (Figure 42) respectively were incorporated into the cordierite matrix. These coatings effectively reduced or eliminated fiber/matrix interaction, allowing pullout to occur. The carbon coatings were applied by the Nextel fiber manufacturer. Nickel coatings were applied using an electroless plating technique at McDonnell-Douglas Research Labs and were primarily investigated to gain a better understanding of the effectiveness of fiber coatings on reducing fiber/matrix interactions. Coating application times ranged from five to forty minutes; longer plating times produced thicker coatings. Figure 42 represents the effects of a plating time of five minutes.

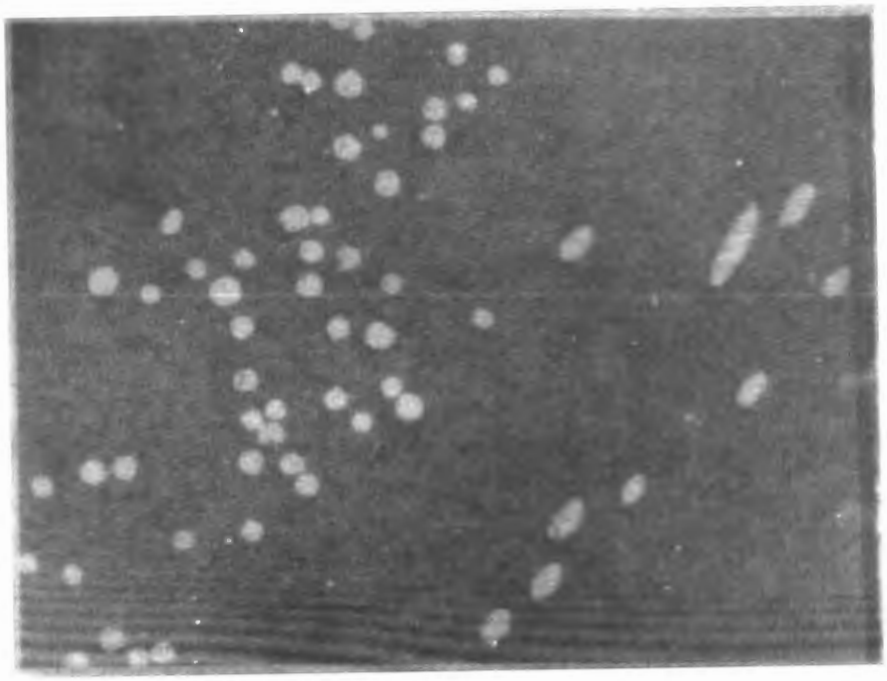

Fig. Optical fractograph Nicalon fiber reinforced cordierite matrix, hot pressed in argon at 950C for 2 minutes, showing brittle fracture.
Bar = 100μm

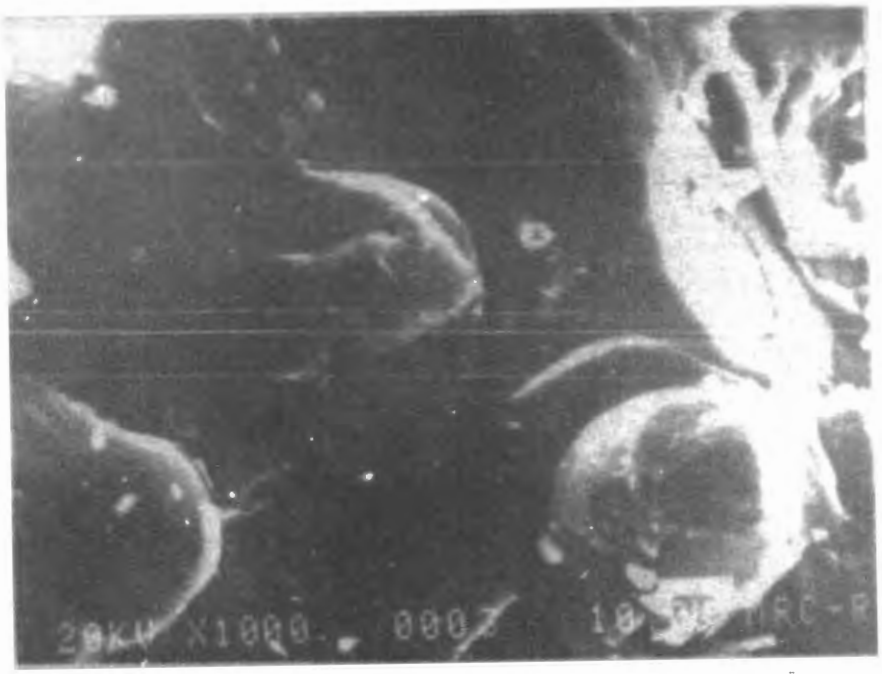

Fig. 36. SEM fractograph depicting hemispherical fracture surfaces surrounding fiber FP in the cordierite matrix, for a specimen hot pressed in argon at 1150C for 15 minutes.

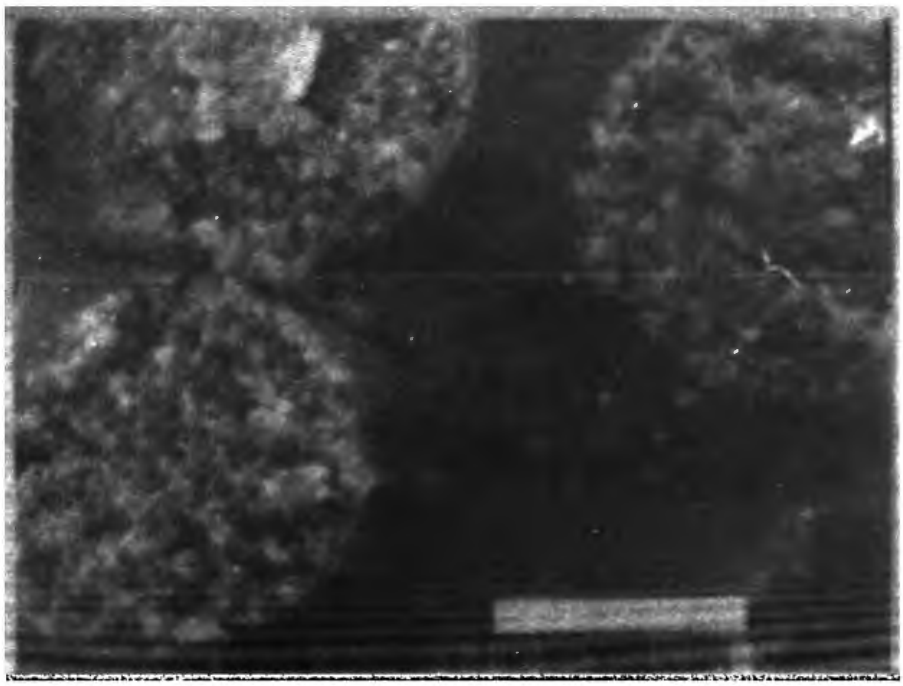

Fig. 37. SEM fractograph of cordierite containing Fiber FP, hot pressed in argon at 1000C for 15 minutes, showing matrix microcracking tangent to fibers.

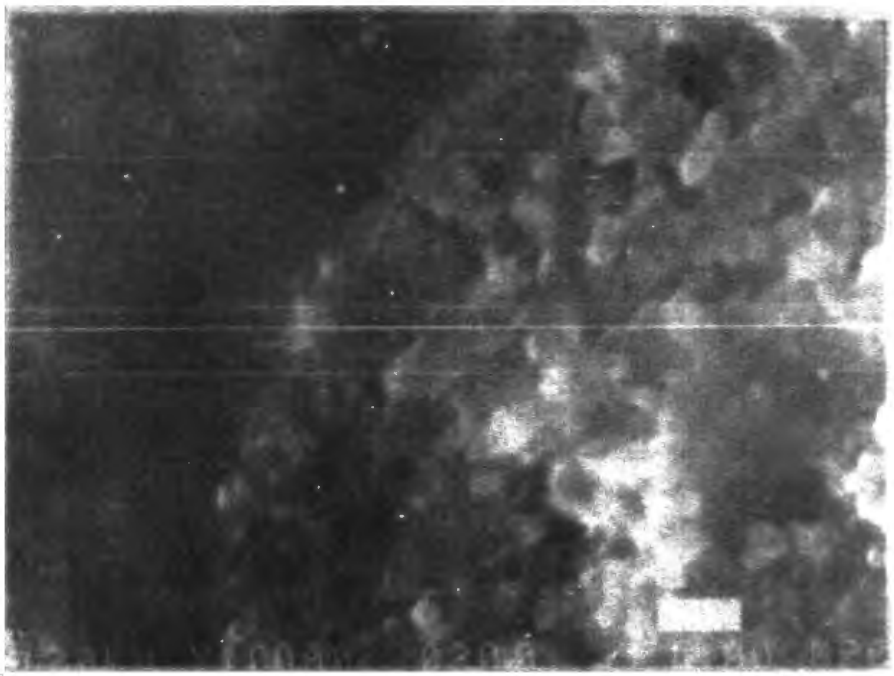

Fig. 38. SEM fractograph depicting the well defined Fiber FP/ cordierite matrix interfacial region in a specimen hot pressed in argon at 1150C for 15 minutes.

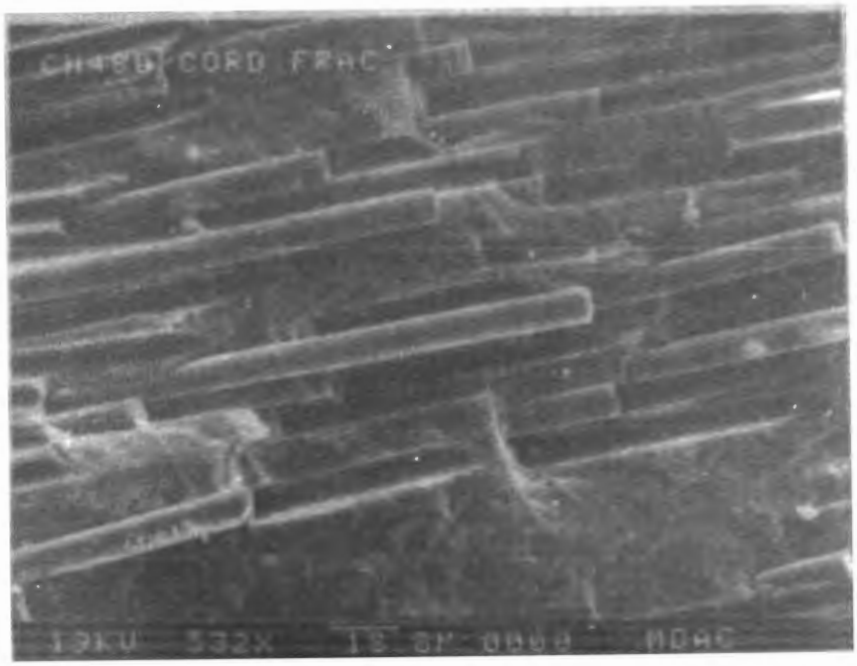

Fig. 39. SEM fractograph of a carbon coated Nextel 480 fiber reinforced cordierite matrix composite, hot pressed in argon at 950C for 1 minute, showing fiber debonding and pullout.

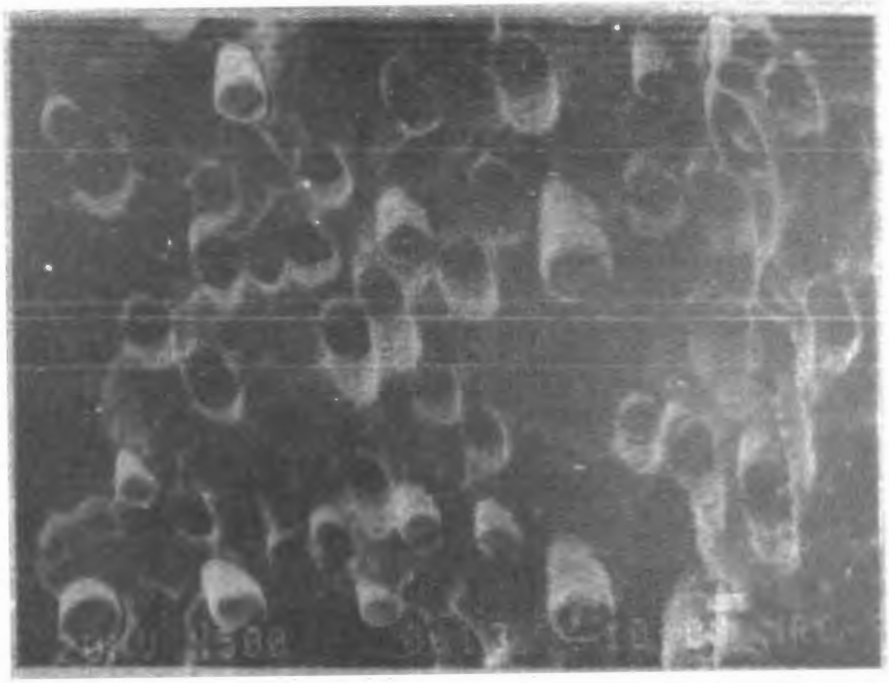

Fig. 40. SEM fractograph of a nickel coated Nicalon fiber reinforced cordierite matrix composite, hot pressed in argon at 1100C for 2 minutes, showing fiber pullout.

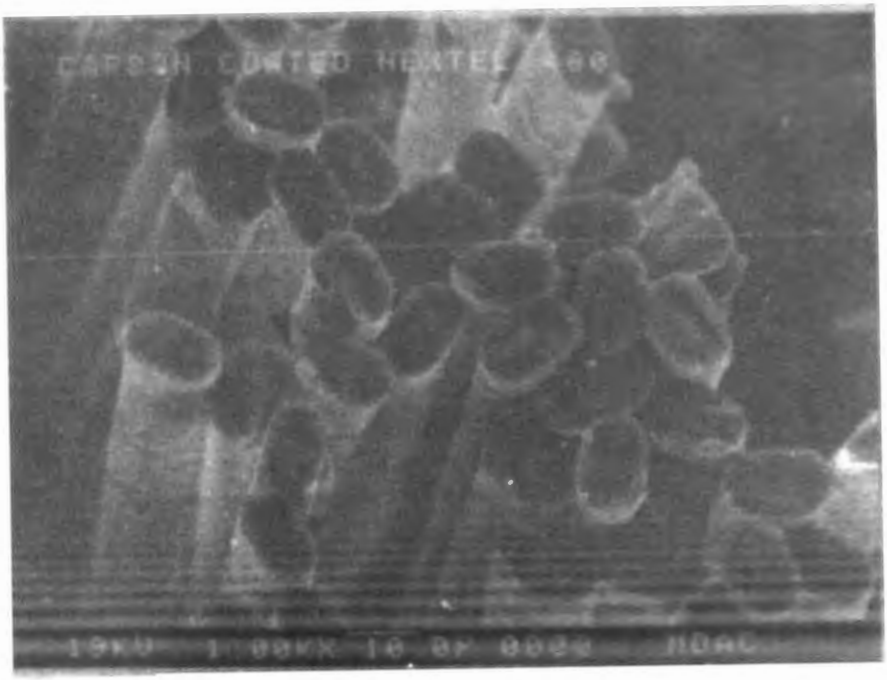

Fig. 41. SEM photomicrograph of carbon coated Nextel 480 fibers.

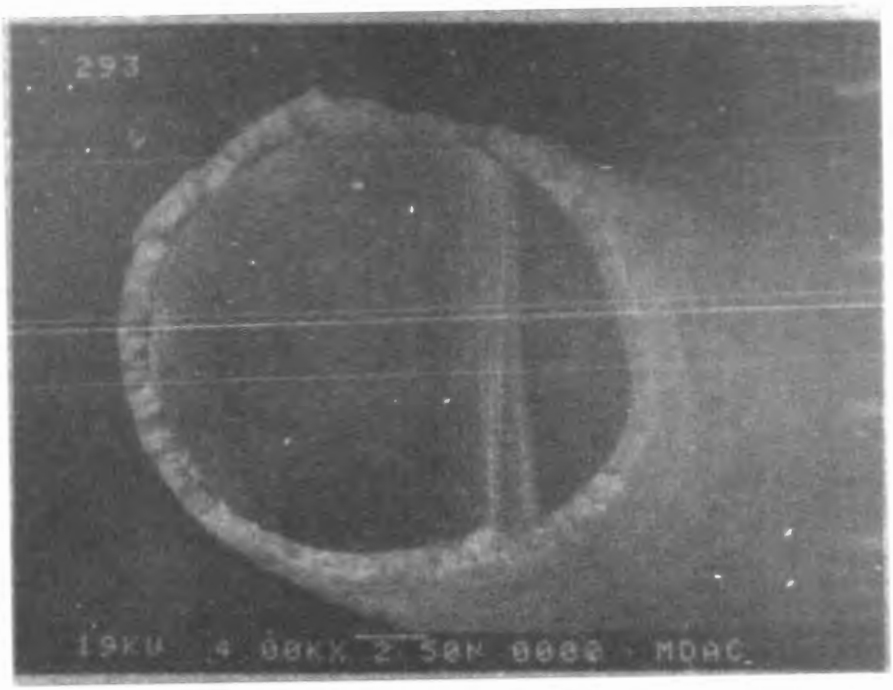

Fig. 42. SEM photomicrograph of a nickel coated Nicalon fiber illustrating a coating thickness of approximately 0.8μm.

Tyranno fiber does not require any coatings because it exhibits pullout when incorporated uncoated into the cordierite matrix. Unlike the behavior Tyranno fiber exhibits in the YAS-7 matrix, mainly that the fiber bonds when hot pressed at low temperature (1000°C) and debonds and pulls out at higher temperature (1150°C), when Tyranno fiber is incorporated into the cordierite matrix fiber debonding and pullout occurs at both of the hot pressing temperatures (Figures 43 and 44).

Table X lists the composite systems investigated, their hot pressing temperatures and the fiber/matrix interaction observed.

D. MECHANICAL TESTING RESULTS

The specimens used for mechanical testing were composed of randomly dispersed chopped fibers, not unidirectionally aligned continuous fibers, so the minimum S/d ratio required to produce In addition, no observations were made as to the failure mechanism of the tested specimens, tensile failure was assumed, for purposes of analysis, and the standard Modulus of Rupture (M.O.R.) equation for three-point flexure of rectangular prisms was used to calculate the strength values listed in Table XI.[85,86]

The observed decrease in strength in tested composite specimens can be attributed to misalignment of the chopped fibers used. Only a small percentage of fibers are parallel to the testing direction and the misaligned fibers would act as stress risers causing a decrease in strength. The low toughness values can also be attributed to a small percentage of crack-bridging fibers. Toughness values reported in the literature for chopped carbon fiber reinforced Pyrex composites are 10 times lower than these values.[53] This may be due to differences in

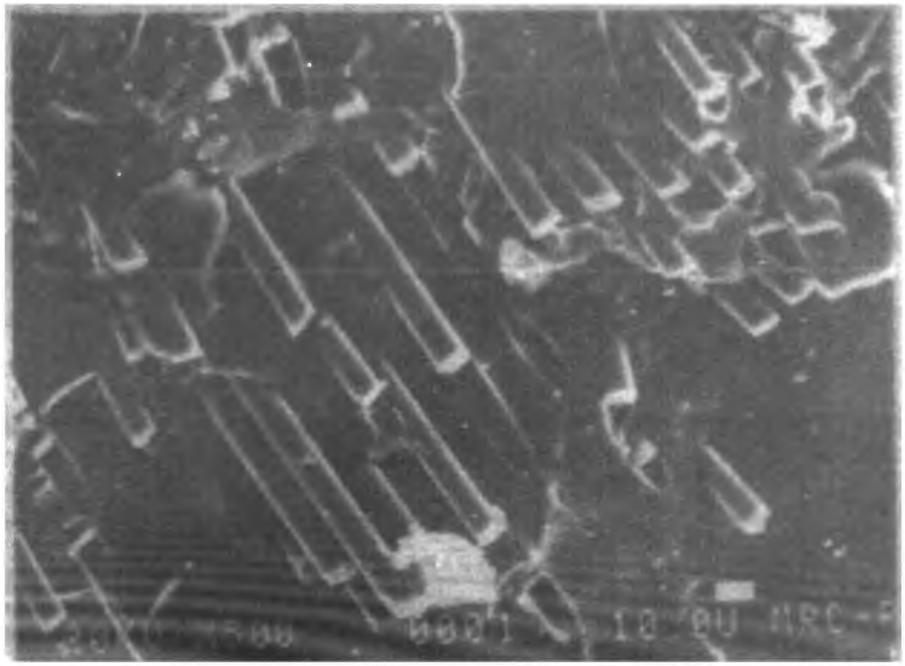

Fig. 43. SEM fractograph of a Tyranno fiber reinforced cordierite specimen, hot pressed in argon at 1000C for 15 minutes, showing fiber debonding and pullout.

Fig. 44. SEM fractograph of a Tyranno fiber reinforced cordierite specimen, hot pressed in argon at 1150C for 15 minutes, showing fiber pullout.

TABLE X

COMPOSITE SPECIMENS WITH YAS-7 OR CORDIERITE MATRIX

Fiber	Fiber Coating	Hot Pressing Temperature (°C)	Fracture Behavior	Figure
YAS-7				
N440	none	1000	Brittle	24
Tyranno	none	1000	Brittle	22
Tyranno	none	1150	Fiber Pullout	25
Fiber FP	none	1000	Brittle	
Fiber FP	none	1150	Brittle	26,27
SCS-6	none	1200	Matrix Cracking	28,29
N480	Carbon	1100*	Fiber Pullout	30,31
N440	SiC	1100	Limited Pullout	32
N440	BN	1100	Limited Pullout	33
Cordierite				
AS-4 (Uni)	none	1000	Fiber Pullout Matrix Cracking	19 20,21
N440	none	1000	Brittle	
Nicalon	none	950	Brittle	35
Nicalon cloth	none	950	Brittle	17
Fiber FP	none	1000	Brittle	37
Fiber FP	none	1150	Brittle	36,38
N480	Carbon	915*	Fiber Pullout	39
Nicalon	Nickel	930	Fiber Pullout	40
Tyranno	none	1000	Fiber Pullout	43
Tyranno	none	1150	Fiber Pullout	44

*Vaccum hot pressed, all other specimens hot pressed in argon.

TABLE XI

MECHANICAL TESTING RESULTS

Material	Average Value	Standard Deviation
M.O.R. Testing (Strength)	(MPa)	
Cast YAS-7	198	42
YAS-7 Matrix	161	30
YAS-7 Heat Treated at 1100°C	186	26
YAS-7 + 10% Nextel	144	19
YAS-7 + 20% Nextel	165	31
YAS-7 + 30% Nextel	108	26
YAS-7 + 20% CCN 480*	123	23
Cordierite Matrix	135	23
Cordierite + 20% CCN 480*	133	19
SENB Testing (Toughness), K_{Ic}	(MPa$\sqrt{m}$)	
YAS-7 + 20% CCN 480*	4.2	2.3
Cordierite + 20% CCN 480*	3.3	0.8
Elastic Modulus (From Bending Data)	(GPa)	
YAS-7 Matrix	171.	30.6
Cordierite Matrix	97.4	14.8

*CCN 480 = Carbon Coated Nextel 480

the matrix materials and the toughness of the matrix without fiber additions. The fibers, although intimately mixed with the matrix, formed clumps which aligned perpendicular to the pressing direction to produce a two-dimensional lamina rather than a three-dimensional random distribution. This clumping would cause two problems: the first problem is the non-uniformity of the dispersion; the second problem is the anisotropy which results from that non-uniform dispersion. The toughness values listed in Table XI were calculated based on S/d ratios of approximately 4 using single edged notched beams (SENB).[86]

The average elastic modulii for cast monolithic YAS-7 and hot pressed monolithic cordierite are 171 GPa and 97.4 GPa, respectively. These values were calculated using ASTM Standard Method C674-81p from the load/deflection curves generated during flexure testing.[85] Raw testing data and sample calculations are presented in Appendix C.

E. CRYSTALLIZATION STUDIES

This study focuses primarily on the utility of YAS-7 as a candidate glass-ceramic matrix for ceramic composites because it has not been previously investigated. Experiments with the cordierite matrix were primarily conducted to help develop the fabrication processes and to provide comparative results when applicable. The scope of this study expanded considerably when experimental results using the YAS-7 matrix material indicated the possibility of a polymorphic phase transformation in the YAS-7 glass-ceramic matrix.

1. Effect of Dopants on the Crystallization of YAS-7. In order to determine the crystallization parameters of the YAS-7 glass, the glass powder was initially doped separately with 2.0% of TiO_2, ZrO_2,

and CaO which are known to be good nucleation agents in other glass systems. DTA was performed on the doped glass powders, but, as illustrated in Figure 45, no effect was observed in the position or size of the crystallization exotherm. The dopant additions did not appear to effect the crystallization of the glass, and no further work was attemted to enhance crystallization of the YAS-7 with nucleation agents.

2. Effects of Heat Treatments on Cast and Hot Pressed YAS-7.

Heat treatments of cast glass slivers (Table VIII) revealed no visual evidence of crystallization. The specimens softened at these heat treatment temperatures and deformed. Hot pressed specimens, determined to be amorphous using powder XRD, were heat treated, but no softening was detected by visual observation up to 1200°C.

The hot pressing of YAS-7 apparently causes an increase in refractoriness of the glass. Hot pressed specimens are light gray in color, probably a result of carbon and/or boron nitride (BN) diffusion into the hot pressed billet during hot pressing. Carbon or BN could act as nucleation sites promoting nucleation and crystallization in the glass, increasing its refractoriness. If only five percent $Y_2Si_2O_7$ (density = 4.6 g/cm^3)[40] crystallized from the glass during hot pressing the density of the resulting hot pressed specimen would be approximately 3.5 g/cm^3. This density corresponds to the measured density of hot pressed specimens. In addition, this small amount of crystalline material would not be detectable with standard powder XRD techniques. Transmission electron microscopy (TEM) would be effective in determining whether the crystallites are actually present and their approximate size.[23]

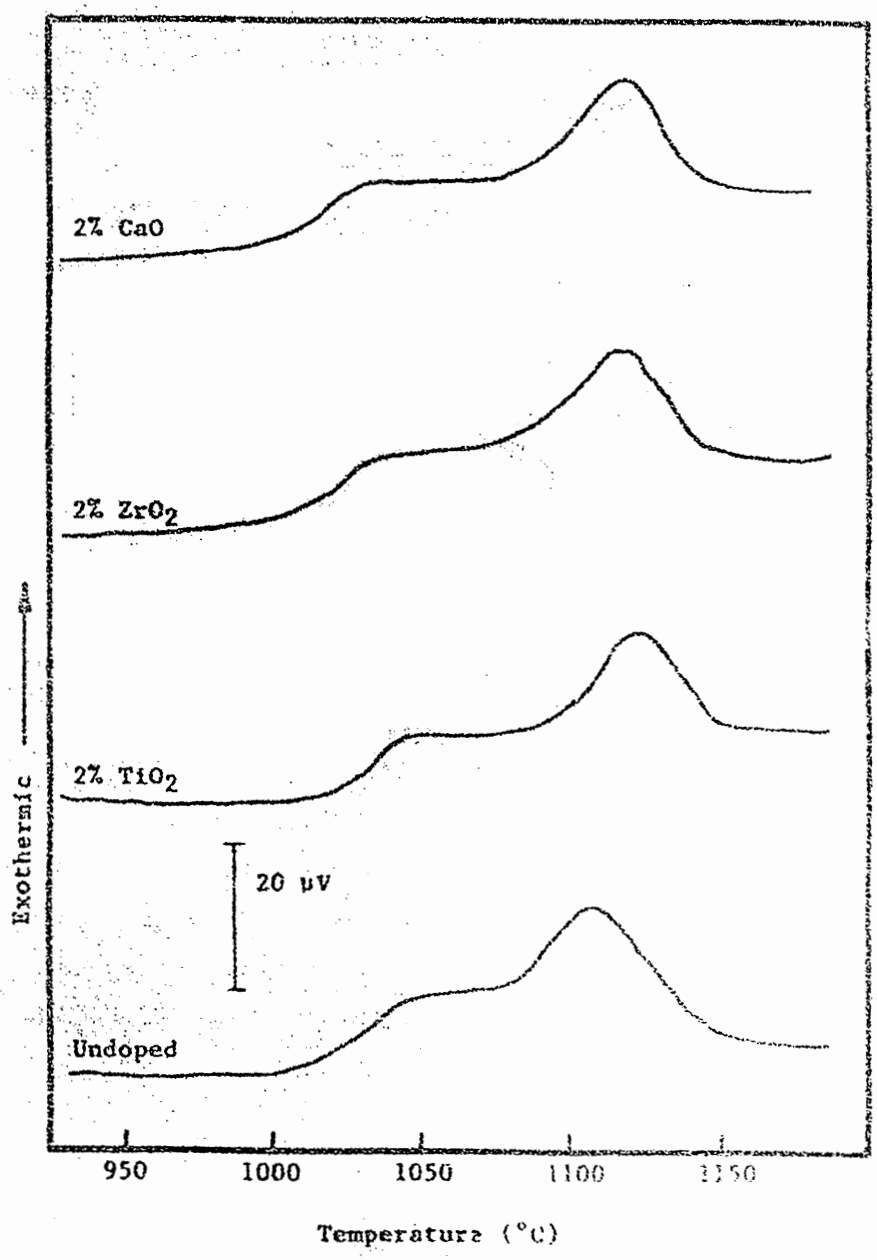

Fig. 45. The effect of dopants on the DTA exotherms associated with the crystallization of YAS-7 glass.

3. C.T.E. Studies and the Polymorphic Transformation. A specimen of cast YAS-7 and a YAS-7 specimen hot pressed at 1000°C for two minutes were each cut into specimens for C.T.E. measurement. Both these specimens generated C.T.E. curves (Figure 46) which show the glass softening point to be approximately 900°C. The slightly concave C.T.E. curve for the hot pressed billet suggests that the specimen contained some residual stress typical of incompletely annealed glass. The dilatometric softening temperatures for these two specimens corresponds with the observed hot pressing behavior of YAS-7.

In keeping with the purpose of this project, to develop ceramic composites, YAS-7 glass powder was mixed with 20% and 30% uncoated Nextel 440 fiber to form specimens for mechanical testing. Two specimens were cut from each hot pressed billet to be used for C.T.E. measurement. Typically, when a glass softens, the dilatometer specimen will first expand as melting begins, then, as melting progresses, soften and deform causing a decrease in length. At approximately 900°C, the specimens appeared to exhibit behavior typical of a glass specimen but instead of deforming, the specimens stopped expanding and exhibited essentially zero thermal expansion between 900°C and 1200°C even though heating continued at a constant rate (Figure 47). At approximately 1200°C both specimens started to deform so the dilatometer run was halted at 1275°C for the specimen containing 20% fiber and 1260°C for the specimen containing 30% fiber. This halt in expansion at 900°C is presumably due to the fibers supporting the dilatometer load when the glass began to soften.

The hot pressed specimen containing 10% Nextel 440 fiber was allowed to continue heating above 1275°C. The 10% specimen then underwent a abrupt expansion of 0.6% over the temperature range of

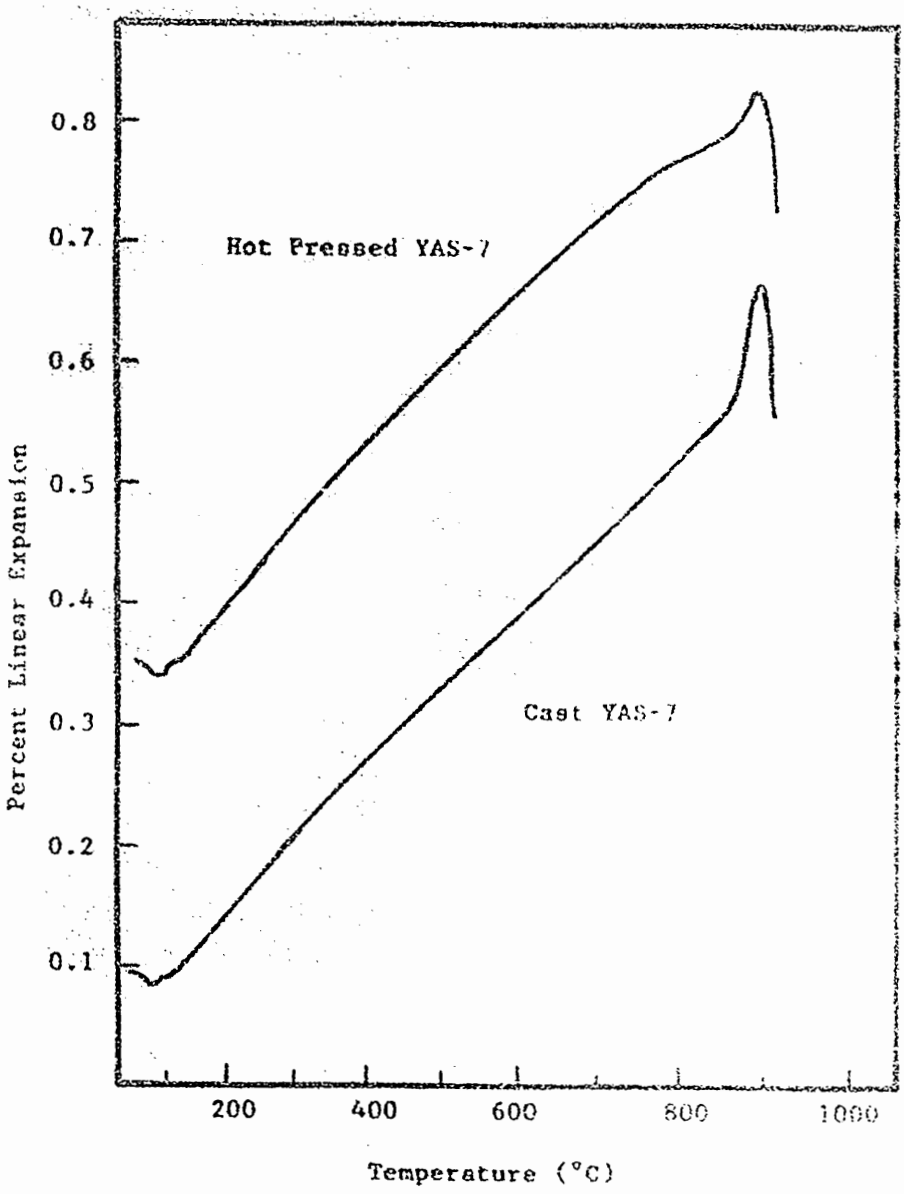

Fig. 46. Thermal expansion curves for cast and hot pressed YAS-7.

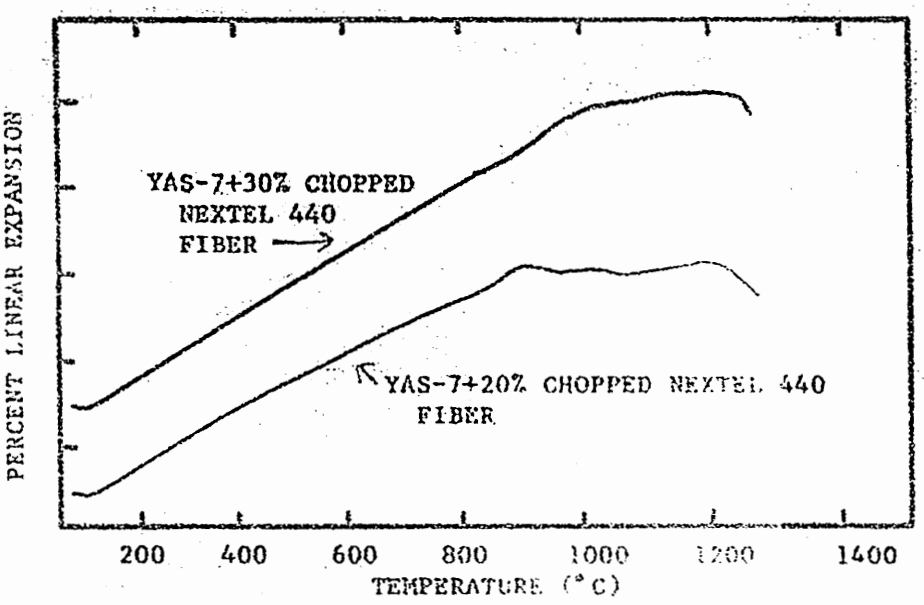

Fig. 47. Thermal expansion curves for YAS-7 containing 20% and 30% Nextel 440 fiber, hot pressed in argon at 980°C and 1000°C, respectively.

1300°C to 1350°C. Identical behavior occurred again in another specimen cut from the same hot pressed billet. Both specimens underwent a permanent expansion of approximately 0.5%. A second test of the previously measured specimen indicated softening beginning at approximately 1150°C, a behavior similar to a viscous solid (Figure 48). The C.T.E. between the first and the second thermal expansion test decreased from 6.3×10^{-6}/°C (400°C to 850°C) to 5.0×10^{-6}/°C (400°C to 1000°C).

a. Discussion of the Abrupt Expansion. Previous work by others on the thermal expansion of composites showed no evidence of such an abrupt expansion.[87-90] Thermal expansions of composites and multiphase systems usually follow the ROM.[17,87-90] Liquid formation due to partial melting of the specimen could result in a volume increase; the liquid formed, however, would probably not be able to support the dilatometer load, and the specimen would deform rather than expand.[91]

Because the C.T.E. is expected to follow the ROM in a multiphase system, if one phase relaxed the overall expansion of the material would assume the C.T.E. of the remaining phase. If the lower C.T.E. material softened, the thermal expansion of the material could suddenly increase. This is not likely to occur in this particular case, however, unless the remaining phase had an extremely high C.T.E. which could then cause the rapid expansion at 1280°C as observed. The only other phenomena which could cause such an abrupt expansion in a material would be a polymorphic phase transformation.[88,91] Large, sudden expansions are often observed during polymorphic transformations such as the α- to β-quartz inversion which is accompanied by a sudden volume expansion of approximately 4.5% at 573°C.[12]

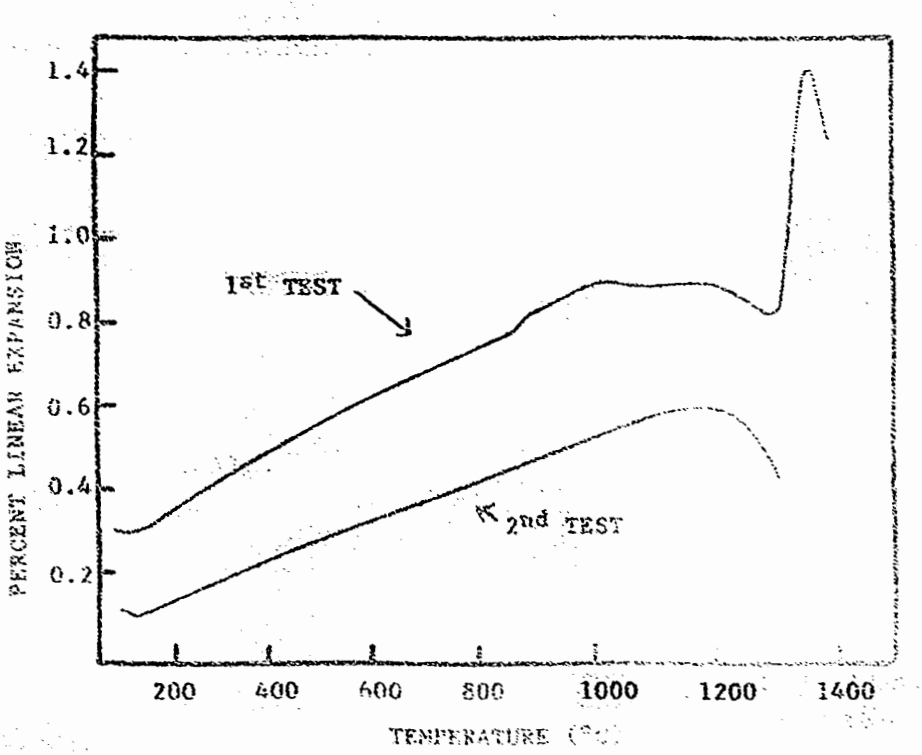

Fig. 48. Thermal expansion curves for YAS-7 containing 10% Nextel 440 fiber, hot pressed in argon at 1010°C.

A specimen of YAS-7, hot pressed at 1000°C for 15 minutes, produced a normal expansion curve when tested in the dilatometer up to 1285°C, expanded 0.86% between 1285°C and 1345°C, deformed 0.06% between 1345°C and 1375°C, expanded another 0.4% between 1375°C and 1390°C, and then began to melt (Figure 49). Visual observation revealed that this specimen had begun to foam on the top surface (Figure 50); since this bloating effect was mainly confined to the surface, it could have been caused by volatilization of carbon or BN inclusions from hot pressing. SEM examination of the exterior of the bloated surface showed needle-like crystals in a smooth porous matrix (Figure 51). Analysis of the crystals and the surrounding matrix using EDAX showed the crystals to be composed mainly of an yttrium silicate; the matrix was composed primarily of an aluminum silicate. SEM analysis of the unbloated, as hot pressed surface (Figure 52), showed a much different microstructure than that of the foamed surface.

Another specimen of YAS-7, hot pressed at 1000°C for 15 minutes, was tested in the dilatometer; this specimen abruptly expanded at 1270°C, the dilatometer was shut off at 1300°C, and the cooling curve was recorded (Figure 53). The C.T.E. of this specimen on cooling was 5.8×10^{-6}/°C (350°C to 1150°C) compared to the C.T.E. of 7.2×10^{-6}/°C (400°C to 1000°C) on heating. When retested, this specimen exhibited behavior similar to the retested specimen of YAS-7 containing 10% Nextel 440 fiber: the C.T.E. curve was linear and has a C.T.E. of 5.3×10^{-6}/°C up to 1200°C, at which point it began to soften (Figure 53). Powder XRD of the hot pressed billet and the C.T.E. specimen after this second test revealed that the crystalline phases α-$Y_2Si_2O_7$ and mullite originally present in the hot pressed specimen had changed to β-$Y_2Si_2O_7$ and mullite.

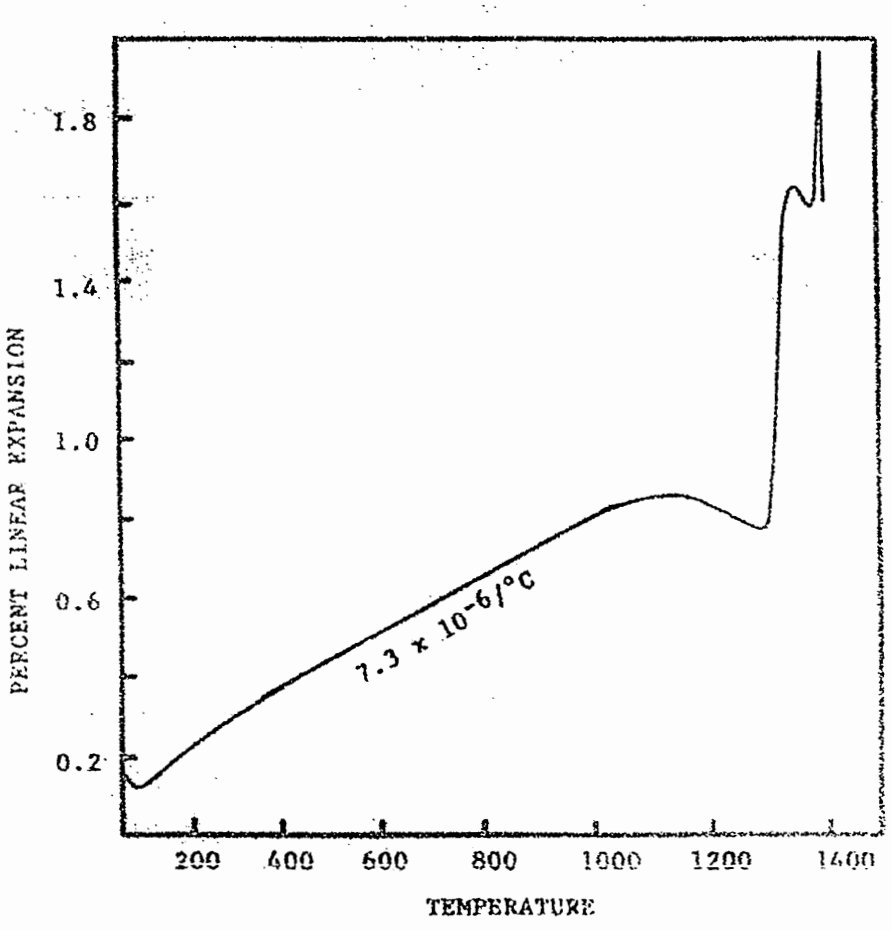

Fig. 49. Thermal expansion curves for monolithic YAS-7 glass-ceramic, hot pressed in argon at 1000°C for 15 minutes.

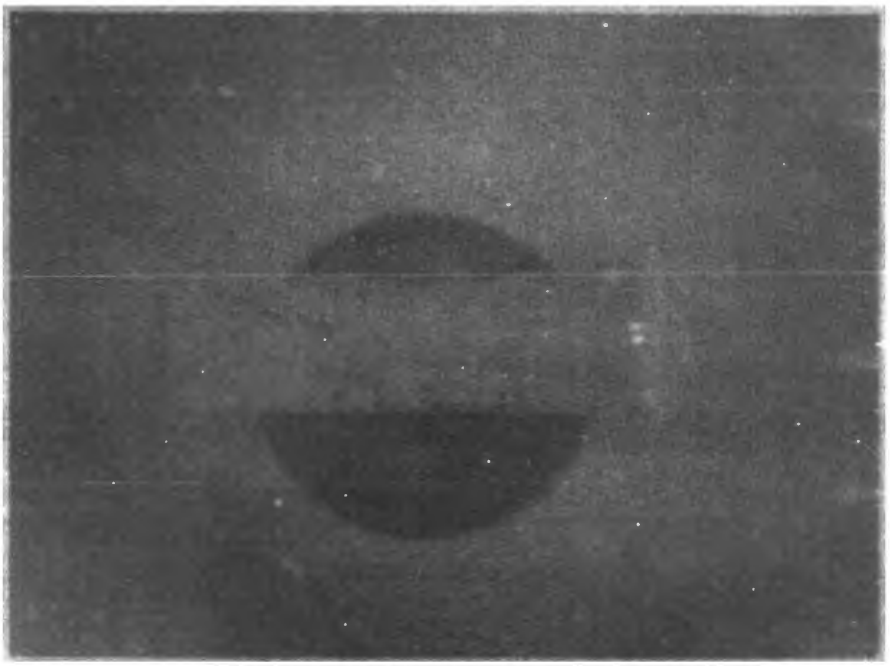

Fig. 50. Photomicrograph of the bloated thermal expansion specimen, which produced the thermal expansion curve illustrated in Figure 49.
Specimen Length = 1 inch

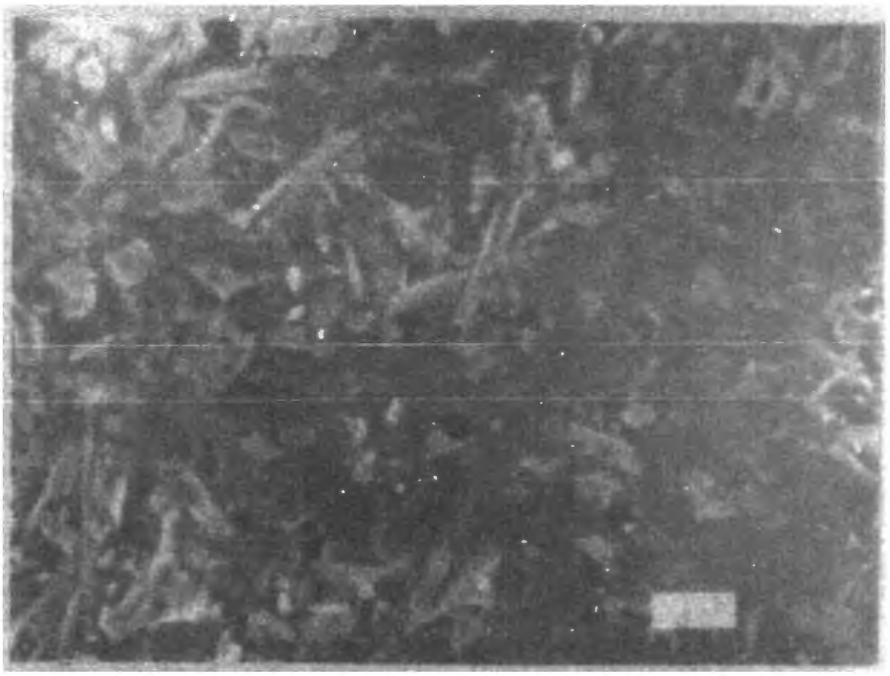

Fig. 51. SEM photomicrograph of the bloated surface of the specimen depicted in Figure 50.
Bar = 10μm

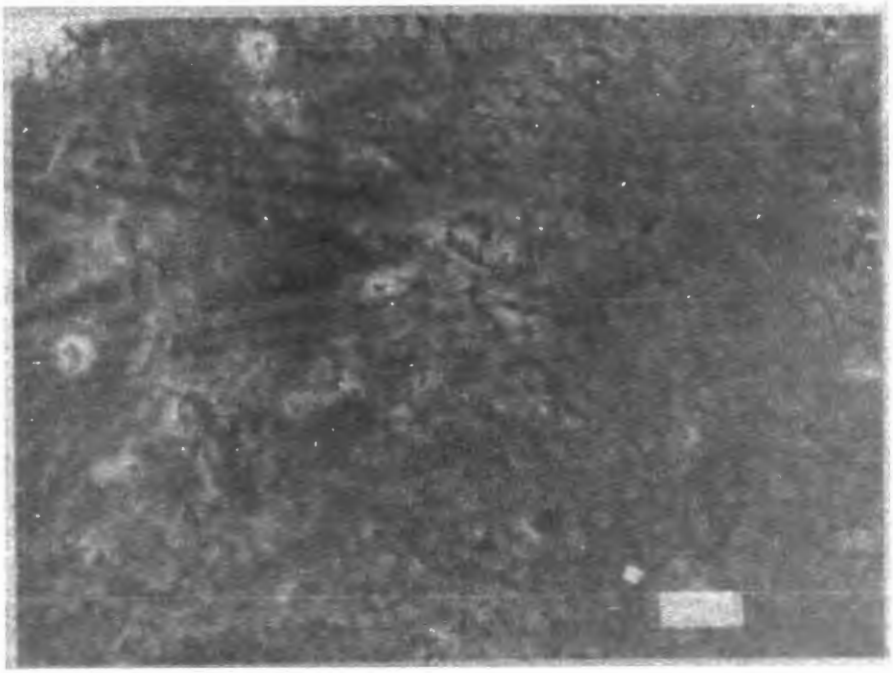

Fig. 52. SEM photomicrograph of the hot pressed, unbloated surface of the specimen depicted in Figure 50.
Bar = 10μm

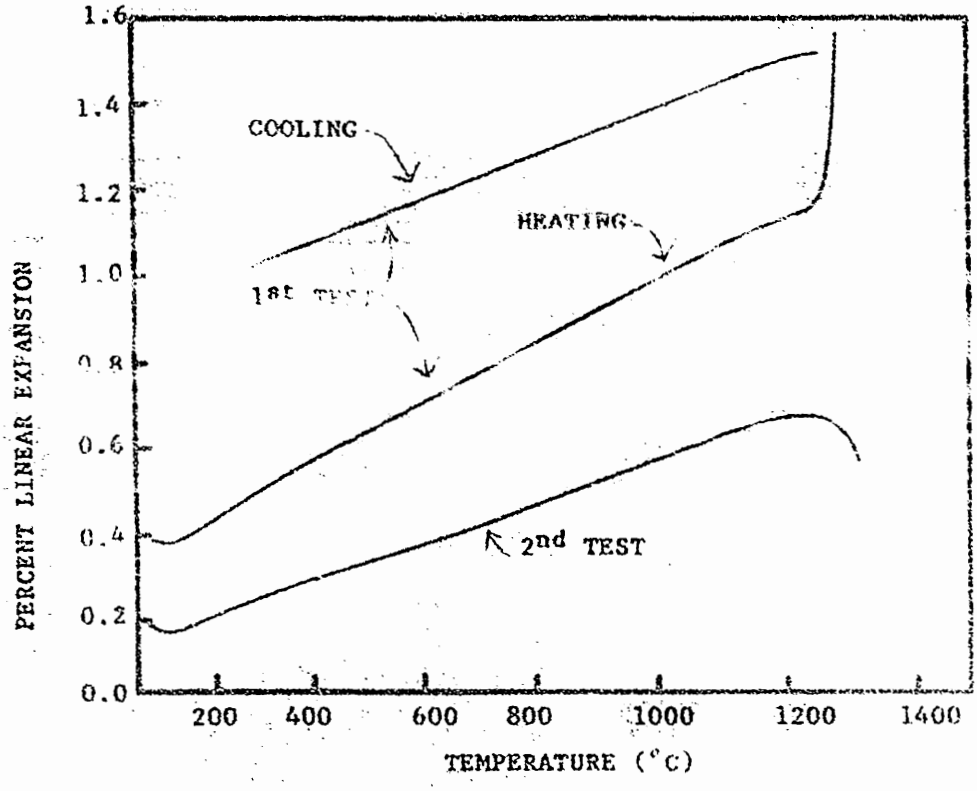

Fig. 53. Thermal expansion curves for monolithic YAS-7 specimen, hot pressed in argon at 1000°C for 15 minutes.

A specimen of YAS-7, hot pressed at 1300°C for 15 minutes, yielded a C.T.E. curve similar to the retested specimen in Figure 53. A second test of this specimen showed a 0.48% expansion beginning at 1345°C, illustrated in Figure 54. This specimen appeared similar to the specimen depicted in Figure 50. Examination of the dilatometer apparatus showed the alumina specimen holder was off-center in the furnace which could have resulted in a thermal gradient, heating the top of the specimen more rapidly than the bottom. This could explain the bloating observed in the upper surface of the specimen. Powder XRD of YAS-7, hot pressed at 1300°C for 15 minutes, indicated it contained mullite and β-$Y_2Si_2O_7$. The C.T.E.s for the above specimens and the identified crystal phases are listed in Table XII.

b. DTA Analysis. To determine whether a polymorphic phase transformation was occurring in the YAS-7 glass at or around 1300°C, DTA was performed on a small block of hot pressed YAS-7 plus 10% Nextel and on a crushed specimen from the same hot pressed billet. Comparison of the DTA curves of hot pressed YAS-7 plus 10% Nextel fiber and YAS-7 glass show that fiber additions cause a small decrease in the crystallization temperature (Figure 55). The position of the crystallization peak for the specimen containing fiber was not affected by crushing the specimen, indicating that the YAS-7 glass is not sensitive to surface crystallization effects. A change of slope which occurred at approximately 1280°C could correspond to the polymorphic phase transformation, particularly if the transformation does not require or produce heat.[24] Melting of the DTA specimen begins at 1360°C and is denoted by a sharp endothermic dip. A second DTA measurement of the crushed specimen showed no exothermic or endothermic reactions up to 1350°C, the temperature at which the test

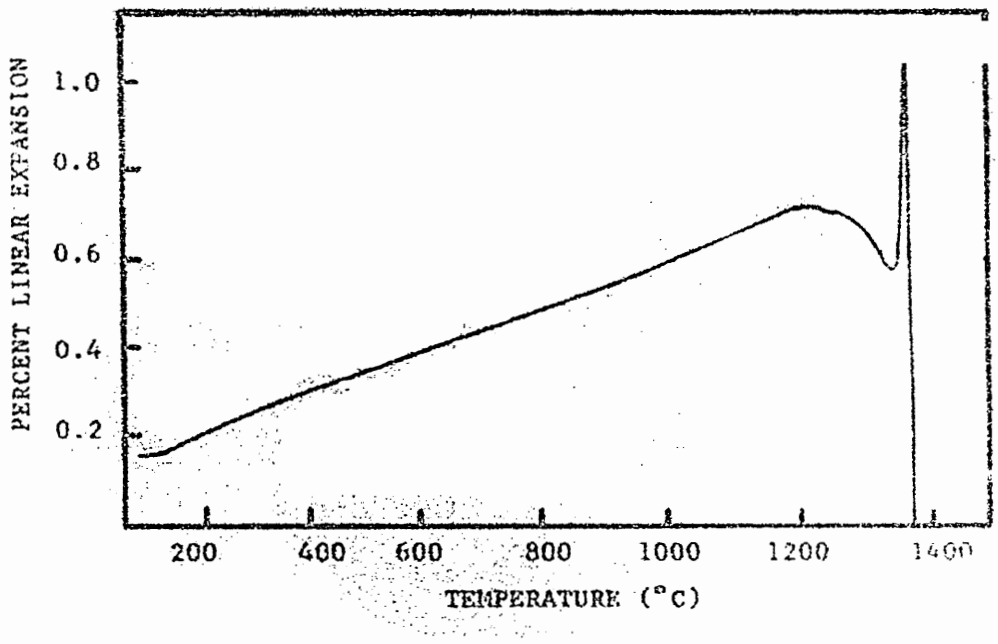

Fig. 54. Thermal expansion curves for monolithic YAS-7 specimen, hot pressed in argon at 1300°C for 15 minutes.

TABLE XII

YAS-7 C.T.E VALUES AND CRYSTALLIZATION PRODUCTS

Specimen	C.T.E. (10^{-6}/°C)	Temperature Range (°C)	Maximum Temp. (°C)	Crystalline Phases Before	After	Figure
Cast	6.31	350-800	915	Amorphous		46
HP	6.17	400-700	915	Amorphous		46
+20% N440	6.33	400-700	1275	α-Y·2S		47
+30% N440	7.2	550-900	1265	α-Y·2S		47
+10% N440						
(Test 1)	6.33	400-850	1385	α-Y·2S		48
(Test 2)	5.03	400-1000	1300			48
HP at 1000°C	7.3	500-1000	1395	α-Y·2S,3A·2S	β-Y·2S,3A·2S	49
HP at 1000°C						
(Test 1 Heat)	7.15	400-1000	1300	α-Y·2S,3A·2S		53
(Test 1 Cool)	5.83	350-1150			β-Y·2S,3A·2S	53
(Test 2 Heat)	5.25	700-1000	1320	β-Y·2S,3A·2S	β-Y·2S,3A·2S	53
HP at 1300°C	4.56	400-900	1370	β-Y·2S,3A·2S		54

Y·2S = $Y_2Si_2O_7$
3A·2S = Mullite

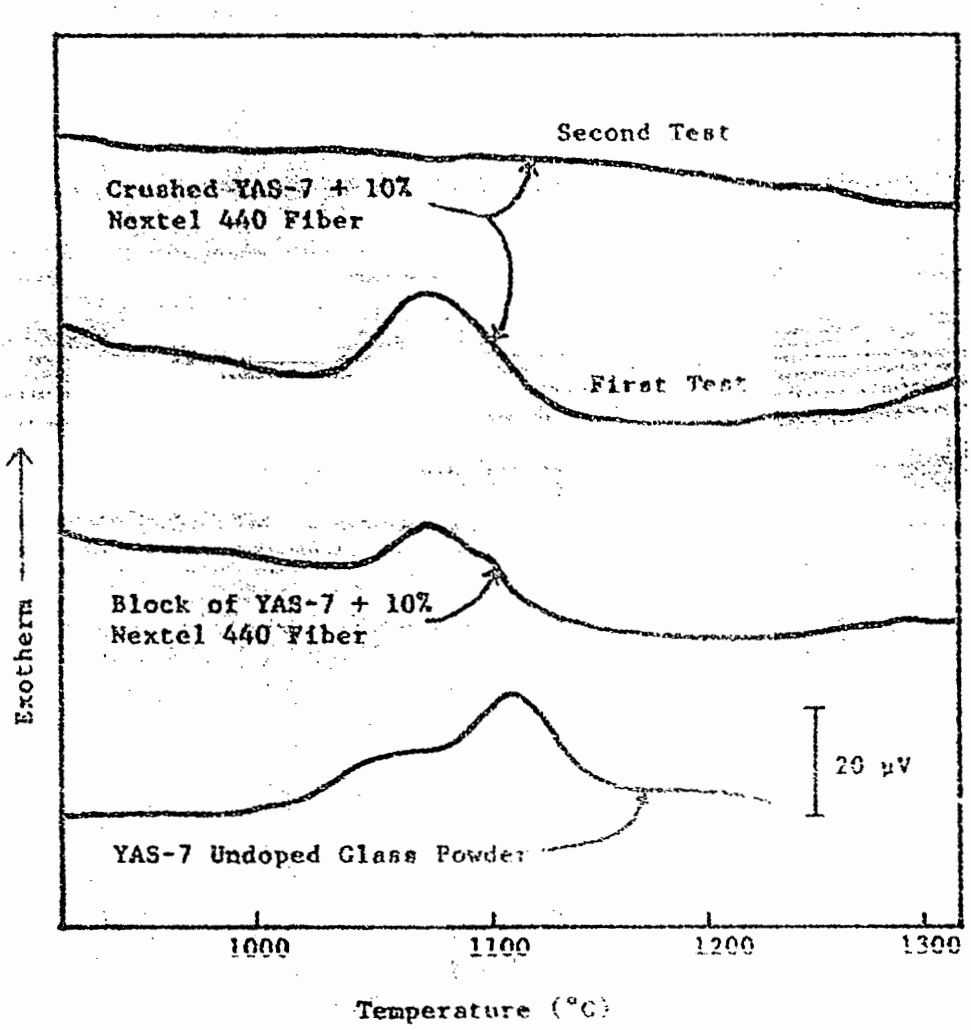

Fig. 55. DTA curves for undoped YAS-7 powder and hot pressed YAS-7 containing 10% Nextel 440 fiber, bulk and crushed specimens.

was terminated. DTA was also performed on a specimen of Nextel 440 fiber to determine if the fiber is thermodynamically stable in air up to 1300°C. No reactions were observed.

c. The Polymorphic Phase Transformation. A previous study on the crystallization of YAS-7 showed the crystallization products of YAS-7 to be β-$Y_2Si_2O_7$, γ-$Y_2Si_2O_7$, and $SiAl_2O_5$, or sillimanite.[92] However, the crystallization temperatures used in that study were below the reported transformation temperatures for α- to β-$Y_2Si_2O_7$ and β- to γ-$Y_2Si_2O_7$ of 1225°C and 1445°C respectively.[41-45] The formation of sillimanite only occurs under very rigid temperature and pressure conditions, and it is doubtful that these conditions could have occurred during the heat treatment of YAS-7.[93] Therefore, the formation of sillimanite is highly unlikely and the aluminosilicate phase is more probably mullite ($Si_2Al_6O_{13}$); the XRD patterns for sillimanite and mullite are very similar, and one can easily be mistaken for the other. Previous work by others with $Y_2Si_2O_7$ describes the α- to β-$Y_2Si_2O_7$ polymorphic phase transformation to occur at 1225°C (Table I);[41-45] there is no mention, however, whether this transformation is a displacive transformation and as such could account for the large expansion which begins at 1280°C. The transformation is also described as reversible in previous work,[41-45] but is not observed as reversible in this study. If the observed expansion is due to the polymorphic phase transformation of α-$Y_2Si_2O_7$ to β-$Y_2Si_2O_7$, it is possible that the Al_2O_3 in the YAS-7 glass is acting as a dopant in the structure of the $Y_2Si_2O_7$ thereby shifting the transformation temperature upwards from 1225°C to 1280°C.

The compound $Y_2Si_2O_7$ was fabricated using hydrothermal processing techniques from reagent grade yttrium nitrate and TEOS. The raw

chemicals were put into solution using ethanol and gently heated until gelling occurred. The material was then dried at 110°C for three days then heat treated at 500°C for 24 hours to remove the organics and nitrates. The resulting powder was determined to be amorphous using powder XRD techniques. DTA showed an exothermic peak associated with crystallization to begin at 960°C with the maximum occurring at 1050°C. At 1200°C an endothermic discontinuity began which ended at 1243°C, another exothermic reaction began at 1420°C and the last reaction, an exothermic discontinuity, occurred at 1535°C (Figure 56). These last three reactions correspond to the polymorphic transformation temperatures of 1225°C, 1445°C, and 1535°C as reported in the literature.[41,42] A specimen for thermal expansion testing measuring 1/4" x 1/4" x 1-1/4" was compacted and placed in a small furnace to sinter. The specimen was heated at 900°C for 5 hours,; the temperature increased to 1000°C and held for 5 hours, then was increased to 1100°C and held for 12 hours. It was hoped that the material, which was amorphous, would sinter to sufficient strength to use as a thermal expansion specimen. When the specimen was examined after holding for 12 hours at 1100°C the specimen had disintegrated into a fine powder. Powder XRD showed the specimen to be pure α-$Y_2Si_2O_7$. It appears that the crystallization causes a change in volume which is sufficient to destroy the specimen.

Using the unit cell volumes[41] for α- and β-$Y_2Si_2O_7$ a volume expansion of 6.66% was calculated for the phase transformation. The linear expansion resulting from the phase transformation for a rectangular prism of $Y_2Si_2O_7$ was calculated assuming 100% conversion of α- to β-$Y_2Si_2O_7$. From this value, data from the YAS phase diagram and the percentage of the abrupt expansion from the C.T.E. of the

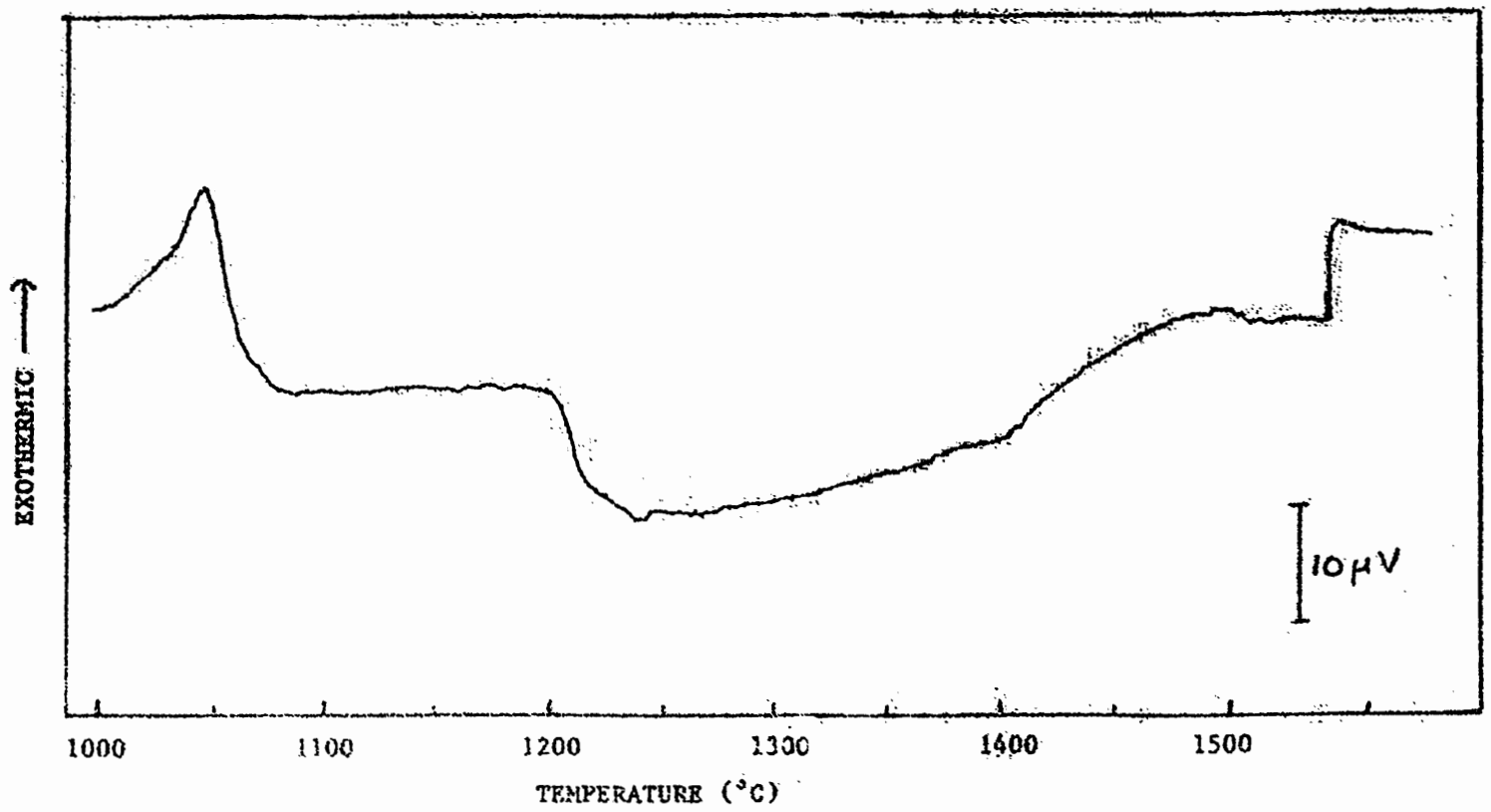

Fig. 56. DTA curve of yttrium diorthosilicate prepared using hydrothermal processing techniques.

YAS-7 specimen (Figure 49), hot pressed at 1000°C, the weight percentages of crystalline phases were calculated to be 47.1 weight % β-$Y_2Si_2O_7$, 24.1 weight % $3Al_2O_3.2SiO_2$ (mullite), and 5.7 weight % Al_2O_3 with the remainder (23.1 weight %) to be a glass of composition YAS-7. This correlates well with the crystalline phases identified with powder XRD and the observed peak intensities. These calculations are presented in Appendix D.

4. Effect of Hot Pressing on the Matrix Crystallization. Powder XRD analysis of hot pressed YAS-7 matrices revealed that if the specimens were held at a maximum temperature below 1150°C for a short time, i.e. less than three minutes, the specimens would remain X-Ray amorphous. SEM analysis of these specimens showed a bi-phase material which appeared to have glassy inclusions in a crystalline matrix (Figure 57). Holding the YAS-7 glass under pressure at the maximum hot pressing temperature for approximately 15 minutes will cause YAS-7 to crystallize. Ideally, the YAS-7 should be hot pressed at 1300°C to allow the α- to β-$Y_2Si_2O_7$ polymorphic phase transformation to occur while in the confines of the hot press, thereby stabilizing the matrix and allowing YAS-7 matrix composites to be utilized up to 1200°C.

Hot pressing SG-266M for 15 minutes at temperatures from 950°C to 1250°C causes SG-266M to crystallize to α-cordierite. SEM analysis indicates that the fracture surface of monolithic SG-266M contains multiple fractures following the blocky grain structure; the material appears well densified with very little porosity (Figures 58 and 59). DTA analysis showed that doping SG-266M separately with 2.0% TiO_2 and ZrO_2 resulted in a considerable change in the exothermic peaks associated with crystallization (Figure 60). With the discovery that the cordierite matrix would readily crystallize through the use of longer hot pressing times, additional work with dopants was suspended.

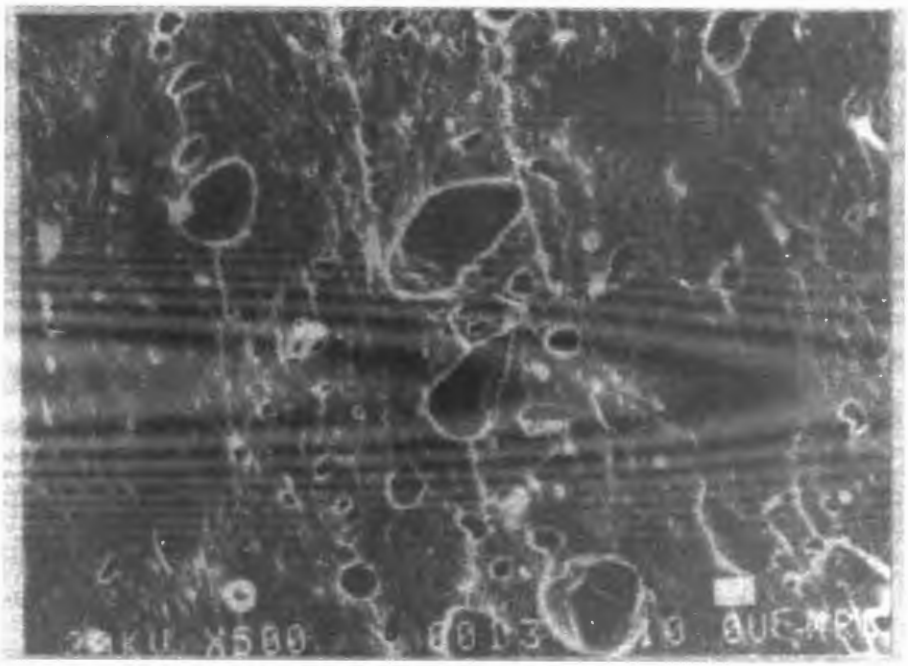

Fig. 57. SEM fractograph showing glassy inclusions in monolithic YAS-7, hot pressed in argon at 1000C for 15 minutes.

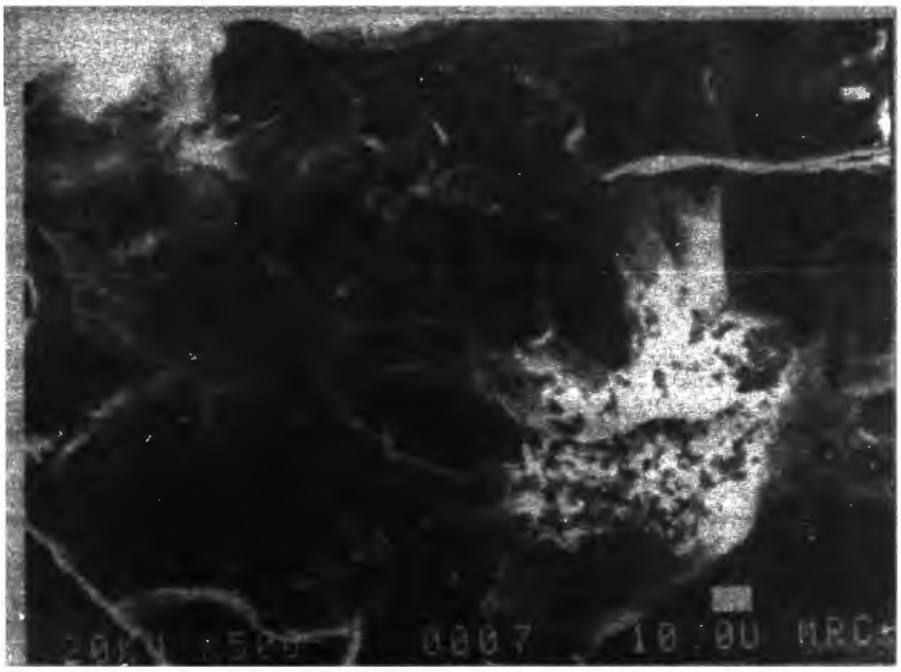

Fig. 58. SEM fractograph of monolithic cordierite glass-ceramic, hot pressed in argon at 950C for 15 minutes.

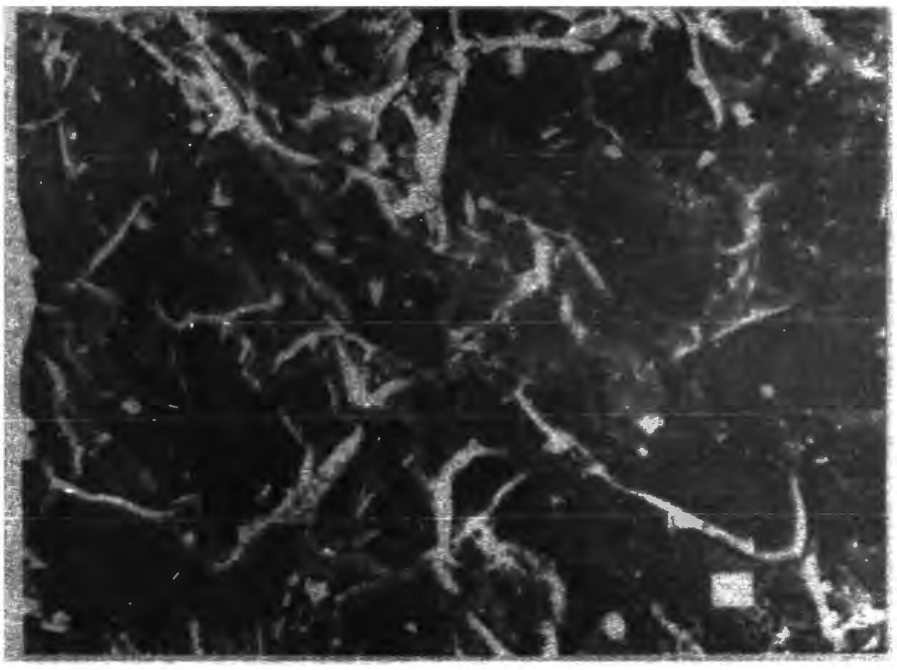

Fig. 59. SEM fractograph of monolithic cordierite glass-ceramic, hot pressed in argon at 1250C for 15 minutes.

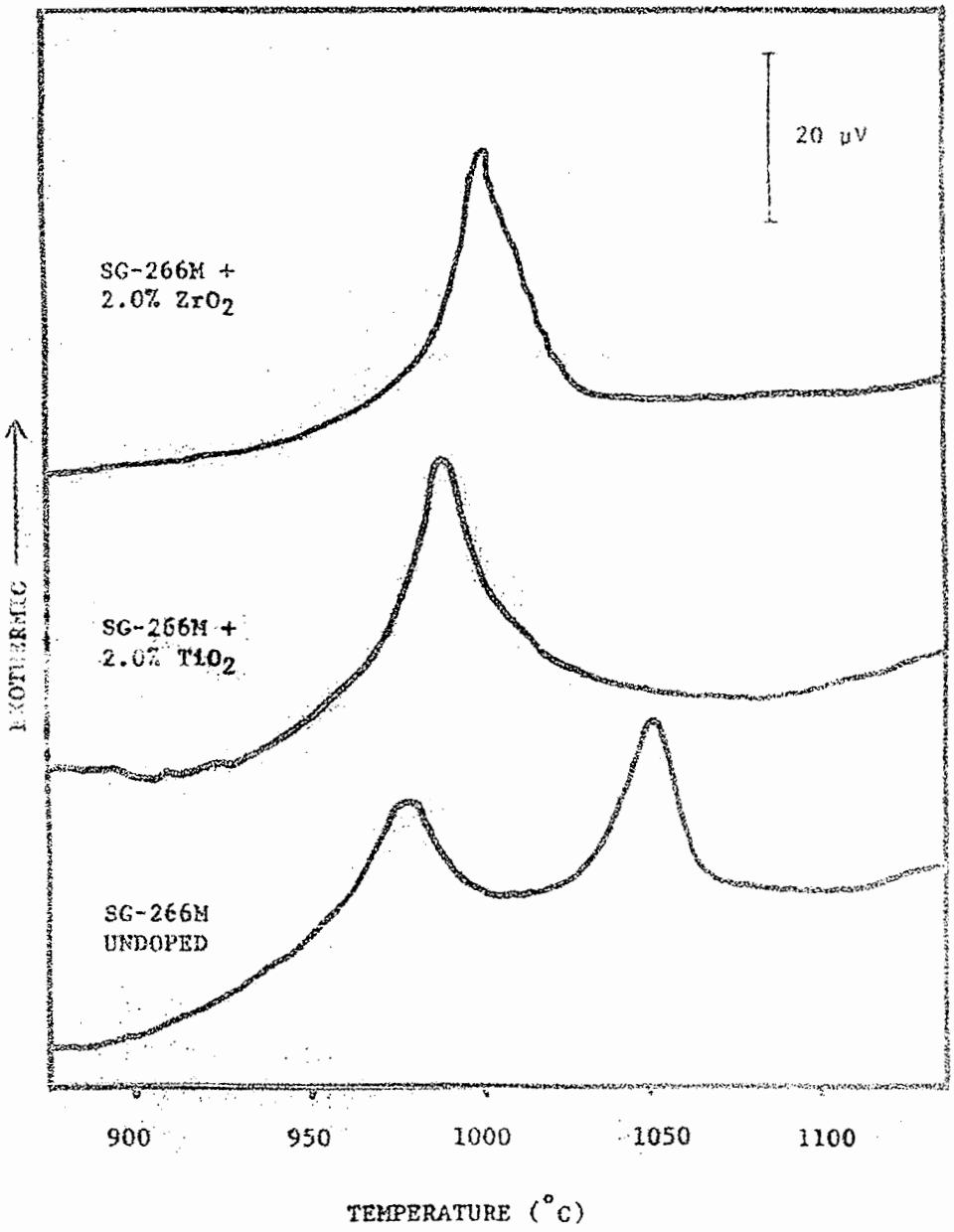

Fig. 60. The effect of dopants on the DTA exotherms associated with the crystallization of cordierite glass.

V. SUMMARY OF RESULTS AND CONCLUSIONS

A. PROCESSING

Techniques were developed for the production of discontinuous fiber reinforced composites using a slurry method and a roller casting method. These techniques provided specimens for determining the extent of fiber/matrix interaction as a function of hot pressing temperature, and for determining the effectiveness of using various fiber coatings to reduce fiber/matrix interaction. Roller casting methods produced promising results for the fabrication of large two dimensionally orientated chopped fiber laminas. A filament winder was designed and built to facilitate the fabrication of unidirectional lamina prepregs.

The optimum hot pressing parameters were determined for the YAS-7 and cordierite matrices. Dense specimens were produced at hot pressing temperatures as low as 980°C and 915°C for the YAS-7 and the cordierite matrix, respectively. The optimum densification pressure was determined to be 3.5 MPa (500 psi) and higher densification pressures were deemed unneccessary. Hot pressing specimens in an argon atmosphere produced satisfactory results and vacuum hot pressing did not show any significant advantages.

B. COMPOSITE SPECIMENS

Specimens fabricated with uncoated Nextel, Nicalon, Fiber FP, and SCS-6 exhibited brittle fracture due to fiber/matrix interactions and chemical bonding. Coatings of carbon, BN, nickel, and silicon carbide reduced fiber/matrix interaction to allow fiber debonding and pullout.

Uncoated Tyranno fiber exhibited fiber debonding and pullout when incorporated into the cordierite matrix at both hot pressing temperatures (1000°C and 1150°C). Tyranno fiber bonded to the YAS-7 matrix at low temperature (1000°C) producing brittle fracture but debonded and pulled out at a higher bonding temperature (1150°C).

Discontinuous fiber reinforced composite specimens exhibited lower strengths than the monolithic matrix specimens, when tested in flexure, presumably due to misalignment of the reinforcing fibers in the composite specimens. It is expected that optimum composite mechanical properties will only be realized through the use of unidirectionally aligned continuous fibers. The elastic moduli, calculated from flexure data, of monolithic YAS-7 and cordierite were 171 GPa and 97.4 GPa, respectively.

C. CRYSTALLIZATION OF THE GLASS-CERAMIC MATRICES

Differential thermal analysis showed that dopant additions do not affect the crystallization of the YAS-7 glass, but greatly affect the crystallization of the cordierite glass. Fiber additions did affect the crystallization of YAS-7 and also appear to act as porosity sinks causing a dramatic decrease in the YAS-7 matrix porosity during hot pressing. Hot pressing also appears to increase the high temperature dimensional stability of the YAS-7 glass provided the glass is not under an applied load. The glass remains X-ray amorphous when hot pressed below 1050°C for short times, i.e. 2 minutes or less.

Hot pressing greatly enhances crystallization in both the cordierite and the YAS-7 matrices when the specimens are held in the hot press at the maximum hot pressing temperature for 15 minutes. Powder XRD was used to identify the crystalline phases formed in the

glass-ceramics. Cordierite crystallizes to α-cordierite. YAS-7 crystallizes to mullite and α-$Y_2Si_2O_7$ when hot pressed at or below 1250°C and crystallizes to mullite and β-$Y_2Si_2O_7$ when hot pressed at 1300°C.

An abrupt expansion of approximately 0.8% begins at 1280°C, detected during thermal expansion measurements of hot pressed YAS-7. This expansion is due to the displacive polymorphic phase transformation of α-$Y_2Si_2O_7$ to β-$Y_2Si_2O_7$ which, although listed as reversible in the literature, was not observed to be reversible in this study. The shift of transformation temperature from 1225°C to 1280°C may be due to alumina, present in the YAS-7 glass, acting as a dopant in the $Y_2Si_2O_7$ structure. The C.T.E. decreases from 7.2 x 10^{-6}/°C to 5.3 x 10^{-6}/°C as a result of the transformation. Attempts to fabricate a specimen and measure the thermal expansion behavior of the $Y_2Si_2O_7$ phase alone were unsuccessful. If YAS-7 is hot pressed at 1300°C, β-$Y_2Si_2O_7$ and mullite result and the matrix is dimensionally stable up to 1200°C.

D. ADDITIONAL DISCUSSION ON THE YAS PHASE DIAGRAM

Figure 61 illustrates the composition triangles determined using the invariant points and their respective equilibrium phases on the YAS phase diagram.[37] The composition YAS-7 lies in the Y-2S, 3A-2S, 2Y-3S composition triangle and therefore, under equilibrium conditions would contain those three compounds. It is also evident that there would be approximately equal amounts of Y-2S and 2Y-3S judging from the position of YAS-7 inside the composition triangle. The binary phase diagram (Figure 62) shows that 2Y-3S decomposes to Y-S and Y-2S at 1650°C and would not be stable at room temperature. In the YAS phase diagram, alumina must somehow stabilize the 3Y-2S structure to

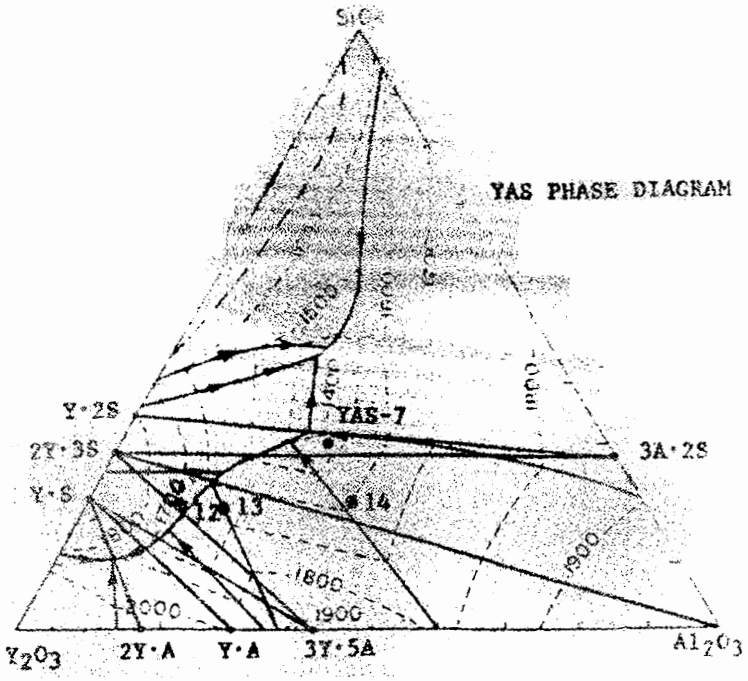

Fig. 61. Composition triangles in the YAS system.

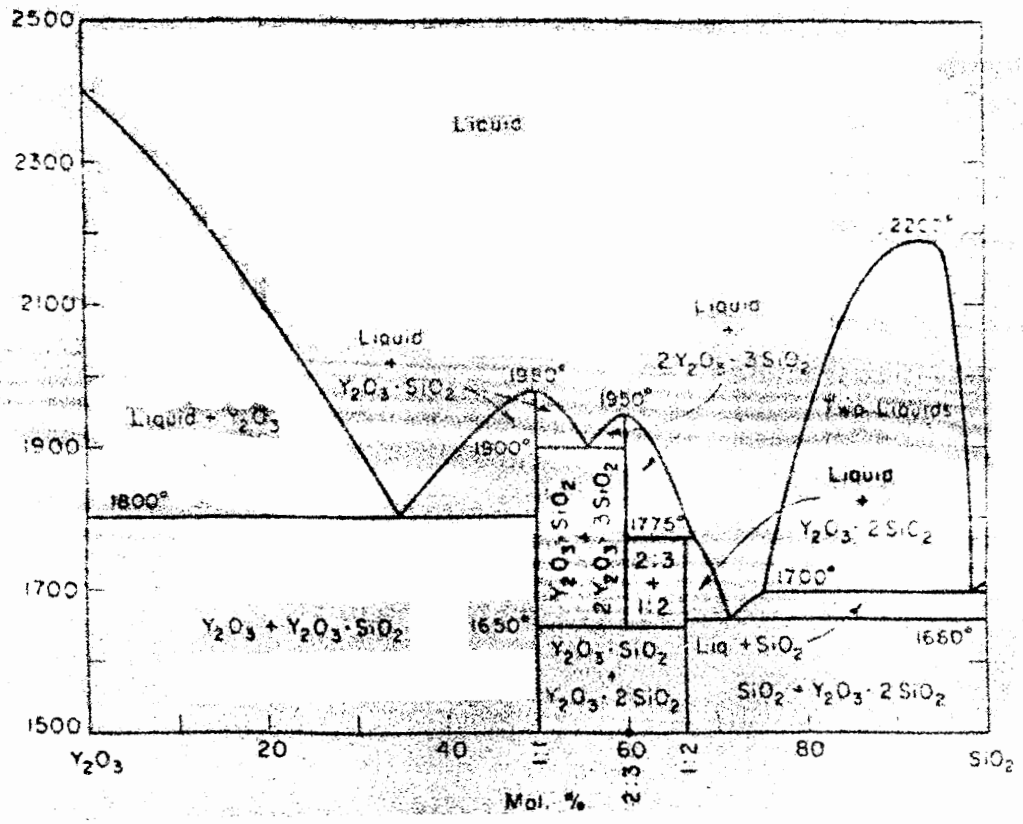

Fig. 62. Yttria silica binary phase diagram.

allow the compound to be stable below 1400°C. YAS-7 under these circumstances should crystallize to 3A-2S, Y-2S, and Y-S however, no Y-S is observed in any of the crystallized specimens. A recent study of the yttrium silicates[41] suggests that there is not sufficient evidence to support the existence of the 3A-2S compound while another study[34] simply ignores the 3Y-2S compound. Similar discrepancies in the crystallization products in the YAS phase diagram have been observed by another investigator.[94] Table XIII lists the experimental and theoretical crystallization products for compositions in the YAS phase diagram. These results suggest that the Y-2S region is considerably larger than it appears on the current YAS phase diagram assuming the crystallized specimens are in equilibrium.

If the 3A-2S compound does not exist, the YAS phase diagram and the accompanying composition triangles could be altered as illustrated in Figure 63. This proposed phase diagram would correspond to the experimental results with the exception of composition 13 (Table XIII). This proposed phase diagram could also be feasible if the 2Y-3S compound is not stable below 1400°C and was used to calculate the percent crystallization of the YAS-7 composition presented earlier and further discussed in Appendix D.

In order to verify the existence of the 2Y-3S compound, high temperature XRD should be performed on powders, prepared by hydrothermal methods, in both the yttria-silica binary and the YAS ternary diagram at temperatures above which the 2Y-3S compound is stable. If high temperature XRD is impractical, rapidly quenching the compound may retain the structure for analysis at roc. temperatures.

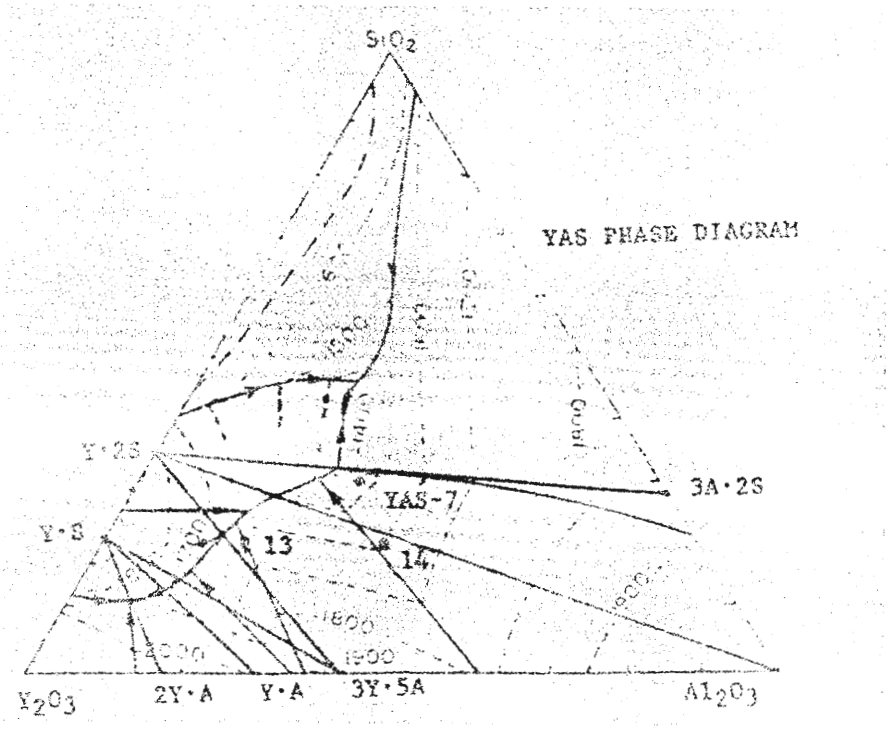

Fig. 63. Proposed composition triangles in the YAS system.

EXPERIMENTAL AND THEORETICAL CRYSTALLIZATION PRODUCTS FOR COMPOSITIONS IN THE YTTRIA ALUMINA SILICA SYSTEM

Designation	Composition (weight %) Y-A-S	Theoretical Crystallization Products	Experimental Crystallization Products
YAS-7	40-30-30	3A-2S Y-2S 2Y-3S	3A-2S Y-2S
9 (Ref. 94)	41-31-28	3A-2S Y-2S 2Y-3S	Glass β-Y-2S
12 (Ref. 94)	67-13-20	3Y-5A A 2Y-3S	3Y-5A Y-2S Y-S
13 (Ref. 94)	60-20-20	3Y-5A A 2Y-3S	3Y-5A Y-2S Y-S
14 (Ref. 94)	42-38-20	3A-2S A 2Y-3S	3Y-5A A Y-2S

Y = Y_2O_3

A = Al_2O_3

S = SiO_2

VI. DIRECTIONS FOR FUTURE WORK

The primary goal of future work should be the development of processing parameters for the fabrication of unidirectional fiber reinforced glass-ceramic composites. The temperature stability of the Tyranno fiber needs to be determined and unidirectional Tyranno fiber reinforced composite specimens should be fabricated. This fiber is the most promising candidate for use in glass-ceramic matrix composites because it does not require a coating. New high temperature fiber coatings need to be developed and evaluated for use with Tyranno and other available fiber ceramic fibers.

The effect of hot pressing time on the crystallization of the matrices needs to be investigated further. The optimum holding time and temperature should be determined for both matrices to maximize the crystalline content. Transmission electron microscopy should be used to quantitatively analyze fiber/matrix interactions and the effects of fiber additions on the crystallization of the glass-ceramic matrices.

Cordierite is an excellent matrix candidate for high temperature glass-ceramic matrix composites. Cordierite, when completely crystallized, should be usable to 1100°C. The low C.T.E. of cordierite makes it compatible with the existing ceramic fiber systems.

In order for the YAS-7 composition to be used as a high temperature glass-ceramic matrix, certain problems must be overcome. The source of the matrix porosity, developed during hot pressing, must be identified and the effect of this porosity on mechnical behavior of the matrix should be evaluated. The α- to β-$Y_2Si_2O_7$ phase transformation, the accompanying 6.6% volume expansion, and the 1300°C

processing temperature needed to trigger this transformation, must be investigated to determine their effects on the mechanical and chemical properties on both the matrix and the reinforcing fibers.

BIBLIOGRAPHY

1. T. Chou, R. L. McCullough and R. B. Pipes, "Composites" Scientific American. 255 [10] 192-203 (1986).
2. M. R. Piggott, "Load Bearing Fibre Composites," Pergamon Press, Oxford 1980.
3. R. Wills, M. Pascucci and F. Jelinek, "Ceramic-Ceramic Composites, State-of-the-Art Report," MCIC 86-51, Batelle Columbus Division, January 1986.
4. R. W. Davidge, "Mechanical Behavior of Ceramics," Cambridge University Press, 1979, 111-117.
5. I. W. Donald and P. W. McMillan, "Review: Ceramic-Matrix Composites," Journal of Materials Science. 11 949-972 (1976).
6. R. W. Davidge, "Fiber Reinforced Ceramics," Composites, 18 [2] (1987).
7. A. A. Griffith, "The Phenomena of Rupture and Flow in Solids," Philosophical Transactions of the Royal Society of London, A221 163-198, (1920).
8. D. C. Larsen, S. L. Stuckly, and S. A. Bortz, "Test Methodology for Ceramic Fiber Composites: Results for SiC/LAS, SiC/SiC, and C/SiC Composites," Metal Matrix, Carbon and Ceramic Matrix Composites, 1985, 313-334.
9. K. M. Prewo, "Fiber Reinforced Metal and Glass Matrix Composites," Frontiers in Materials Science. Sandia National Labs, October 1983.
10. B. D. Agarwal and L. J. Broutman, "Analysis and Performance of Fiber Composites," John Wiley and Sons, New York 1980.

11. A. K. Khaund, V. D. Krstic and P. S. Nicholson, "Influence of Elastic and Thermal Mismatch on the Local Crack-Driving Force in Brittle Composites," Journal of Materials Science, 12 2269-2273 (1977).

12. W. D. Kingery, H. K. Bowen and D. R. Uhlmann, "Introduction to Ceramics, 2nd Edition," John Wiley and Sons, New York 1976.

13. K. M. Prewo, "The Development of Fiber Reinforced Glasses and Glass Ceramics," Tailoring Multiphase and Composite Ceramics, Pennsylvania State University, July, 1985.

14. K. M. Prewo, J. J. Brennan, and G. K. Layden, "Fiber Reinforced Glasses and Glass-Ceramics for High Performance Applications," American Ceramic Society Bulletin, 65 [2] 305-313 (1986).

15. J. A. Cornie, Y. Chiang, D. R. Uhlmann, A. Mortensen, and J. M. Collins, "Processing Techniques for Fiber-Reinforced Ceramic Matrix Composites," American Ceramic Society Bulletin, 65 [2] 297-304 (1986).

16. R. Pampauch, W. Slomka, and J. Chlopek, "Determination of the Influence of Matrix-Ceramic Fibre Reactions on Strength of Composites," Ceramics International, 12 9-18 (1986).

17. R. R. Tummala and A. L. Friedlberg, "Thermal Expansion of Composite Materials," Journal of Applied Physics, 41 [13] 5104-5107 (1970).

18. J. K. Wells and P. W. R. Beaumont, "Debonding and Pull-out Processes in Fibrous Composites," Journal of Materials Science, 20 1275-1284 (1985).

19. R. H. Doremus, "Glass Science," John Wiley and Sons, New York 1973.

20. M. J. Hyatt, "Glass Formation and Properties in the Y_2O_3-Al_2O_3-SiO_2 System," M. S. Thesis, University of Missouri-Rolla, 1984.

21. T. S. Sedykh, A. I. Pustil'nik and V. I. Mikheikin, "Refractive Indexes in the Yttrium Oxide-Silicon Dioxide-Aluminum Oxide System in the Vitrification Region," Inorganic Materials, 11 [6] 987-988 (1975). Translated from: Izvestiya Akademii Nauk SSSR, Neorganicheskie Materialy, 11 [6] 1153-1154 (1975).

22. P. W. McMillan, Glass-Ceramics, 2nd Edition," Academic Press, London 1979.

23. W. Vogel, Tranlated by N. Kreidl, "Chemistry of Glass," The American Ceramic Society, Inc., Columbus, Ohio 1985.

24. M. I. Pope and M. D. Judd, "Differential Thermal Analysis," Heyden and Sons LTD., London 1977.

25. E. E. Hermes and K. S. Mazdiyasni, "Processing and Characterization of SiC Fiber Reinforced Magnesium Aluminum Silicate Composites," Metal Matrix, Carbon and Ceramic Matrix Composites, 1985, 217-228.

26. J. J. Brennan, Personal Communication.

27. T. Mah, "Fiber-Reinforced Ceramic-Matrix Composites," Metal Matrix, Carbon and Ceramic Matrix Composites, 1984, 245-260.

28. W. Zdaniewski, " Crystallization and Structure of a MgO-Al_2O_3-SiO_2-TiO_2 Glass-Ceramic," Journal of Materials Science, 8 192-202 (1973).

29. W. Zdaniewski, "DTA and X-Ray Analysis Study of Nucleation and Crystallization of MgO-Al_2O_3-SiO_2 Glasses Containing ZrO_2, TiO_2 and CeO_2," Journal of the American Ceramic Society, 58 [5-6] 163-169 (1975).

30. A. G. Gregory and T. J. Veasey, "Review: The Crystallisation of Cordierite Glass - Part III," Journal of Materials Science, 8 324-332 (1973).

31. A. G. Gregory and T. J. Veasey, "Review: The Crystallization of Cordierite Glass - Part II," Journal of Materials Science, 7 1327-1341 (1972).

32. A. G. Gregory and T. J. Veasey, "Review: The Crystallisation of Cordierite Glass - Part I," Journal of Materials Science, 6 1312-1321 (1971).

33. C. H. Drummond, III, and K. S. Mazdiyasni, "SiC/Zirconia-Cordierite Glass-Ceramic Composites," Metal Matrix, Carbon and Ceramic Matrix Composites, 1985, 197-204.

34. D. P. Thompson, "Phase Relation in Y-Si-Al-O-N Ceramics," Presented at the Penn State Conference on Tailoring Multiphase and Composite Ceramics, July 1985.

35. "Aluminosilicate Glasses Containing Yttrium," Patent: Japan Kokai Tokkyo Koho, #JP 8469443 A2, JP5969443, 19 April 1984. Chemical Abstract #101 (14) 115671r Patent.

36. "Aluminosilicate Glasses Containing Rare Earth Metal Oxides," Patent: Japan Kokai Tokkyo Koho, #JP 8302236 A2, JP5802236, 7 January 1983. Chemical Abstract #98 (24) 203245e Patent.

37. I. A. Bondar and F. Y. Galakhov, "Phase Equilibria in the Y_2O_3-Al_2O_3-SiO_2 System," Bulletin of the Academy of Sciences of the USSR, Division of Chemical Science, 7 1231-1232 (1964); Translated from Izvestiya Akademii Nauk SSSR, Seriya Khimicheskaya, 7 1325-1326 (July, 1964).

38. A. Makishima, H. Kubo and T. Shimohira, "Formation and Crystallization of Yttrium Aluminosilicate Glasses Containing Calcium Oxide," Journal of the American Ceramic Society, 69 [6] C130-C136 (1986).

39. A. Makishima, H. Kubo, K. Kotani, M. Tsutsumi, and M. Asami, "Formation and Crystallization in the Yttrium Aluminosilicate Glasses Containing Zinc Oxide," Journal of the American Ceramic Society, 69 [12] C294-C296 (1986).

40. W. R. Schoeller and A. R. Powell, "The Analysis of Minerals and Ores of the Rarer Earths," Charles Griffin and Co. LTD., London 1919, 69.

41. K. Liddell and D. P. Thompson, "X-Ray Diffraction Data for Yttrium Silicates," British Ceramic Transactions Journal, 85 17-22 (1986).

42. J. Ito and H. Johnson, "Synthesis and Study of Yttrialite," The American Mineralogist, 53 [11-12] 1940-1952 (1968).

43. A. N. Lazarev, T. F. Tenisheva and I. A. Bondar', "More on the Polymorphism of Rare-Earth Pyrosilicates," Inorganic Materials, 1 [7] 1104-1106 (1965). Translated from Izvestiya Akademii Nauk SSSR, Neorganicheskie Materialy, 1 [7] 1207-1209 (1965).

44. N. G. Batalieva and Y. A. Pyatenko, "Artificial Yttrialite ("y-Phase") -- A Representation of a New Structure Type in the Rare Earth Diorthosilicate Series," Soviet Physics - Crystallography 16 [5] 786-789 (1972). Translated from Kristallografiya 16 [5] 905-910 (1971).

45. J. Felsche, "Crystal Data on the Polymorphism Disilicate $Y_2Si_2O_7$," Die Naturwissenschaften, 57 [3] 127-128 (1970).

46. S. Yajima, J. Hayashi, M. Omori, and K. Okamura, "Development of a Silicon Carbide Fibre with High Tensile Strength," Nature 261 June 24, 1976, 683-685.

47. G. Simon and A. R. Bunsell, "Mechanical and Structural Characterization of the Nicalon Silicon Carbide Fibre," Journal of Materials Science, 19 3649-3657 (1984).

48. S. R. Levitt, "High-Strength Graphite Fibre/Lithium Aluminosilicate Composites," Journal of Materials Science, 8 793-806 (1973)

49. T. Foltz, Personal Communication.

50. D. D. Johnson, A. R. Holtz, and M. F. Gunther, "Properties of Nextel 480 Ceramic Fiber," Presented at the 11th Annual Conference on Composites and Advanced Ceramic Materials, Cocoa Beach, FL, January 18-23, 1987.

51. K. M. Prewo and J. J. Brennan, "High Strength Silicon Carbide Fibre-Reinforced Glass-Matrix Composites," Journal of Materials Science, 15 463-468 (1980).

52. J. V. Milewski, "Efficient Use of Whiskers in the Reinforcement of Ceramics," Advanced Ceramic Materials, 1 [1] 36-41 (1986).

53. R. A. J. Sambell, D. H. Bowen, and D. C. Phillips, "Carbon Fiber Composites with Ceramic and Glass Matrices. Part I. Discontinuous Fibres, " Journal of Materials Science, 7 663-675 (1972).

54. B. A. Bender, D. Lewis III, W. S. Coblenz, and R. W. Rice, "Electron Microscopy of Ceramic Fiber-Ceramic Matrix Composites - Comparison with Processing and Behavior," Metal Matrix, Carbon and Ceramic Matrix Composites, 1984, 171-190.

55. W. S. Coblenz, R. W. Rice, D. Lewis III, D. Shadwell, B. A. Bender and C. Cm. Wu, "Progress in Ceramic Refractory Fiber Composites," Metal Matrix, Carbon and Ceramic Matrix Composites, 1984, 191-215.

56. K. M. Prewo and J. J. Brennan, "Silicon Carbide Yarn Reinforced Glass Matrix Composites," Journal of Materials Science, 17 1201-1206 (1982).

57. J. J. Brennan and K. M. Prewo, "Silicon Carbide Fiber Reinforced Glass-Ceramic Matrix Composites Exhibiting High Strength and Toughness," Journal of Materials Science, 17 2371-2383 (1982).

58. J. J. Brennan, "Interfacial Characterization of Glass and Glass-Ceramic Matrix/Nicalon SiC Fiber Composites," Tailoring Multiphase and Composite Ceramics, Plenum Publishing Co., 1986 549-560.

59. R. Chaim and A. H. Heuer, "The Interface Between (Nicalon) SiC Fibers and a Glass-Ceramic Matrix," Advanced Ceramic Materials 2 [2] 154-158 (1987).

60. D. C. Phillips, "Interfacial Bonding and the Toughness of Carbon Fiber Reinforced Glass and Glass-Ceramics," Journal of Materials Science, 9 1847-1854 (1974).

61. J. R. Hellmann, "Fiber Reinforced Ceramic Composites," Unpublished Work, Sandia National Laboratories, 1985.

62. D. C. Phillips, "The Fracture Energy of Carbon-Fibre Reinforced Glass," Journal of Materials Science, 7 1175-1191 (1972).

63. L. J. Schioler and J. J. Stiglich, Jr., "Ceramic Matrix Composites: A Literature Review," American Ceramic Society Bulletin, 65 [2] 289-292 (1986).

64. K. M. Prewo. "A Compliant, High Failure Strain, Fibre-Reinforced Glass-Matrix Composite," Journal of Materials Science, 17 3549-3563 (1982).

65. R. A. J. Sambell, A. Briggs, D. C. Phillips, and D. H. Bowen, "Carbon Fibre Composites with Ceramic and Glass Matrices. Part II, Continuous Fibres," Journal of Materials Science, 7 676-681 (1972).

66. M. A. Herron and S. H. Risbud, "Characterization of SiC-Fiber-Reinforced Ba-Si-Al-O-N Glass-Ceramic Composites," American Ceramic Society Bulletin, 65 [2] 342-346 (1986).

67. D. Lewis and R. W. Rice, "Furthur Assesment of Ceramic Fiber Coating Effects on Ceramic Fiber Composites," Metal Matrix, Carbon and Ceramic Matrix Composites, 1985, 13-26.

68. B. Bender, D. Shadwell, C. Bulik, L. Inorvati, and D. Lewis III, "Effect of Fiber Coatings and Composite Processing on Properties of Zirconia-Based Matrix SiC Fiber Composites," American Ceramic Society Bulletin, 65 [2] 363-369 (1986).

69. V. A. Lavrenko and A. F. Alexeev, "High Temperature Oxidation of Boron Nitride," Ceramics International, 12 [1] 25-31 (1986).

70. R. W. Rice, J. R. Spann, D. Lewis III, and W. S. Coblenz, "The Effect of Ceramic Fiber Coatings on the Room Temperature Mechanical Behavior of Ceramic Fiber Composites," Metal Matrix, Carbon and Ceramic Matrix Composites, 1984, 217-231.

71. D. B. Marshall and A. G. Evans, "Failure Mechanisms in Ceramic Fiber/Ceramic Matrix Composites," Journal of the American Ceramic Society, 68 [5] 225-231 (1985).

72. J. J. Mecholsky, "Evaluation of Mechanical Property Testing Methods for Ceramic Matrix Composites," American Ceramic Society Bulletin, 65 [2] 315-322 (1986).

73. D. C. Phillips and R. W. Davidge, "Test Techniques for the Mechanical Properties of Ceramic Matrix Fibre Composites," British Ceramic Transactions Journal, 85 123-130 (1986).

74. T. Mah, M. G. Mendiratta, A. P. Katz, R. Ruh, and K. S. Mazdiyasni, "High-Temperature Mechanical Behavior of Fiber-Reinforced Glass-Ceramic Matrix Composites," Journal of the American Ceramic Society, 68 [9] C248-C251 (1985).

75. T. Mah, M. G. Mendiratta, A. P. Katz, R. Ruh, and K. S. Mazdiyasni, "Room-Temperature Mechanical Behavior of Fiber-Reinforced Ceramic-Matrix Composites," Journal of the American Ceramic Society, 68 [1] C27-C30 (1985).

76. M. G. Jenkins, A. S. Kobayashi, M. Sakai, K. W. White and R. C. Bradt, "Fracture Toughness Testing of Ceramics Using a Laser Interferometric Strain Gage," To be Published in the American Ceramic Society Bulletin.

77. E. Y. Luh and A. G. Evans, "High Temperature Mechanical Properties of a Ceramic Matrix Composite," Journal of the American Ceramic Society, 70 [7] 446-469 (1987).

78. D. B. Marshall, "An Indentation Method for Measuring Matrix-Fiber Frictional Stresses in Ceramic Composites," Journal of the American Ceramic Society, 67 [12] C259-C260 (1984).

79. R. Gonzalez, Y Chen and K. L. Tsang, "Diffusion of Deuterium in Amorphous Cordierite," Journal of the American Ceramic Society, 67 [12] 775-777 (1984).

80. G. N. Howatt, R. G. Breckenridge, and J. M. Brownlow, "Fabrication of Thin Ceramic Sheets for Capacitors," Journal of the American Ceramic Society, 30 [8] 237-242 (1947).

81. P. W. D. Mitchell, "Chemical Method for Preparing $MgAl_2O_4$ Spinel, "Journal of the American Ceramic Society, 55 [9] 484 (1972).

82. D. R. Messier and G. E. Gazza, "Synthesis of $MgAl_2O_4$ and $Y_3Al_5O_{12}$ by Thermal Decomposition of Hydrated Nitrate Mixtures," American Ceramic Society Bulletin, 51 [9] 692-697 (1972).

83. W. C. Luth and C. O. Ingamells, "Gel Preparation of Starting Materials for Hydrothermal Experimentation," The American Mineralogist, 50 [1] 255-258 (1965).

84. R. Roy, "Aids in Hydrothermal Experimentation: II, Methods of Making Mixtures for Both "Dry" and "Wet" Phase Equilibrium Studies," Journal of the American Ceramic Society, 39 [4] 145-146 (1956).

85. "1986 Annual Book of ASTM Standards," Volume 15.02, Class: Ceramic Whitewares, Procedure C674-81p, 259-263.

86. W. F. Brown and J. E. Srawley, Plane Strain Crack Toughness Testing of High Strength Metallic Materials, ASTM Special Technical Publication #410, 1966.

87. S. E. Salibekov, K. L. Portnoi and V. M. Chubarov, "Experimental Investigation of Thermal Expansion in Composite Fibrous Materials," High Temperature, March 1973, 702-706; Translated from Teplofizika Vysokikh Temperatur, 10 [4], 783-787. (July-August, 1972).

88. J. B. Austin, "Thermal Expansion of Nonmetallic Crystals," Journal of the American Ceramic Society, 35 [10] 243-253 (1952).

89. S. S. Tompkins, "Thermal Expansion of Selected Graphite Reinforced Polyimide-, Epoxy-, and Glass-Matrix Composites," NASA Technical Memorandum #87572, (July, 1985).

90. A. A. Fahmy and A. N. Ragai, "Thermal Expansion of Two-Phase Solids," Journal of Applied Physics, 41 [13] 5108-5111 (1970).

91. K. Chyung, Personal Communication.

92. A. F. Helma, "Crystallization Characteristics of YAS Glasses," Unpublished work.

93. W. Eitel, "Silicate Science, Volume III, Dry Silicate Systems," Academic Press, New York, 1965, 111-137.

94. A. D. Miller and D. W. Gilbert, "Silicon Nitride Wettability Studies," Attachment I, Low-Cost, Net-Shape Ceramic Radial Turbine Program, Phase I Final Technical Report, 21-3991(4), Garrett Turbine Engine Company, Phoenix, AZ, December 24, 1981.

95. F. A. Hummel, "Introduction to Phase Equilibria in Ceramic Systems," Marcel Dekker, Inc., 1984.

REFERENCES

1. W. Eitel, "System Silica-Alumina-Magnesia," Silicate Science, Volume III, Dry Silicate Systems, Academic Press, New York, 1965, 208-220.

2. D. J. Pysher, K. C. Goretta, R. E. Tressler, and R. S. Hodder, Jr., "High Temperature Strengths of Ceramic Fibers," Pennsylvania State University, Unpublished Work.

3. B. Budiansky and J. W. Hutchinson, "Matrix Fracture in Fiber-Reinforced Ceramics," Journal of the Mechanics, Physics and Solids, 34, [2], 167-189. (1986).

4. K. Okamura, "Ceramic Fibres from Polymer Precursors," Composites, 18, [2], 107-120, (1987).

5. J. J. Brennan, "Additional Studies of SiC Fiber Reinforced Glass-Ceramic Matrix Composites," Office of Naval Research Report #R84-916018-4, Annual Report, April 1, 1984.

6. J. J. Brennan, "Additional Studies of SiC Fiber Reinforced Glass-Ceramic Matrix Composites," Office of Naval Research Report #R85-916777-2, Annual Report, May 31, 1985.

7. J. J. Brennan, "Interfacial Studies of SiC Fiber Reinforced Glass-Ceramic Matrix Composites," Office of Naval Research Report #R86-917546-2, Annual Report, September 30, 1986.

8. F. D. Gac, J. V. Milewski, J. J. Petrovic, and P. D. Shalek, "Silicon Carbide Whisker Reinforced Glass and Ceramics," Metal Matrix, Carbon and Ceramic Matrix Composites, 1985, 53-72.

9. P. L. Higby and J. E. Shelby, "Properties of Some Simple Glass/Ceramic Systems," Journal of the American Ceramic Society, 67 [7] 445-449 (1984).

10. B. H. Mussler and M. W. Shafer, "Preparation and Properties of Cordierite-Based Glass-Ceramic Containing Precipitated ZrO_2," American Ceramic Society Bulletin, 64 [11] 1459-1462 (1985).

11. K. P. Gadkaree and K. Chyung, "Silicon-Carbide-Whisker-Reinforced Glass and Glass-Ceramic Composites," American Ceramic Society Bulletin, 65 [2] 370-376 (1986).

12. M. R. Piggott, "The Effect of Aspect Ratio on Toughness in Composites," Journal of Materials Science, 9 494-502 (1974).

13. J. Aveston and A. Kelly, "Theory of Multiple Fracture of Fibrous Composites," Journal of Materials Science, 8 352-362 (1973).

14. W. A. Zdaniewski, "Microstructure and Kinetics of Crystallization of MgO-Al2O3-SiO2 Glass-Ceramics," Journal of the American Ceramic Society, 61 [5-6] 199-204 (1978).

15. A. Makishima, Y. Tamura, and T. Sakaino, "Elastic Moduli and Refractive Indices of Aluminosilicate Glasses Containing Y_2O_3, La_2O_3, and TiO_2," Journal of the American Ceramic Society, 61 [5-6] 247-249 (1978).

VITA

William Michael Carty was born September 28, 1962 in Belleville, Illinois. He graduated with honors from Belleville Township High School West in May, 1980 and enrolled in Belleville Area College the following August. In January, 1981 he transferred to the University of Missouri at Rolla. He entered the cooperative engineering program with Wisconsin Porcelain Company, Sun Prairie, Wisconsin from January to May, 1982, and Sunnen Products Company, St. Louis, Missouri from January to August, 1984. He was granted a Bachelor of Science Degree in Ceramic Engineering in May, 1985. Immediately thereafter he enrolled in the Graduate School at the University of Missouri at Rolla studying for the Master of Science Degree in Ceramic Engineering.

APPENDIX A

POWDER XRD PATTERNS

Figures 64-67 illustrate the powder XRD patterns obtained from typical specimens. The peaks in Figures 66 and 67 are designated in the following manner:

m = $3Al_2O_3 \cdot 2SiO_2$ or mullite

A = α-$Y_2Si_2O_7$

B = β-$Y_2Si_2O_7$

The cordierite standard pattern was obtained from a crushed specimen of a cordierite body used in the fabrication of catalytic converter parts. This pattern was chosen because it was cleaner, in terms of contamination from mullite impurities, than a "96% pure" specimen obtained from Baikowski Company. Information regarding the preparation of the mullite XRD standard will be available in the forthcoming master's thesis by A.J. Skoog.

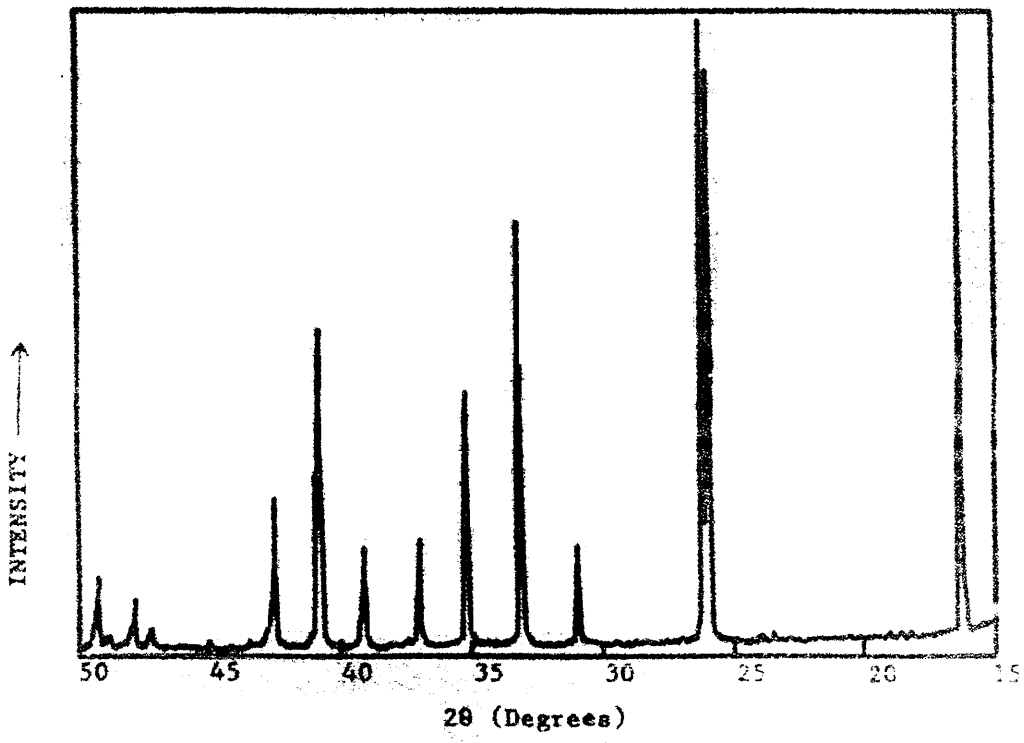

Fig. 64. Standard powder XRD pattern for $3Al_2O_3 \cdot 2SiO_2$ (mullite), courtesy of A.J. Skoog.

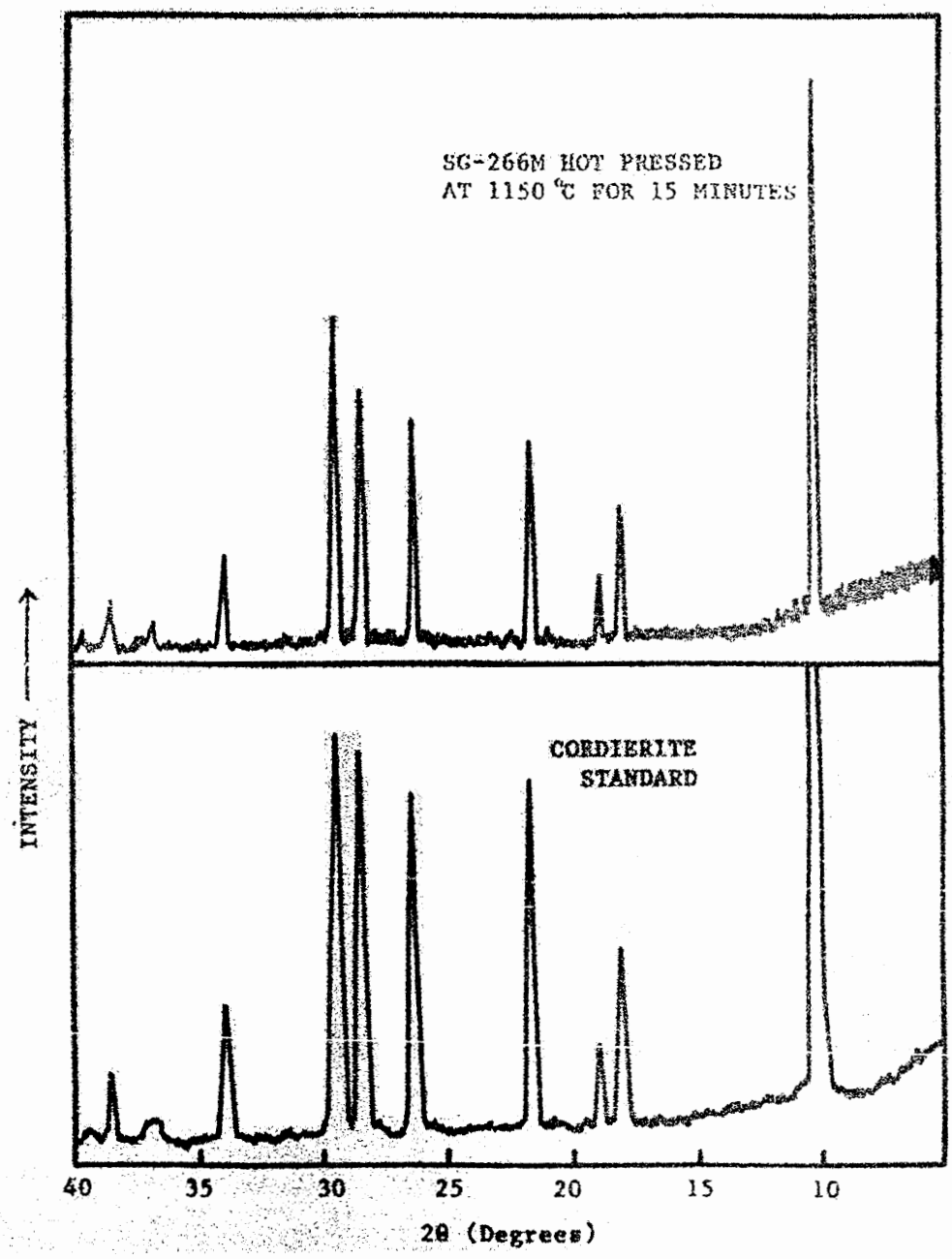

Fig. 65. Powder XRD patterns from a commercial cordierite (standard) and hot pressed SG266M.

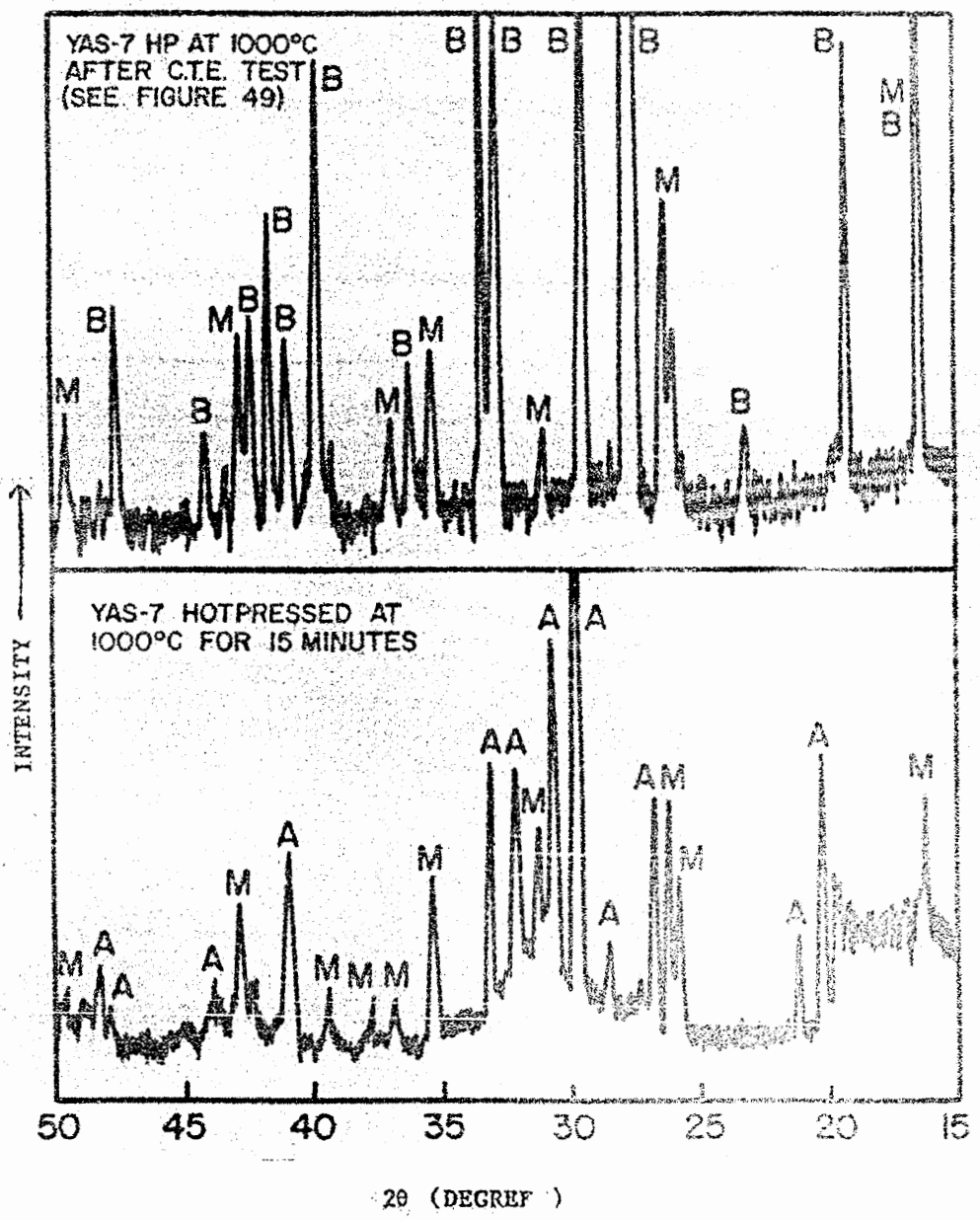

Fig. 66. Powder XRD patterns of hot pressed YAS-7 before and after thermal expansion test.

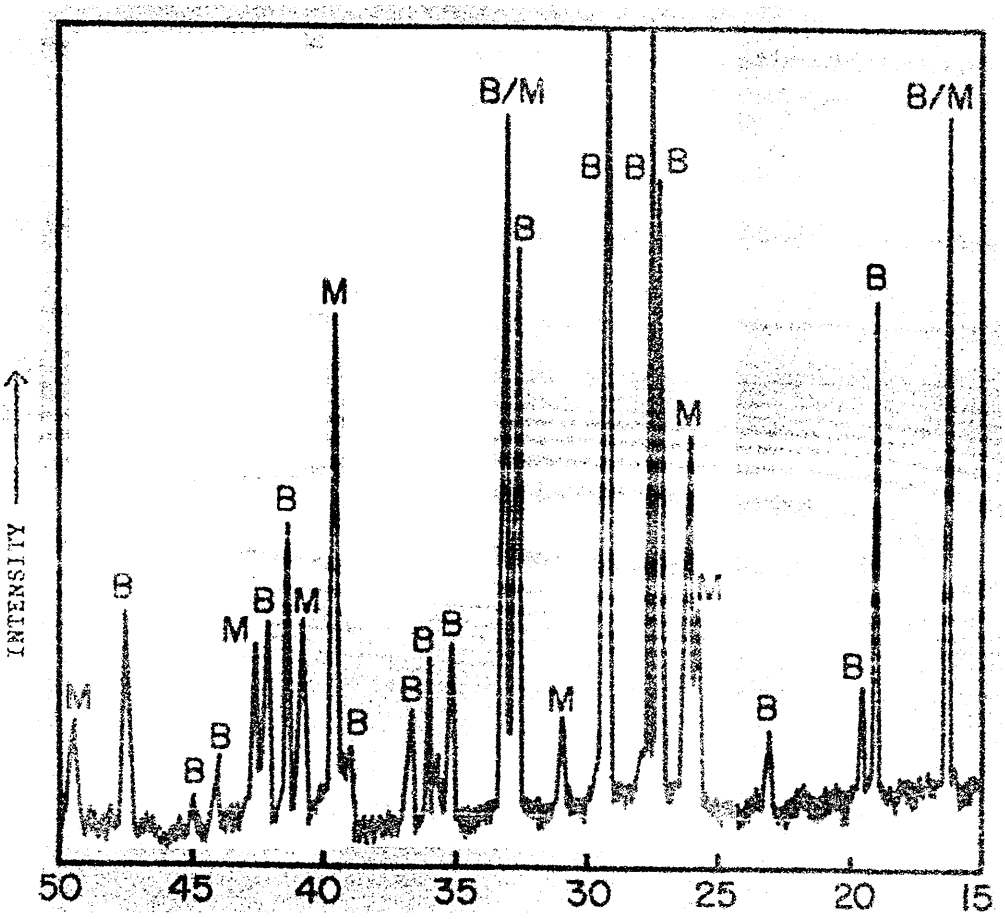

Fig. 67. Powder XRD pattern for YAS-7 hot pressed at 1300°C for 15 minutes.

APPENDIX B

ADDITIONAL DISCUSSION OF AXIAL STRESS DUE TO C.T.E. MISMATCH

To determine the effect of C.T.E. mismatch, in terms of matrix microcracking, of various fiber additions into either the cordierite or YAS-7 matrix, the resulting axial stresses should be calculated before composite fabrication. If the axial stress is greater than the matrix failure strength, then matrix microcracking will occur and the resulting composite system will be useless. Table XIV contains the calculated axial stresses (Equation 5) for hypothetical composite systems using 50 volume % unidirectionally aligned commercially available ceramic fiber and either the cordierite matrix or the YAS-7 matrix. In the case of YAS-7, which has been found to exhibit a considerable change in C.T.E. during crystallization, values for the axial stress have been calculated using the experimentally determined C.T.E. values. It has also been assumed that the elastic moduli for cast YAS-7 glass and crystallized, hot pressed YAS-7 are the same. The change in temperature (ΔT) used for these calculations was picked as the glass softening temperature for cordierite and YAS-7 glass because the matrix would not be able to deform and relieve stresses below that temperature. The ΔT for crystallized YAS-7 was picked, based on experimental results, as the minimum temperature required to allow the α- to β-$Y_2Si_2O_7$ phase transformation and hence, the lower C.T.E.

Negative axial stress means the matrix will be placed in compression and no matrix microcracking will occur. A perfect C.T.E. match between the fiber and the matrix is optimum. Some toughening of

TABLE XIV

AXIAL STRESSES RESULTING FROM C.T.E. MISMATCH FOR HYPOTHETICAL GLASS-CERAMIC MATRIX COMPOSITE SYSTEMS

	Axial Stress, σ_z (MPa)		
		YAS-7	
Fiber V_f=0.5	Cordierite ΔT=850°C	Glass ΔT=900°C	Crystalline ΔT=1280°C
AS-4	287*	757*	912*
NICALON	-21.9	259*	219*
NEXTEL 440	-97.6	164	73.9
FIBER FP	-191	39.3	-65.2
TYRANNO	-21.9	259*	219*

*Expected Matrix Microcracking
-Denotes Compressive Axial Stress

the composite may result from significant compressive stresses in the matrix as discussed earlier.

Based on the calculated axial stress values listed in Table XIV, YAS-7 will only be useful as a glass-ceramic matrix when reinforced with Fiber FP or Nextel 440. Cordierite, however, is a candidate for all of the listed ceramic fibers. Carbon AS-4 fiber reinforced cordierite matrix composites would exhibit microcracking which has been observed experimentally.

APPENDIX C

MECHANICAL TESTING DATA AND SAMPLE CALCULATIONS

A. M.O.R. RESULTS AND CALCULATIONS

Table XV contains the mechanical testing data used to calculate the 3-point flexure strength (M.O.R.) values listed in Table XI using the following equation:

$$M.O.R. = (3\ P\ L)/(2\ b\ d^2)$$

where L equals the testing span which was one inch for all tested specimens in this thesis. For the first specimen listed in Table XV,

$$M.O.R. = (3)(265)(1)/2(0.223)(0.320)^2 = 17,400 \text{ psi}$$

$$(17,400 \text{ psi})(6.9 \text{ MPa}/1000 \text{ psi}) = 120 \text{ MPa}$$

the averages and standard deviations were calculated using the standard equations. Only specimens in which fracture initiated approximately midway between the testing supports were used in the calculation of the averages and standard deviations. Values obtained from specimens which did not exhibit ideal fracture were discarded and are marked with an asterisk in Table XV.

B. TOUGHNESS MEASUREMENT DATA AND CALCULATIONS

The values for toughness (K_{1c}), listed in Table XI, were calculated from the data listed in Table XVI using the following equation:[86]

$$K_{1c} = Y[(3PLc) / (2bd^2)] \qquad (7)$$

where c equals the notch depth. The calibration coefficient, Y, is a function of (c/d) and the testing configuration, i.e. 3- or 4-point bending, and can be calculated using this fourth-degree polynomial:

TABLE XV

3-POINT FLEXURE TESTING DATA

HOT-PRESSED CORDIERITE

d (in.)	b (in.)	P (lbs.)	M.O.R. (MPa)
0.320	0.223	265	120
0.320	0.233	260	113
0.320	0.205	295	145
0.318	0.235	195	85
0.312	0.226	347	163

HOT-PRESSED CORDIERITE + 20% CARBON COATED NEXTEL 480

d (in.)	b (in.)	P (lbs.)	M.O.R. (MPa)
0.268	0.335	260	112
0.260	0.347	205	90
0.254	0.366	319	140
0.228	0.339	252	148
0.253	0.365	193	85

CAST YAS-7

d (in.)	b (in.)	P (lbs.)	M.O.R. (MPa)
0.199	0.366	125	89*
0.239	0.354	362	185
0.231	0.346	358	200
0.265	0.330	135	60*
0.261	0.339	343	154
0.238	0.366	510	254

HOT-PRESSED YAS-7

d (in.)	b (in.)	P (lbs.)	M.O.R. (MPa)
0.239	0.277	273	178
0.242	0.270	97	65*
0.241	0.260	283	194
0.240	0.274	194	127
0.278	0.170	184	145

TABLE XV (Cont.)

HOT-PRESSED YAS-7 HEAT TREATED AT 1100C

d (in.)	b (in.)	P (lbs.)	M.O.R. (MPa)
0.225	0.258	183	145
0.207	0.257	230	216
0.252	0.255	304	194
0.253	0.213	248	188
0.268	0.243	312	185

HOT-PRESSED YAS-7 + 10% UNCOATED NEXTEL 440

d (in.)	b (in.)	P (lbs.)	M.O.R. (MPa)
0.246	0.161	151	160
0.248	0.164	145	149
0.256	0.147	115	123

HOT-PRESSED YAS-7 + 20% UNCOATED NEXTEL 440

d (in.)	b (in.)	P (lbs.)	M.O.R. (MPa)
0.238	0.162	177	199
0.236	0.159	134	156
0.245	0.158	128	140

HOT-PRESSED YAS-7 + 30% UNCOATED NEXTEL 440

d (in.)	b (in.)	P (lbs.)	M.O.R. (MPa)
0.263	0.161	87	81*
0.261	0.159	140	134
0.262	0.153	113	111

HOT-PRESSED YAS-7 + 20% CARBON COATED NEXTEL 480

d (in.)	b (in.)	P (lbs.)	M.O.R. (MPa)
0.249	0.198	75	63*
0.264	0.259	228	131
0.259	0.266	184	107
0.275	0.262	294	153
0.281	0.261	204	102

TABLE XVI

SENB TOUGHNESS TESTING DATA

CORDIERITE + 20% CARBON COATED NEXTEL 480

d (in.)	b (in.)	c (in.)	Y	P (lbs.)	K_{1c} (MPa·m$^{\frac{1}{2}}$)
0.388	0.269	0.058	1.725	195	3.3
0.357	0.265	*			
0.368	0.249	0.079	1.747	160	3.8
0.379	0.258	0.054	1.726	179	3.2
0.365	0.267	0.065	1.728	242	4.9

YAS-7 + 20% CARBON COATED NEXTEL 480

d (in.)	b (in.)	c (in.)	Y	P (lbs.)	K_{1c} (MPa·m$^{\frac{1}{2}}$)
0.275	0.259	0.054	1.736	127	4.3
0.295	0.262	0.067	1.759	237	8.0
0.265	0.264	0.038	1.725	91	2.7
0.257	0.258	0.040	1.725	65	2.1
0.280	0.262	0.067	1.768	107	3.9

$$Y = A_0 + A_1(c/d) + A_2(c/d)^2 + A_3(c/d)^3 + A_4(c/d)^4 \qquad (8)$$

Table XVII contains coefficients for A_n depending on the testing method employed. The testing specimen used in this study had a span to depth ratio of approximately 3 so the values listed in Table XVII for S/d = 4 were used to calculate Y.

The toughness values calculated from the data in Table XVI initially had the units ksi·in$^{\frac{1}{2}}$. These values were converted to MPa·m$^{\frac{1}{2}}$ using the following equality:

$$\text{ksi}\cdot\text{in}^{\frac{1}{2}} = [6.9/(0.0254)]\,\text{MPa}\cdot\text{m}^{\frac{1}{2}}.$$

C. ELASTIC MODULUS CALCULATIONS

The elastic modulus, E, of a material can be calculated from flexure testing data using the equation

$$E = P L^3 / 4 \Delta b d^3 \qquad (9)$$

where Δ is the deflection of each specimen determined from the load/deflection curve generated during testing. For the first specimen in Table XVIII,

$$E = (285)(1)^3/[(4)(7.09\times10^{-4})(0.223)(0.320)^3] = 12{,}790 \text{ ksi}$$

$$(12{,}790 \text{ ksi})(6.9 \text{ GPa}/1000 \text{ ksi}) = 88 \text{ GPa}.$$

TABLE XVII

COEFFICIENTS FOR DETERMINING THE CALIBRATION FACTOR FOR TOUGHNESS MEASUREMENTS USING FLEXURE TESTING (REF. 86)

	A_0	A_1	A_2	A_3	A_4
4-Point Bending	+1.99	-2.47	+12.97	-23.17	+24.80
3-Point Bending					
S/D = 8	+1.96	-2.75	+13.66	-23.98	+25.22
S/D = 4	+1.93	-3.07	+14.53	-25.11	+25.80

TABLE XVIII

3-POINT FLEXURE DATA USED TO CALCULATE ELASTIC MODULI

HOT-PRESSED CORDIERITE

P (lbs.)	Δ (10-4 in.)	d (in.)	b (in.)	E (MPa)
265	7.09	0.320	0.223	88.3
260	6.89	0.320	0.233	85.6
295	6.79	0.320	0.205	112.
195	5.71	0.318	0.235	86.3
347	7.38	0.312	0.226	115.

CAST YAS-7

P (lbs.)	Δ (10-4 in.)	d (in.)	b (in.)	E (MPa)
125	5.61	0.199	0.366	133
362	6.69	0.239	0.354	193
359	6.99	0.231	0.346	208
135	3.44	0.265	0.330	152
343	6.69	0.261	0.339	147
510	9.25	0.238	0.366	193

APPENDIX D

CALCULATIONS OF THE PERCENT CRYSTALLINITY OF A HOT-PRESSED YAS-7 SPECIMEN

Theoretically, the volume change associated with the α- to β-$Y_2Si_2O_7$ polymorphic phase transformation can be calculated using the unit cell dimensions of 133.6Å^3 and 142.5Å^3 for α- and β-$Y_2Si_2O_7$, respectively (Table I).

$$\% \text{ Volume Change} = [(V_i - V_f)/V_i] * 100 \qquad (10)$$

V_i and V_f equal the initial and final volumes, respectively. In this case, when a specimen of $Y_2Si_2O_7$ is heated through the transformation temperature of 1225°C, V_i = 133.6Å^3 and V_f = 142.5Å^3 and the volume change equals -6.66%. The negative sign denotes expansion.

This expansion can be coordinated to the linear expansion of a rectangular prism, such as used for thermal expansion test specimens, provided the dimensions of the test specimen are known. The specimen used to generate the curve illustrated in Figure 49 had the initial dimensions b_i = 0.219", d_i = 0.240" and l_i = 1.002" to give a volume of 0.0527 in^3. If the initial specimen was 100% α-Si_2O_7, upon complete conversion to β-Si_2O_7 the specimen would undergo a volume increase of 0.0035 in^3 assuming isotropic behavior. Based on this assumption, the final dimensions of the C.T.E. test specimen, having the initial dimensions listed above, are b_f = 0.224", d_f = 0.245" and l_f = 1.024". Therefore, the percent linear expansion due to the polymorphic phase transformation of a pure specimen of $Y_2Si_2O_7$ equals:

$$[(l_i - l_f)/(l_i] * 100 = -2.20\% \qquad (11)$$

The percentage of $Y_2Si_2O_7$ present in the YAS-7 specimen, which generated the C.T.E. curve in Figure 49, is calculated based on the percent expansion due to the phase transformation divided by the theoretical expansion due to the phase transformation:

$$(0.864/2.20) * 100 = 39.3 \text{ Volume \% } Y_2Si_2O_7 \qquad (12)$$

The relative amounts of Al_2O_3, mullite, and $Y_2Si_2O_7$ present in a fully crystallized specimen of YAS-7 can be calculated using the lever rule.[95] Figure 68 illustrates the YAS phase diagram, the composition triangle ABC, and the YAS-7 composition. The theoretical weight percentage of A, B, and C (Al_2O_3, $Y_2Si_2O_7$ and mullite, respectively) using the following equations:[95]

$$\%A = \frac{B-E}{B-A} * 100 = 7.4 \text{ weight \% } Al_2O_3$$
$$\%B = \frac{G-A}{B-A} * 100 = 61.1 \text{ weight \% } Y_2Si_2O_7 \qquad (13)$$
$$\%C = \frac{E-G}{B-A} * 100 = 31.5 \text{ weight \% mullite}$$

The volume percentages, based on the reported densities for each species, are listed in Table XIX. The "Estimated Volume %" was calculated by multiplying each volume percent by the ratio of experimental volume % $Y_2Si_2O_7$, from equation 12, to the calculated volume % $Y_2Si_2O_7$, from equation 13. The total of the estimated volume percentages, subtracted from 100% gives the volume percent glass of composition YAS-7. Weight percentages of each species, Al_2O_3, $Y_2Si_2O_7$, mullite, and YAS-7 were calculated using the reported densities of each and are listed in the last column of Table XIX.

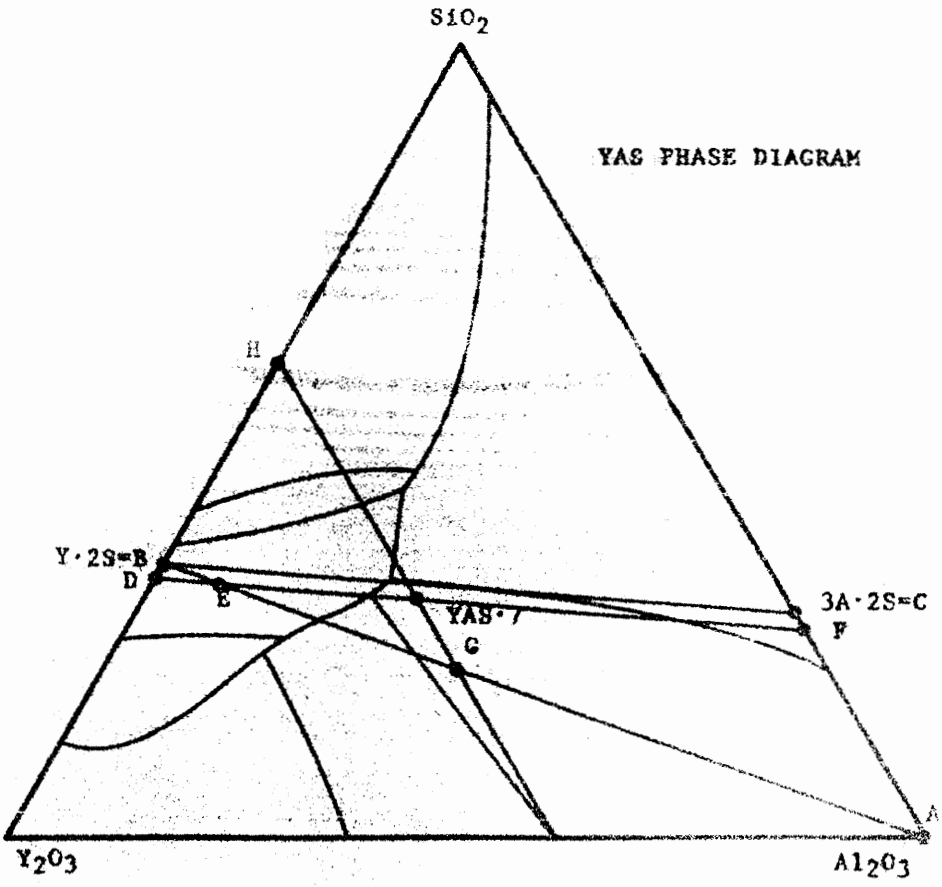

Fig. 68. YAS phase diagram for calculating crystalline phase percentages.

TABLE XIX

PERCENTAGES OF CRYSTALLINE SPECIES IN A YAS-7 SPECIMEN

	Weight %	Density g/cm^3	Volume cm^3	Volume %	Estimated Vol %	Estimated Wt %
Al_2O_3	7.4	3.9	1.9	7.6	5.6	5.7
$Y_2Si_2O_7$	61.1	4.6	13.3	53.2	39.3	47.1
Mullite	31.5	3.2	9.8	39.2	28.9	24.1
Totals	100.0		25.0	100.0	73.8	76.9
YAS-7 Glass		3.39			26.2	23.1